CHARACTERIZATION OF ROABIBA SANDSTONES RESERVOIR IN BINTUNI FIELD, PAPUA, INDONESIA

A Thesis

by

RIENE VERA

Submitted to the Office of Graduate Studies of
Texas A&M University
in partial fulfillment of the requirements for the degree of

MASTER OF SCIENCE

December 2009

Major Subject: Geology

CHARACTERIZATION OF ROABIBA SANDSTONES RESERVOIR IN BINTUNI FIELD, PAPUA, INDONESIA

A Thesis

by

RIENE VERA

Submitted to the Office of Graduate Studies of
Texas A&M University
in partial fulfillment of the requirements for the degree of

MASTER OF SCIENCE

Approved by:

Chair of Committee,	Wayne M. Ahr
Committee Members,	Yuefeng Sun
	Walter B. Ayers
Head of Department,	Andreas Kronenberg

December 2009

Major Subject: Geology

ABSTRACT

Characterization of Roabiba Sandstones Reservoir in Bintuni Field, Papua, Indonesia.

(December 2009)

Riene Vera, B.S., Trisakti University, Jakarta (Indonesia)

Chair of Advisory Committee: Dr. Wayne M. Ahr

Bintuni Field has two Middle Jurassic gas reservoirs, Upper and Lower Roabiba Sandstone reservoirs, with the estimated reserve from eight appraisal drilled wells of 6.08 tcf. The field has not been producing commercially. The main gas reservoir is the Upper Roabiba Sandstone. It was deposited in a tidal-dominated shoreface delta and consists of a moderately sorted, fine to medium grain, quartzarenite with average porosity of 12% and average permeability of 250 md. Lower Roabiba Sandstone was deposited in estuarine channel and marsh and consists of lower fine to lower coarse grained quartzarenites with average porosity of 12% and permeability 215 md.

This study is considered necessary since the field is considered to be a giant field and there are a limited number of studies on the Roabiba Sandstones reservoir specifically in Bintuni Field that have been published. The purpose of this study was to develop geological and petrophysical analysis that will identify reservoir quality and distribution of best, intermediate, and poor reservoir zones by characterizing distribution of porosity-permeability values in lithofacies and mercury injection capillary pressure .

The methods to characterize the reservoir included core-based lithofacies determination, well logs analysis, and mercury injection capillary pressure analysis. As a result from core descriptions, three main units of lithofacies could be identified. Lithofacies massive sandstones (ms), slightly bioturbated sandstones (sb1), and cross-laminated sandstones (xls) have the highest average permeability (>100 md) and porosity (>10%). Petrophysical properties from core data show that porosity varies only slightly regardless of lithofacies characteristic whereas permeability variations are greater and correspond closely with the lithofacies.

When grouped according to the dominant pore throat dimension, distinct collections or grouping of rocks and their associated lithofacies were observed. Winland plot was engaged to do clustering of rock types since Winland R_{35} pore port sizes represent 'cut off values' for good and bad flow unit quality. The analyses of porosity-permeability plots were confirmed with the Winland plot that the best reservoir rock (rock type 1) consists of lithofacies ms, xls, and sb1. From this development, four petrophysical rock types were defined and characterized. Rock type 1 (the best reservoir rock) consists of lithofacies ms, xls, and sb1. Therefore, associated lithofacies in rock type 1 may be used as a pore-proxy rock property for the determination of best reservoir rock and corresponding flow units at the reservoir scale.

ACKNOWLEDGEMENTS

I would like to express my sincere appreciation and gratitude to Dr. Wayne Ahr, chair of my advisory committee, for his support, patience, guidance, constructive criticism, and aggressive encouragement. I would also like to thank my committee members, Dr. Yuefeng Sun and Dr. Walter Ayers, for their guidance and support during this study.

I am deeply indebted to the BP Tangguh Reservoir and Well Team, especially Achmadi T. Kasim, John S. Petler, Joaquin Naar, and May Sari Hendrawati for their support and willingness to assist me with data.

Thanks also go to my friends and colleagues and the department faculty and staff for making my time at Texas A&M University a great experience.

I also would like to thank my beloved husband, Mom and Dad, and the rest of my family for all of their support throughout this endeavor. You have always encouraged me with love, patience, and understanding and I owe much of my success to you. Finally, all of this would not happen without the mercy of Allah the Almighty.

TABLE OF CONTENTS

Page

Page

LIST OF FIGURES

FIGURE Page

FIGURE Page

FIGURE Page

LIST OF TABLES

1. INTRODUCTION

The Bintuni Field in Bintuni Basin, Papua-Indonesia, contains dry gas with low condensate gas ratio (4.0 bbl/MMscf of full well stream). Estimated reserves from eight appraisal drilled wells are 6.08 Tcf (Marcou et al., 2004), but the field is still undeveloped. Bintuni Field has two Middle Jurassic reservoirs and one Paleocene reservoir. This study focuses on the upper and lower sandstones of Middle Jurassic-age. These sandstones are separated by non reservoir shales. Initially the upper sandstone was called the Roabiba Sandstone reservoir and the lower one was named the Aalenian Sandstone (Yoshino et al., 2003). Later, these sands were known simply as the Upper and Lower Roabiba. The Upper Roabiba Sandstone is the main gas reservoir. It is about 200 ft thick, laterally continuous, and consists of a moderately sorted, fine-to-medium grain, quartzarenite with average porosity of 12% and average permeability of 250 mD. The Lower Roabiba Sandstone was deposited in an estuarine channel and marsh and consists of lower fine to lower coarse grained quartzarenites with average porosity of 12% and permeability 215 md.

This study is considered necessary since the field is considered to be a giant field and there are a limited number of studies on the Roabiba Sandstones reservoir characterization in the Bintuni field that has been published. As a commitment to BP Indonesia, the field, well name and depth were not the real data.

_____

This thesis follows the style of American Association of Petroleum Geologists Bulletin.

1.1. OBJECTIVES OF THE STUDY

A major objective of this thesis is to develop a work-flow process to understand the pore-scale rock properties by integrating both large-scale geologic elements and small-scale petrology with the petrophysical properties such as core analysis and wireline log data.

The ultimate objective of this study is to develop geological and petrophysical analysis that will identify reservoir quality and distribution of best, intermediate, and poor reservoir zones. Essential components of process models are identification, specification/description, mapping and interpretation of the principal reservoir zones of Roabiba Sandstone in the Bintuni Field. These objectives will be accomplished by using the following steps:

1. Describing lithofacies from the core data in order to understand the reservoir;
2. Analyzing the well logs to determine the distribution of porosity-permeability values and to calculate the net pay; and
3. Determining reservoir quality by petrophysical rock type from capillary pressure data.

1.2. LOCATION

Bintuni Field is located in the Bintuni Basin, which is interpreted as a deep foreland basin in the northwest portion of Papua, commonly referred to as 'Bird's Head' in English (Figure 1). The field covers an area of 205 km² with approximately 50% of the field onshore.

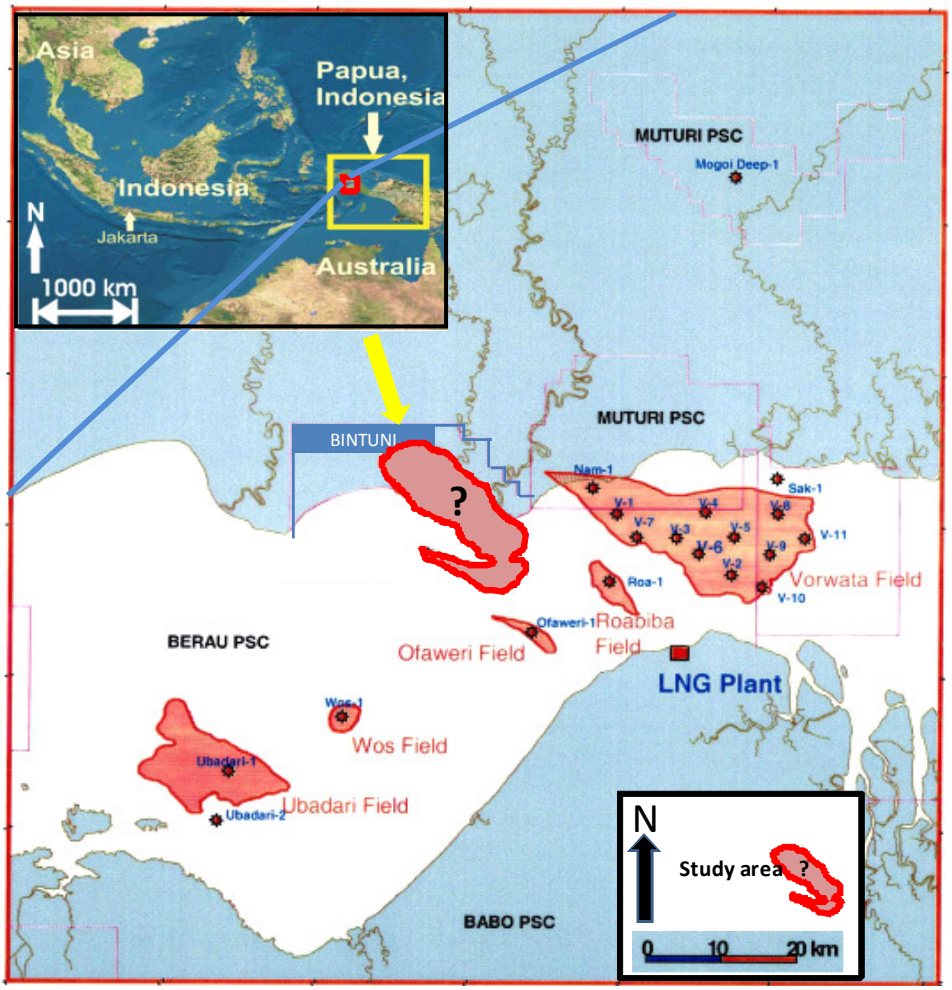

Figure 1. Location of the study area in Bintuni Field, Papua, Indonesia (modified after Marcou et al. 2004)

1.3. FIELD HISTORY

The first well, B1, was drilled by Arco Indonesia Inc. in 1994. B1 well originally drilled as an oil play, encountered a series of gas-charged sands in Middle Jurassic, Cretaceous and Paleocene reservoirs (Yoshino et al., 2003). The discovery of Jurassic sandstone reservoirs by Arco had its root in the previous exploration history of the area.

Conoco discovered Tertiary-sourced commercial oil in the shallow limestone formation at Bintuni shallow field by drilling wells in this area since 1981 (Dolan and Hermany, 1988). Then in 1988 Occidental Petroleum discovered dry gas in thick Jurassic sandstone reservoirs south of Bintuni Field (Perkins and Livsey, 1993).

Arco's well B2 drilled in1995 extended the field to the south, and demonstrated the continuity and dimensions of the Upper Roabiba Sandstone along with productive Paleocene reservoirs. It also confirmed that the field is classified as a giant gas accumulation. Since then, another six appraisal wells have been drilled. All wells encountered the Middle Jurassic sand with one wet (well B5) and one non-productive (well B8). Cores were cut in seven wells; six of them penetrated the Roabiba Sandstone.

1.4. REGIONAL GEOLOGY

The main Bintuni structure is a four-way dip closure on the crest of southward-plunging anticline roughly 25km long (NW-SE) and 12km wide. The general structure of the Bintuni Field is the result of tectonic compression folding related to regional NE to SW during the Oligocene. Tectonic activity in this area can be divided into two main periods of activity: Pre-Collision and Post-Collision.

The pre-collision period (Late Paleozoic-Oligocene) represents the period of geologic time when the rocks of Papua Province were believed to be part of the Australian craton. The presence of NW-SE lineaments such as the thrust fold-belts structures, are interpreted to be reactivation of faults within the Jurassic rift event. The

isopach pattern for Jurassic to Oligocene intervals forms a NW-SE trend (Perkins and Livsey, 1993).

The post-collision period (Oligocene to Recent) represents the period of geologic time after the collision of the northern Australia plate margin with the Pacific plate (Hamilton, 1979). The northwestward motion of Pacific plate and the N25°E movement of the Australian plate created a convergent strike-slip movement for the whole of Papua Province, resulting in wrench and thrust faulting across most of the island. The NW-SE and E-W paleo faults, were reactivated as sinistral wrench faults, and thrust faults. They also formed a series of 'en echelon' anticlinal inversion trending NW-SE (Dolan and Hermany, 1988). These early compressional folds would be reactivated in the Miocene (Casarta et al., 2004).

It is the Miocene to present-day compressional inversion that formed the trapping structures for the Bintuni Basin pre-Tertiary hydrocarbon accumulations (Dolan and Hermany, 1988). The Bintuni anticline is crossed by a number of east-west trending wrench faults systems (Figure 2), which have provided two different mechanisms favorable to trapping hydrocarbons, some of which are continuous across the field (Perkins and Livsey, 1993). Some wrench fault systems have provided faults/fractures as conduits for migrating hydrocarbons, and yet other wrench faults have acted as traps and seals for dip/fault closure on some of the smaller 'pop-up' structures (Perkins and Livsey, 1993).

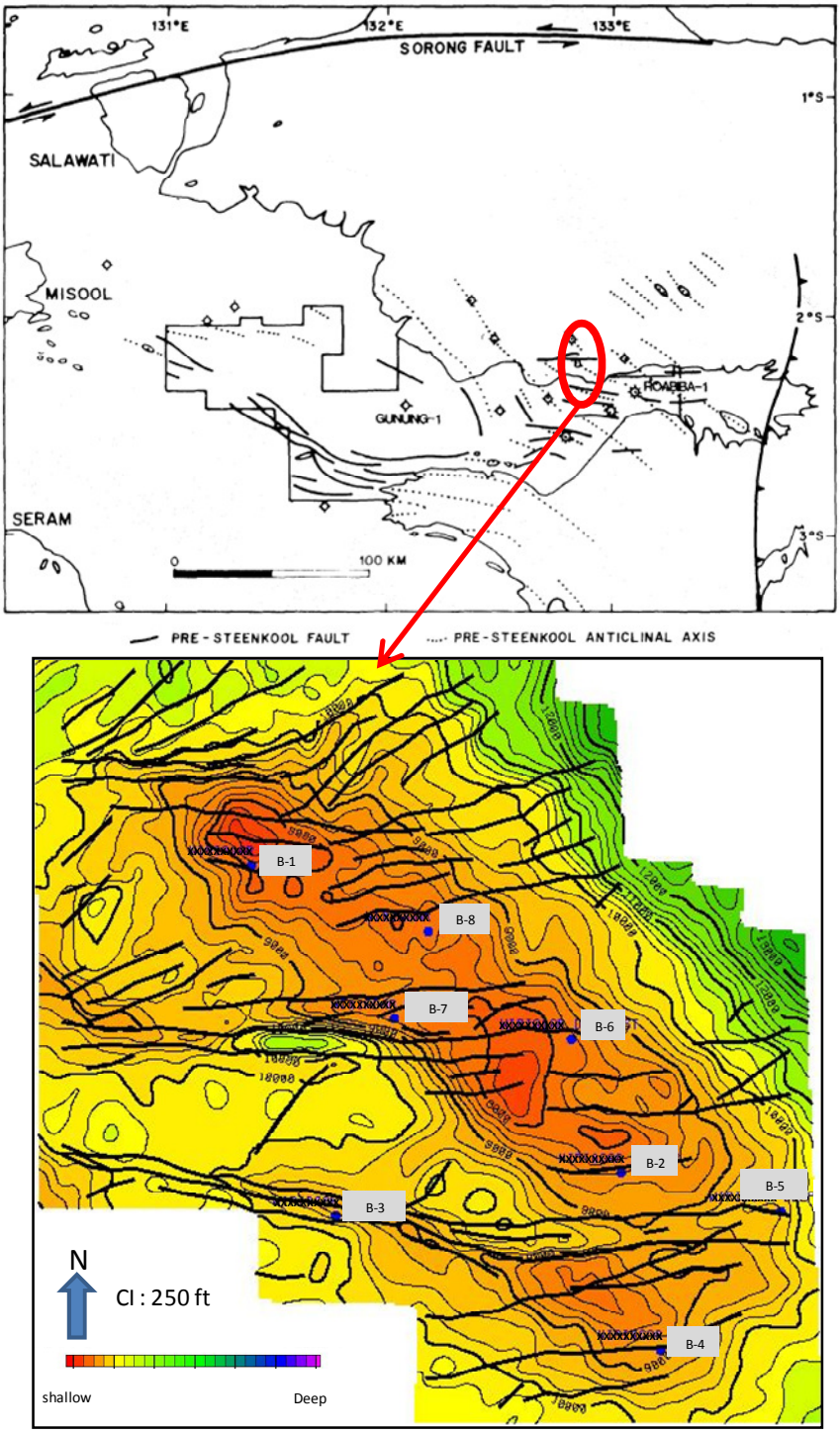

Figure 2. (top picture) Major faults and anticlinal axes in Papua bird's head area (modified after Perkins and Livsey, 1993); (bottom picture) Top Roabiba depth map from seismic with E-W fault crossed the area.

1.5. STRATIGRAPHIC SETTING

The Roabiba and Paleocene Sandstones were deposited during the pre-collision period. Table 1 shows the stratigraphic column of Bintuni Basin.

Table 1. Stratigraphic column for Bintuni Basin (modified after Yoshino et al., 2003)

Geological Age		Formation	Reservoir	
Cenozoic	Upper Miocene - Pleistocene	Steenkool - Sele		
	Mid-Upper Miocene	Kais		
	Mid Eocene - Oligocene	Faumai		
	Lower Eocene	Daram - Waripi		
	Paleocene		Mud Prone	
			Sand Prone	Upper
				Middle
				Lower
Mesozoic	Upper Cretaceous	Upper Kembelangan		
	Upper Jurassic	Lower Kembelangan	Upper Roabiba sand	
	Mid Jurassic		Lower Roabiba sand	
	Triassic	Tipuma		
Paleozoic	Permian	Ainim		

The Upper Permian sedimentation occurred in the continental to shallow marine paleo-depositional environment along the extensionally rifted NW Australian-New Guinea margin of the Tethys Ocean, with widespread coals and carbonaceous shales accumulating in the Bird's Head area (Livsey et al., 1992). Upper Permian paludal and

lacustrine sediments of the Ainim Formation are the primary hydrocarbon source rocks in Bintuni Basin (Perkins and Livsey, 1993).

The subaerial exposure and extensive faulting in the Bintuni area has resulted in a widespread unconformity between the Upper Permian and the Jurassic, with Triassic sediment generally absent (Perkins and Livsey, 1993). Figure 3 illustrates the chronostratigraphy of Bintuni Basin.

A global marine transgression and subsequent highstand had a major impact on the local geology. Jurassic sands consist of a series of shallow marine units deposited in the transgressive systems tract, onlapping the Permo-Triassic rift unconformity (Dolan and Hermany, 1988). The Roabiba Sandstone is a member of the Jurassic transgressive sequence. Tilting and erosion occurred during the Middle-Upper Jurassic. Uplifting during Cretaceous time formed the Intra-Cretaceous Unconformity, and resulted in the removal of Lower Cretaceous sediments in Bintuni Basin (Perkins and Livsey, 1993). During Upper Cretaceous through Eocene times, a marine transgression led to the deposition of widespread carbonate and clastics successions in the Upper Kembelangan Formation. These deposits formed seals for the underlying Jurassic reservoirs in the Bintuni Basin.

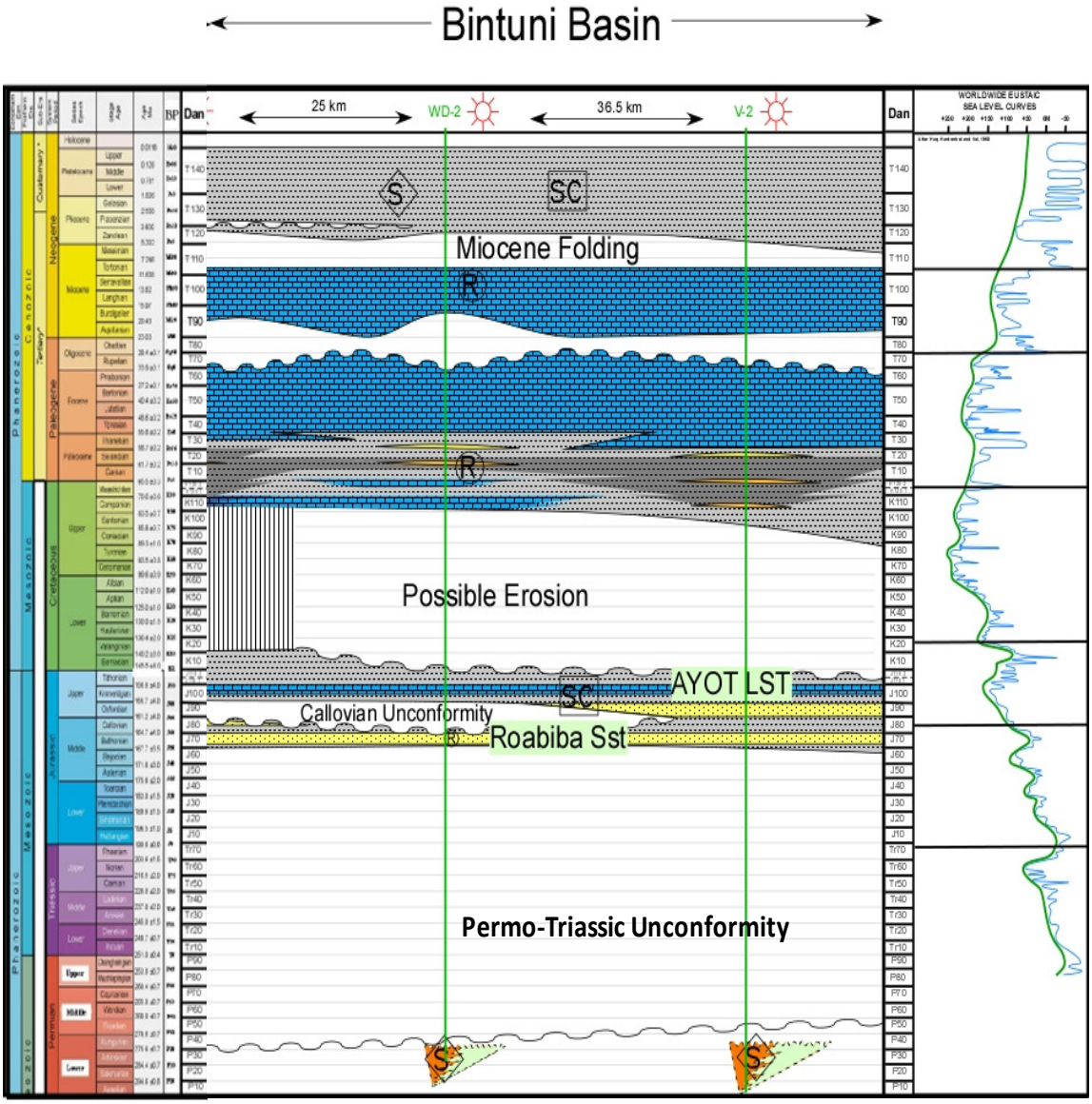

Figure 3. The chronostratigraphy of Bintuni Basin, R=Reservoir, SC=Seal Capacity, S=Source.

Subsequently, during Oligocene to Upper Miocene times, the New Guinea Limestone Group, a thick carbonate sequence that includes the Kais Limestone Formation was deposited (Dolan and Hermany, 1988). Subsidence in the foreland

inboard from the Lengguru Thrust Fold Belt resulted in the formation of the Bintuni Basin and accompanying increases in accommodation space for Upper Miocene to Pleistocene fine grained clastic sediments of the Steenkool Formation. These clay-rich Plio-Pleistocene successions form the top seal for the Miocene Kais Limestone reservoir (Dolan and Hermany, 1988; Perkins and Livsey, 1993).

1.5.1. SEQUENCE STRATIGRAPHIC EVOLUTION

The stratigraphic evolution of Bintuni Basin in early Middle Jurassic was started by tectonically driven lowstand system tract deposited Lower Roabiba Sandstone fluvial and estuarine sediments during Bajocian. The Middle Roabiba section was deposited during a major flooding event in upper Bajocian to lower Bathonian in depositional environment of offshore and brackish water. In lower Bathonian, the base of Upper Roabiba Sandstone was deposited during a forced regression, followed by rapid progradations of sandbars and channels. The Upper Roabiba continued to be deposited in the middle to upper Bathonian during the highstand tract which accumulated tidal-dominated shoreface deposition.

Erosion of Upper and Lower Roabiba towards the north of Bintuni Basin occurred during Bathonian /Callovian. The deposition of an overall progradations in Callovian to Oxfordian produced a succession of shallow marine deposits. Faulting driven deformation, subsidence and deposition continued in the Upper Jurassic. Further erosion marked the onset of the lower Cretaceous unconformity. Pre-Cretaceous faults were buried below lower Cretaceous unconformity (Naar et.al, 2008)

1.6. PREVIOUS WORK

There is a limited amount of information on the Roabiba Sandstone, none of which includes reservoir descriptions. Yoshino et al. (2003) identified gas/condensate reservoirs in Paleocene turbidites, Cretaceous carbonates and Middle Jurassic sandstones. This study determined that the Roabiba Sandstone reservoir has average porosity of about 12% and average permeability of about 261 md, while Aalenian Sandstone has average porosity of about 13% and average permeability 232 md.

Unpublished work at BP by Naar et al. (2008) provided new nomenclature for Roabiba reservoir, namely the Upper (UR), Middle (MR), and Lower Roabiba (LR). The Middle Roabiba is defined by Yoshino et al. (2003) as a non-reservoir. Naar et al. (2008) divided Jurassic interval into 15 zones based on high resolution biostratigraphy and well log correlations. 20 lithofacies were identified in the field and those lithofacies were grouped into three main classes based on their rock characteristics. The classes include bioturbated sandstone, cross bedded sandstone, and siltstone-mudstone. The lithofacies were further subdivided into four flow units based on reservoir quality. The lithofacies with the least matrix content is the massive, cross laminated, dewatered, and bioturbated, lower medium to upper fine-grained sandstones with average permeability greater than 200 md. The lowest ranked flow unit is the upper fine-grained, bioclastic sandstone with average porosity less than 10% and average permeability less than 50 md.

1.6.1. FORMATION

Based on palynological analysis, Yoshino et al. (2003) divided Middle Jurassic Lower Kembelangan Formation in Bintuni Basin into two reservoirs: the upper sandstone called Upper Roabiba (UR) and the lower reservoir called Lower Roabiba (LR), whereas Middle Roabiba (MR) is not a reservoir section.

1.6.2. STRATIGRAPHIC ZONATION

Table 2 shows the stratigraphy and zonation of Bintuni Basin for Middle Jurassic-age. The reservoir sections were divided into zones based on high resolution palynostratigraphy of cored intervals and well log correlations.

Table 2. Stratigraphy and Zonation of Bintuni Basin for Middle Jurassic reservoir (modified after Yoshino et al., 2003).

Geological Age		Formation	Reservoir	Zone
Mesozoic	Mid Jurassic	Lower Kembelangan	Upper Roabiba	UR9
				UR8
				UR7
				UR6
				UR5
				UR4
				UR3
				UR2
				UR1
			Middle Roabiba	MR
			Lower Roabiba	LR4
				LR3
				LR2
				LR1

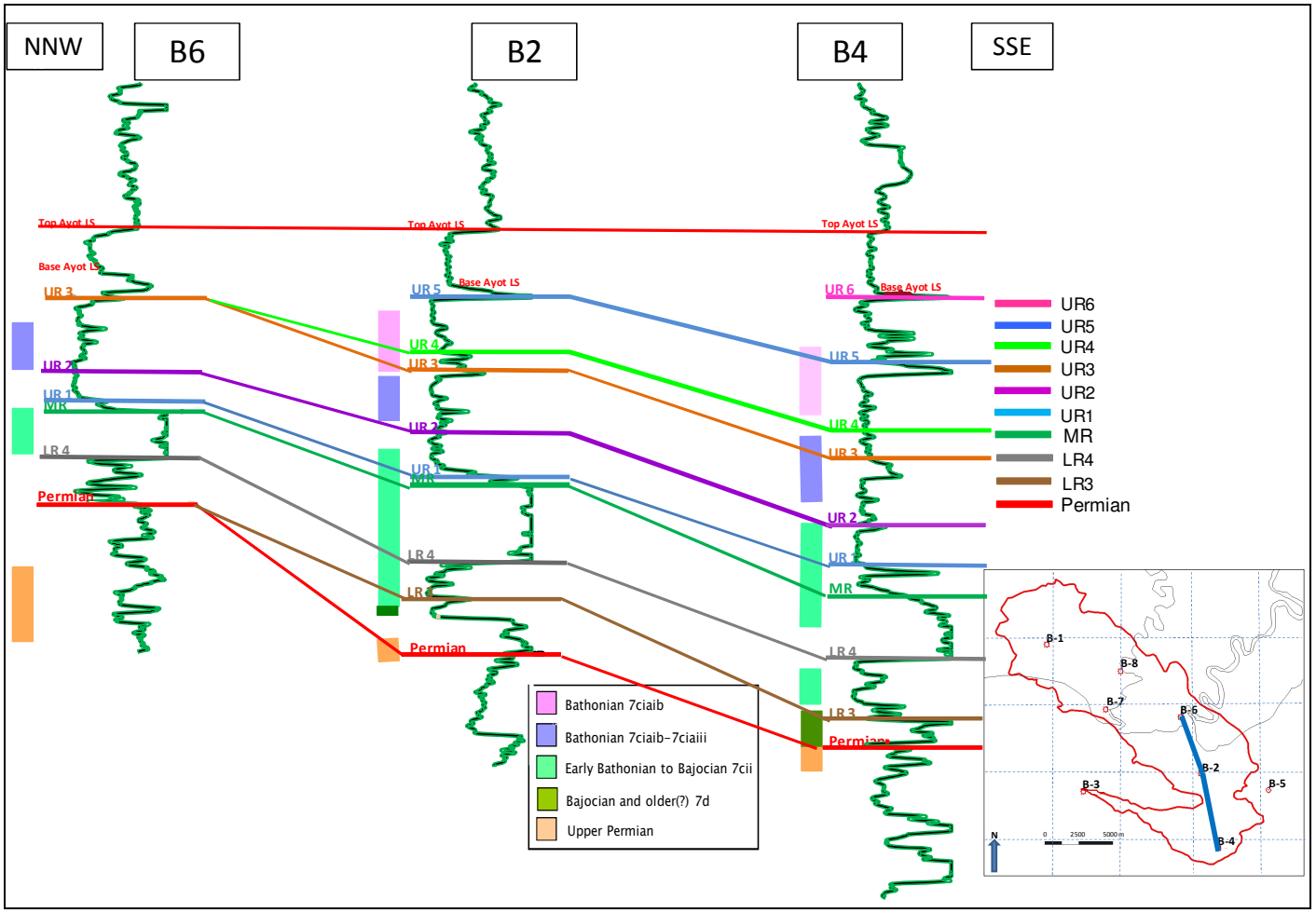

Figure 4. A NNW-SSE cross section illustrating the zonation and correlation of Roabiba Sandstone (datum is top Ayot Limestone).

In Bintuni Field, there are seven zones of UR were determined (UR1-UR6 and UR9) whereas two zones of LR were found (LR3 and LR4). Figure 4 shows a NNW-SSE cross section (wells B6, B2, and B4) with the correlation of zonation between wells and palynological subzones of cored intervals. Wells B6, B2, B4, and B5 consist of UR1 to UR5/UR6 and LR3 to LR4 while B3 (located in the western part of the field) consists of zones UR9 and LR3 to LR4. Wells B1, B8, and B7 (located in the northern part of the field) lack Upper Roabiba section.

1.7. PETROGRAPHY AND MINERALOGY

The Upper and Lower Roabiba Sandstones are very similar in terms of their detrital mineralogy. They can be classified as quartzarenites with several sublitharenites also present in the lower part of Lower Roabiba reservoir.

The sandstones vary in grain size, ranging from lower fine to very coarse. The dominant grains are quartz with minor lithics, feldspar, and accessory grains like carbonaceous material, mica, and unspecified opaques. Quartz is mainly monocrystalline, while lithic fragments are mainly chert. Feldspar grains are principally microcline which is variably leached. The plots of cement-matrix-grains and quartz-lithic-feldspar from all of the wells shows that the lithology is dominated by quartz and grain supported (Figure 5).

The most common authigenic minerals are quartz cement, and kaolinite with less common calcite, siderite, and pyrite. Quartz cement forms syntaxial overgrowth on quartz grains and have preserved primary intergranular pore space from the effects of

burial compaction. Kaolinite fills both intergranular and earlier formed moldic pores and contains microporosity. Calcite and siderite generally occur as isolated intergranular cement. Pyrite occurs in both cementing and replacing roles. Slightly ferroan calcite is locally an important cementing agent. Open fractures were observed in some sandstones and were sometimes partly filled with secondary kaolinite.

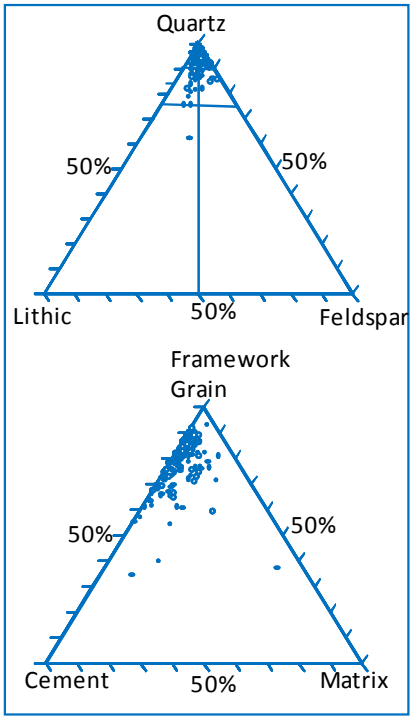

Figure 5. Composition of Roabiba Sandstone from the upper and lower reservoir.

1.8. PETROLEUM SYSTEM

The trap in Bintuni field is a NW-SE trending, plunging anticline with four-way dip closure and E-W trending strike-slip faults systems which created structural highs. The Upper Roabiba Sandstone is absent in some wells due to fault displacement and

erosion (Callovian Unconformity / Ayot Limestone deposition). Other wells such as the B3 well exhibits deeper gas-water contact (10425 ft TVDss) than the main Bintuni Field (10175 ft TVDss).

1.8.1. SOURCE ROCKS

The source rocks for the Bintuni accumulation consist of Upper Permian coals along with Lower-Middle Jurassic coals and shales. The principal gas charge has been interpreted by Yoshino et al. (2003) to have formed during latest Miocene to Recent. The “pod of active source rock” for Bintuni Field lies in the central part of the Bintuni Basin.

1.8.2. SEALS

The immediate top and lateral seals for the Roabiba Reservoir at the anticlinorium are the overlying Ayot Limestone and the Upper Jurassic Shales. Additional regional seal for the Roabiba Reservoir are the Late Cretaceous marl (Salo, 2005).

2. METHODS

2.1. MATERIALS FOR STUDY

The following data for the study were provided by BP Indonesia:

1. Field base map
2. Digital log data from eight wells
3. Conventional cores from six wells
4. Thin sections of the cored interval from six wells
5. XRD and SEM of part of cored interval taken from six wells
6. Mercury injection capillary pressure (MICP) from three wells

The detail data obtained from each well are illustrated in Table 3 (see next page).

2.2. CORE DESCRIPTION

1071 feet of full diameter cores were obtained from six wells: B2, B3, B4, B5, B6, and B7 throughout the entire vertical section, including both reservoirs (Upper and Lower Roabiba) and non-reservoir section (Middle Roabiba). The six cores were described to establish lithofacies to define subdivisions of sedimentary sequences based on lithology, grain size, physical and biogenic sedimentary structures, and to identify stratification that bear a direct relationship to the depositional processes that produced them (Scheihing and Atkinson, 1992).

Table 3. List of wells names, wireline logs, core depth, reservoir cored and additional core analysis data.

Well	Log	FMI	Core Depth	Reservoir cored	Thin section	XRD	SEM	MICP
B-1	GR/Res/ Den/Neu	-	-	-	-	-	-	-
B-2	GR/Res/ Den/Neu	-	#6: 9547-9607 #7: 9607-9667 #8: 9667-9727 #9: 9727-9787	UR, MR, LR	159	2	2	6
B-3	GR/Res/ Den/Neu	Yes	#13: 9294-9385 #14: 9385-9476	UR, MR, LR	19	5	5	17
B-4	GR/Res/ Den/Neu	Yes	#2: 9950-10040 #3: 10040-10098 #4: 10098-10140 #5: 10140-10175 #6: 10175-10242	most of UR, MR, LR	42	10	10	5
B-5	GR/Res/ Den/Neu	Yes	#15: 10501-10515 #16: 10515-10519 #17: 10519-10530 #18: 10530-10559 #19: 10559-10584 #20: 10615-10637 #21: 10751-10753	parts of UR	28	10	8	-
B-6	GR/Res/ Den/Neu	-	#9: 9240-9330	most of UR, MR	12	4	3	-
B-7	GR/Res/ Den/Neu	-	#8: 9431-9521 #9: 9521-9581	MR, LR	25	10	6	-
B-8	GR/Res/ Den/Neu	-	-	-	-	-	-	-
Total			1071 ft		285	41	34	28

Wells B1 and B8 only have wireline log data. Well B8 was cored but the core was lost. Figure 6 shows cored wells' location. From each of the wells, 90 to 292 feet of full diameter cores were used to identify and correlate depositional facies. Conventional (routine) core analyses were obtained for each cored well and special core analyses were performed for wells B2, B3, and B4. Data sets for each well include permeability, porosity, grain density, grain size, and water saturation were obtained by direct

measurement on core plugs. All data from core description and routine core analysis data were compiled in Excel.

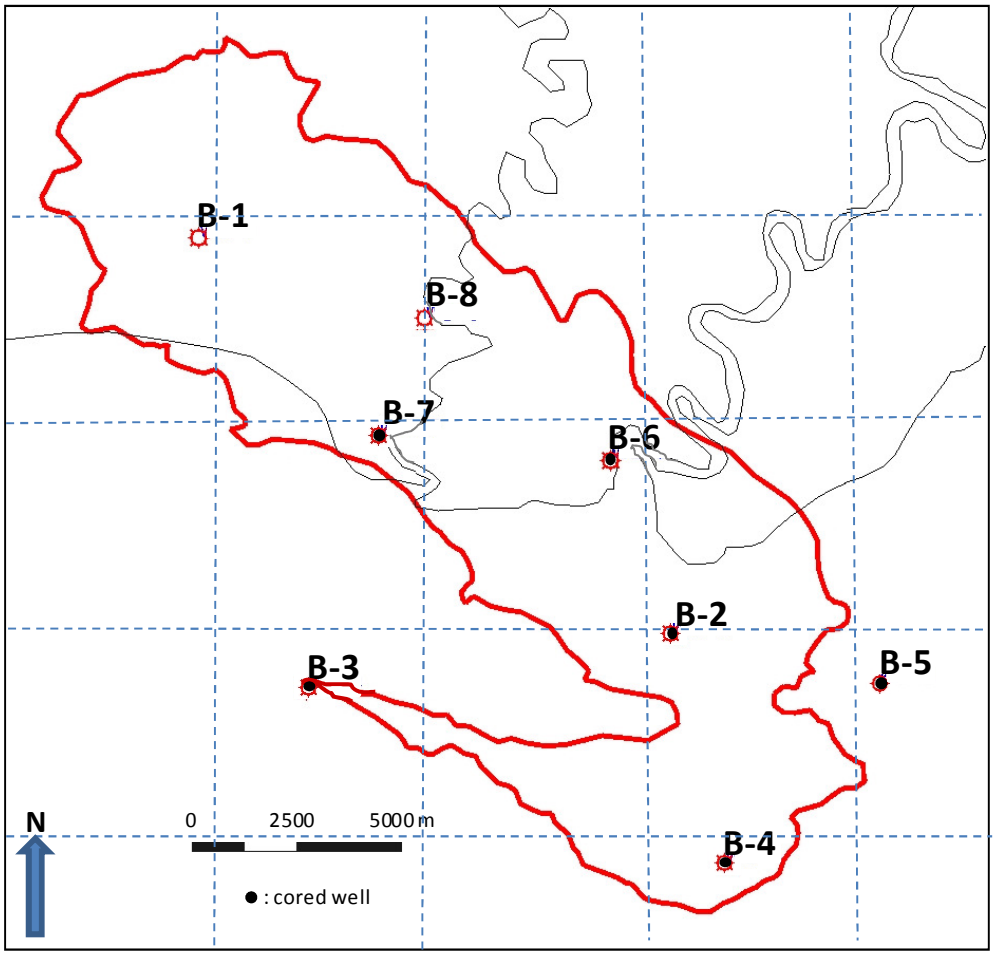

Figure 6. Base map of Bintuni Field and cored wells location.

Core descriptions and core analyses provide a basic reference for subsequent interpretation of borehole log responses and for petrophysical calculations on wells where cores were not available. All cores were described (per 0.5 foot interval) and

classified based on rock type, sedimentary structures, fossils (microfauna) diversity, fossil abundance, and cement content.

2.3. WELL LOG ANALYSIS

An extensive petrophysical analysis of each well using the available logs and cores data was performed to characterize the reservoir. Core descriptions provided a baseline for lithological characteristics of the Roabiba Sandstone. Well log characteristics were compared and correlated with lithological and petrographic features to establish relationships between rock and log properties. Core depth of well B2 has been shifted 14 ft to depth match the log. The ranges of depth shifting for all wells are between -1 to 14 ft.

Core porosity was calculated and compared with log porosity in order to evaluate petrophysical characteristics of the entire reservoir at field scale. After core porosity and log porosity were compared and relationships established, core permeability and core porosity were also compared to determine an empirical relationship that is used to estimate pseudo-permeability from log-derived porosity.

Shale volume (V_{sh}) is a useful discrimination device to help distinguish non reservoir from reservoir rock. V_{sh} calculation depends on gamma ray logs (GR). The equation to estimate V_{sh} is below:

$$V_{sh} = \frac{GR - GR_{Clean}}{GR_{Shale} - GR_{Clean}}$$

The following equation is employed to calculate porosity from density log:

$$\emptyset_d = \frac{\rho_{bulk} - \rho_{matrix}}{\rho_{fluid} - \rho_{matrix}}$$

where ϕ is porosity (%) and ρ is density (g/cm^3). The effective porosity was estimated from porosity logs and shale volume using the formula below:

$$\emptyset_e = \emptyset \times (1 - V_{SH})$$

The method for interpretation of water saturation from logs is the Archie equation (below).

$$S_w = \sqrt[n]{\frac{a}{\emptyset^m} \times \frac{R_w}{R_t}}$$

where *Rt* is true formation resistivity, *Rw* is resistivity of formation water, *a* is tortuosity factor, *m* is cementation factor, and *n* is saturation exponent. *Rw* has been derived from the analysis of logs from the underlying aquifer. The other inputs to the Archie equation, *a*, *m*, and *n*, were measured from the core.

2.4. MERCURY INJECTION CAPILLARY PRESSURE ANALYSIS

Capillary pressure data from mercury injection is an effective technique to analyze pore throat geometry, particularly the size and distribution of pore throat bodies (Purcell, 1949). Mercury is injected in incrementally increasing pressure into the rock pores. Larger pores and throats are saturated initially, followed by the smaller pores and

throats as pressure is increased. The capillary pressure curve provides data on pressure, pore throat size and height of oil column above the free-water level. A capillary pressure curve showing the entry or displacement pressure, the intermediate pressure reading of nonwetting phase saturation, and the maximum pressure reading of irreducible wetting phase saturation (Ahr, 2008). The displacement (entry) pressure is defined as the minimum pressure required for mercury to enter into a wetting fluid with a saturated zone. The magnitude of the displacement pressure reflects the largest connected pore throats in the system. Displacement pressure is higher for small pore throats than for large ones, and their respective curve trajectories differ. Steep trajectories, high displacement pressures, and high wetting phase saturations for any given pressure in the marginal samples, indicating lower accessibility, smaller pore throats, and less pore throat size sorting. Non reservoir curves exhibit characteristics similar to the marginal reservoir samples except that their pressure-saturation trajectories and displacement pressures indicate even smaller pore throat radii, poorer size sorting, and lower pore-pore throat connectivity (Ahr, 2008).

The procedure of MICP test begins with cleaning the samples by extracting hydrocarbons and leaching salts with cool solvents such as mixture of toluene and methanol. The sides of the vertical samples are coated with epoxy prior to drying to prevent lateral penetration of mercury into samples. Both cleaning and drying techniques are designed to minimize clay damage and alteration rock properties (Soeder, 1986). The samples are loaded into the chamber, filled with mercury under a vacuum and pressurized incrementally to a maximum pressure of approximately 50,000psi.

In this study, plugs were cut from cores in three wells that represent the northern (well B2), southern (well B4), and western (well B3) parts of the field. In all, 37 core plugs were obtained and subjected to high pressure mercury injection analysis. Samples are covering both the Upper and Lower Roabiba Sandstone reservoirs and most of the lithofacies. MICP analyses were performed by Corelab Indonesia. Results from the MICP testing includes 1) curvatures of drainage for each sample based on increasing injection pressure and mercury saturation, 2) pore throat radius, and 3) J-function values.

2.5. GRAPHICAL ANALYSIS

The final step in the work-flow process is identification of petrophysical rock types. The Winland method (Winland, 1972) is employed to classify petrophysical rock types using routine permeability-porosity data combined with mercury injection capillary pressure measurements from core plugs. The first step in the Winland method is identification and quantification of dominant pore throat dimensions. The pore throats rather than the overall pore volume control flow capacity in reservoir rocks (Rushing et al., 2008).

To quantify the dominant pore throat dimension, pore throat radii from mercury injection capillary pressure experiments were plotted against incremental mercury saturation. Using the plot, several rock types would be identified and grouped according to the pore throat radius range. Next, R_{35} of the Winland equation which relates absolute permeability to relative porosity as a function of the dominant pore throat radius was applied to investigate porosity-permeability relationship for each rock type.

$$logR_{35} = 0.732 + 0.588\, logK_{air} - 0.864\, log\emptyset_{core}$$

R_{35} is the pore aperture radius corresponding to the 35th percentile of mercury saturation in a mercury porosimetry test, K_{air} is the uncorrected air permeability (in md), and $\emptyset$ is porosity (in %).

The Winland R_{35} permeability-porosity correlation given by equation 5 for dominant pore throats of 0.5, 2, 5, 20, and 30 microns were superimposed on the semilog plot against the porosity-permeability. Ultimately, petrophysical rock types were established by identifying which pore types correspond to high and low porosity-permeability values. Their occurrence and distribution across the reservoir was then established.

3. LITHOFACIES AND DEPOSITIONAL ENVIRONMENT

3.1. LITHOFACIES

Lithofacies are the basic unit for the interpretation of depositional environments. Lithofacies are defined as “mappable stratigraphic units, laterally distinguishable from the adjacent intervals based upon lithologic characteristics such as mineralogical, petrographical, and paleontological signatures that are related with the appearance, texture, or composition of the rock.” (Porras, et al., 1999 and Perez et al., 2003).

Three major unit lithofacies were identified from core descriptions: bioturbated, cross-bedded, and siltstone-mudstone. The bioturbated sandstone lithofacies consists of bioturbated sandstone (sb1), mud-prone moderately to intensely bioturbated sandstone (sb2-sb3), and massive sandstone (ms). The cross-bedded sandstone lithofacies consists of cross-laminated sandstone to matrix rich cross-laminated sandstone (xls- xls-m), low-angle laminated sandstone (lls), and bioclastic sandstone (bs). The siltstone-mudstone lithofacies consists of laminated mudstone (lm), bioturbated mudstone (bm), and massive mudstone (mm). Bioturbated and cross-bedded sandstones are mostly quartzarenites with variable amounts of lithic and feldspar grains. Clay content (matrix) is mostly detrital (pellets and lamina) and kaolinite (filling pores). Table 4 describes lithofacies types that were identified from core descriptions.

Table 4. Lithofacies in Bintuni Field.

Code	Lithofacies Name	Major units	Reservoir/Non Reservoir
ms	Massive sandstone	Bioturbated sandstone	Reservoir
sb1	Moderately bioturbated sandstone		
sb2	Intensely bioturbated sandstone		
sb3	Intensely matrix rich bioturbated sandstone-siltstone		
xls	Cross-laminated sandstone	Cross-laminated sandstone	
xls-m	Cross-laminated matrix rich sandstone		
lls	Low-angle laminated sandstone		
bs	Bioclastic sandstone		
mm	Massive mudstone	Mudstone-siltstone	Non-reservoir
lm	Laminated mudstone		
bm	Bioclastic mudstone		

3.1.1. BIOTURBATED SANDSTONES LITHOFACIES

Bioturbated sandstone is matrix rich sandstone with a range from sb3-sb2-sb1-ms depending on bioturbation type and intensity. The intensity of bioturbation rises from ms to sb3. Bioturbated sandstone is the main lithofacies, wide spread and easy to identify, making up proportion 81% of the Upper Roabiba and 48% of the Lower Roabiba Sandstone (Figure 7).

The sandstones are quartzarenites with upper fine to lower medium grain size, moderately sorted, subangular, and with planar grain contact. Primary porosity is locally degraded by quartz cement (most common in sb lithofacies).

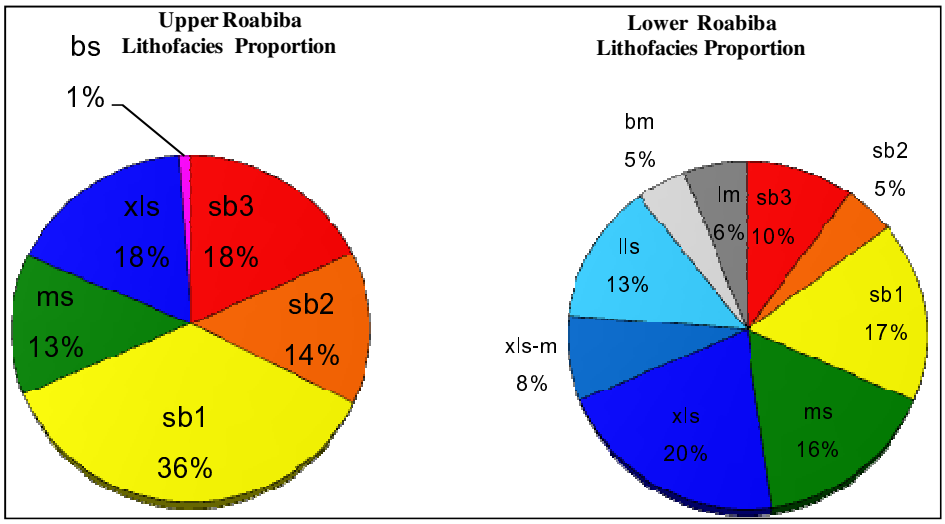

Figure 7. Lithofacies proportions in Upper and Lower Roabiba.

Minor secondary porosity presents feldspar grains. Porosity and permeability values increase as lithofacies change from sb3 to ms as a response of decreasing clay content. The ichnofacies identified in the cores are as follows: *Chondrites*, *Teichichnus*, *Palaeophycus*, *Macaronichnus*, *Opiomorpha*, *Diplocraterium* and *Skolithos*. The massive sandstone (ms) lithofacies bioturbation consists of *Skolithos* and *Palaeophycus* ichnofacies.

Table 5 shows the variation of average permeability as lithofacies changes from sb3 to ms while porosity does not vary significantly between the lithofacies. Lithofacies sb3 and sb2 have low permeability (<100 md) while sb1 and ms have permeability >100 md. The average permeability increases from lithofacies sb3 to ms. Grain size changes from upper fine to lower medium. Figures 8 and 9 show the slabbed cores and thin sections of bioturbated sandstone lithofacies.

Table 5. Porosity–permeability comparison of bioturbated sandstones lithofacies.

Parameter	**sb3**	**sb2**	**sb1**	**ms**
Average porosity (%)	10	12	13	13
Average permeability (md)	10	54	242	393
Average grain size (micron)	230 upper fine	290 upper fine	333 lower medium	330 lower medium

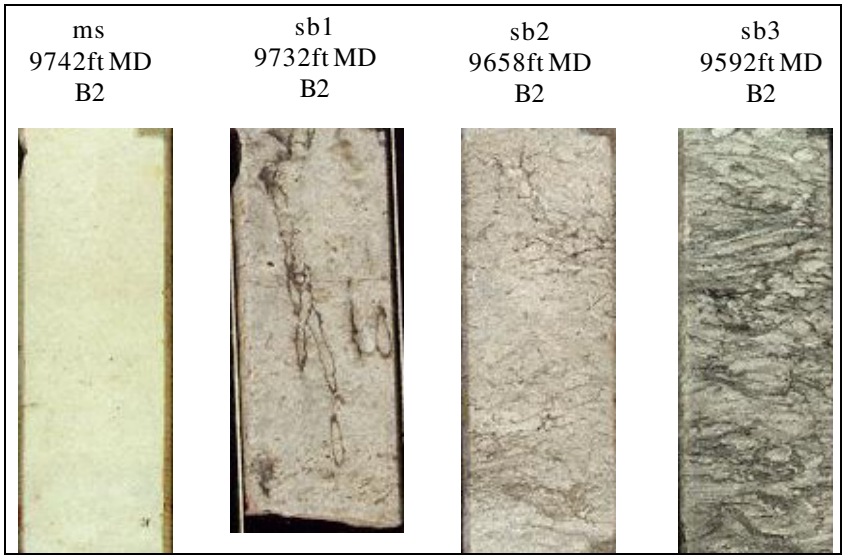

Figure 8. Photos of core from well B2 illustrating the bioturbated sandstones lithofacies.

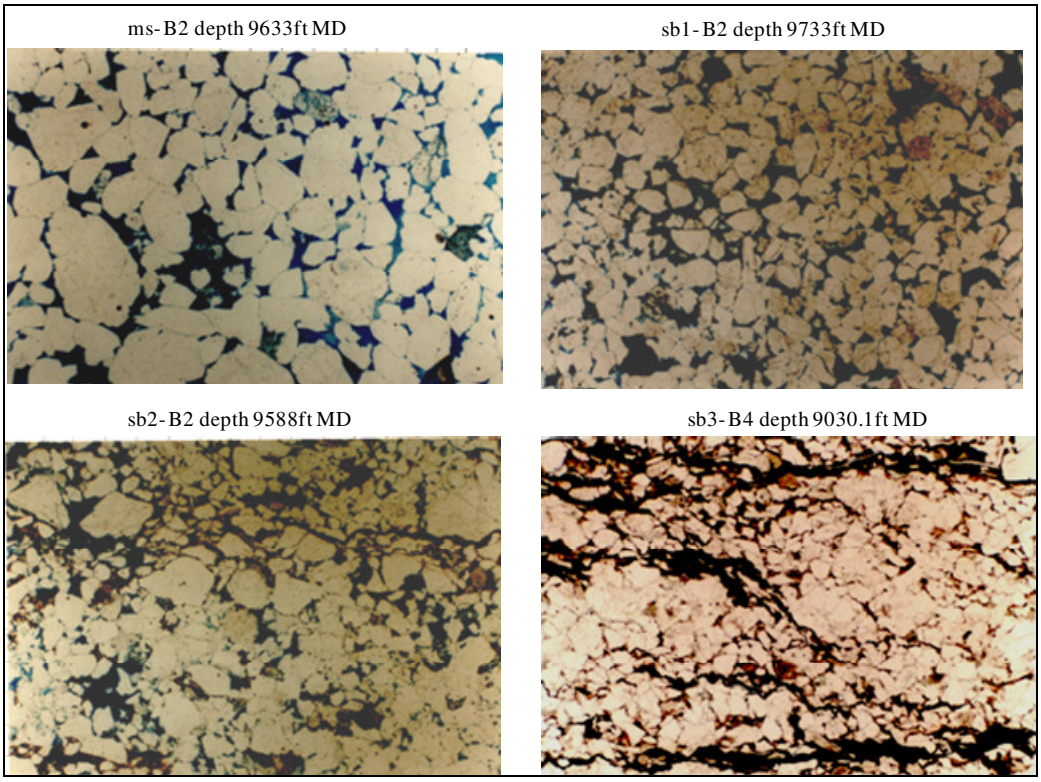

Figure 9. Thin sections view showing bioturbated sandstones lithofacies group.

3.1.2. CROSS-BEDDED SANDSTONES LITHOFACIES

The cross-bedded sandstone lithofacies consists of sandstones with various bedding angles and sandstones with clasts. The main lithofacies in the cross-bedded sandstones exhibit: cross lamination (xls), low-angle lamination (lls), and matrix-rich laminated sandstones (xls-m). The other lithofacies in the unit is the bioclastic sandstone (bs), a sandstone with bioclastic fragments and ferroan calcite cement. Cross-bedded sandstones are the second largest lithofacies group in the Roabiba reservoir. Upper Roabiba Sandstone comprises 19% of cross-bedded lithofacies while Lower Roabiba has 41% (Figure 7) with lithofacies xls as the main lithofacies in the unit.

Based on core descriptions, clay drapes mark low to high angles in cross-bedded sandstones. Grain size changes from coarser to finer occur from lamina to lamina. Bedding-angles typically increase upwards but decrease near the tops of lamination beds. Bioturbation consists of meiofauna between laminae with *Skolithos* and *Palaeophycus* across and parallel to lamination. Figures 10 and11 show the slabbed cores and thin sections of cross-bedded lithofacies.

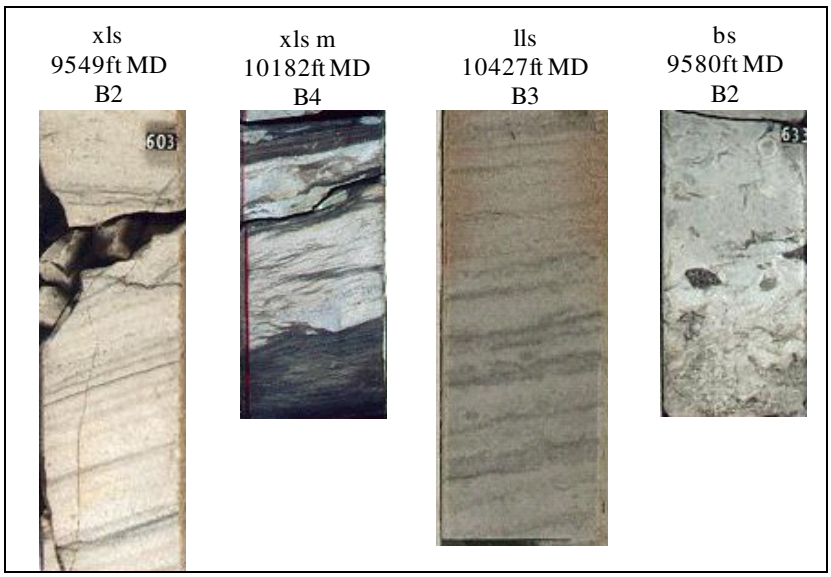

Figure 10. Photos of core from wells B2-B4 illustrating the cross-bedded sandstones lithofacies.

The cross-bedded sandstones lithofacies consist mainly of quartzarenites with medium to coarse grains, moderate to well sorted, subangular, and planar grain contacts. Primary porosity locally was reduced by ferroan calcite cement (most common in bs lithofacies). Clay matrix consists of laminar and pelletal detrital clay with authigenic kaolinite. In addition, porosity in bs lithofacies is locally decreased by calcite cement.

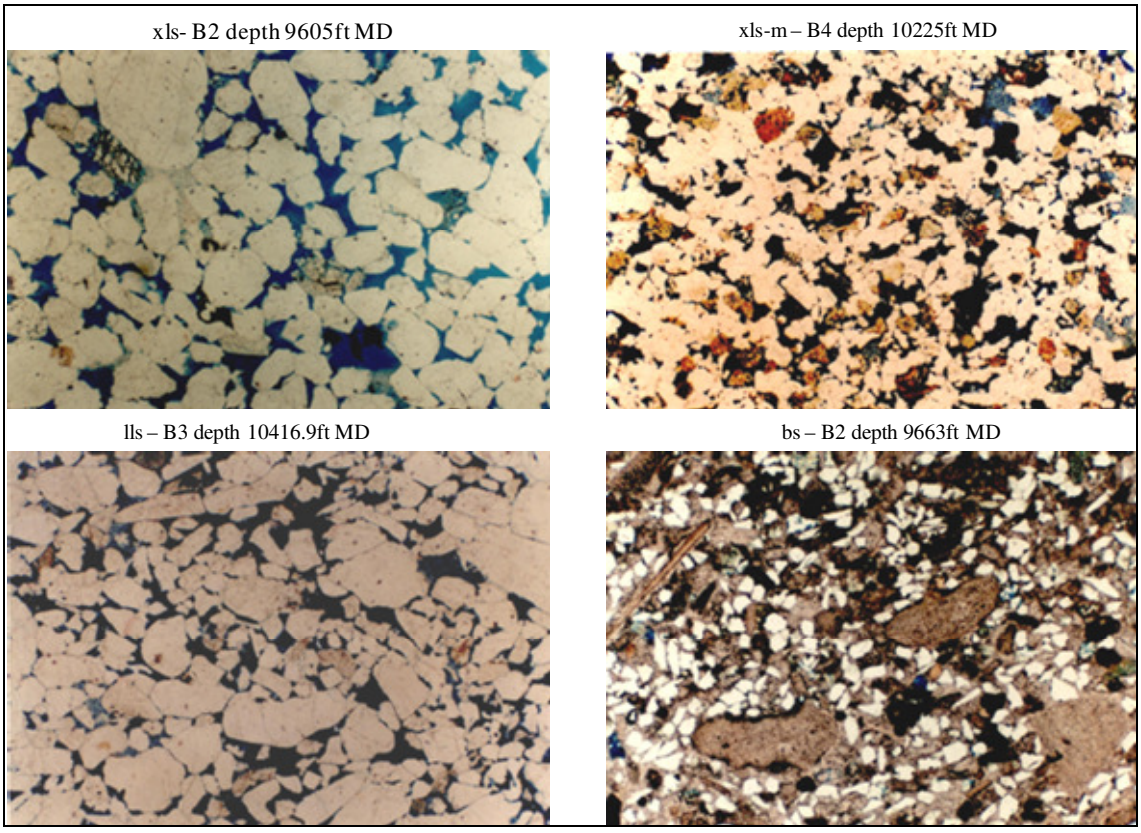

Figure 11. Thin sections view showing cross-bedded sandstones lithofacies.

Average permeability varies as lithofacies changes from lithofacies xls-m to xls. Porosity does not vary significantly between lithofacies, except in lithofacies bs porosity is lowest. Table 6 shows the variation of average permeability and porosity. Low permeability (<100 md) mostly corresponds with lithofacies xls-m and bs while lithofacies xls and lls have permeability >100 md. The average permeability increases from lithofacies xls-m to xls. Grain size changes from lower fine to lower medium.

Table 6. Porosity–permeability comparison of cross-bedded sandstones lithofacies.

Parameter	xls-m	bs	lls	xls
Average porosity (%)	12	7	12	13
Average permeability (md)	15	36	100	450
Average grain size (micron)	170 lower fine	288 upper fine	307 lower medium	378 lower medium

3.1.3. SILTSTONES AND MUDSTONES LITHOFACIES

Siltstones and mudstones lithofacies includes laminated mudstones (lm), bioturbated mudstones (bm) and massive mudstones (mm). Siltstones-mudstones are the least common in the Lower Roabiba Sandstone and they are not present in the Upper Roabiba Sandstone reservoir. There is only limited data in routine core analysis available for this unit. Figure 12 shows the core photos of siltstone-mudstone lithofacies group.

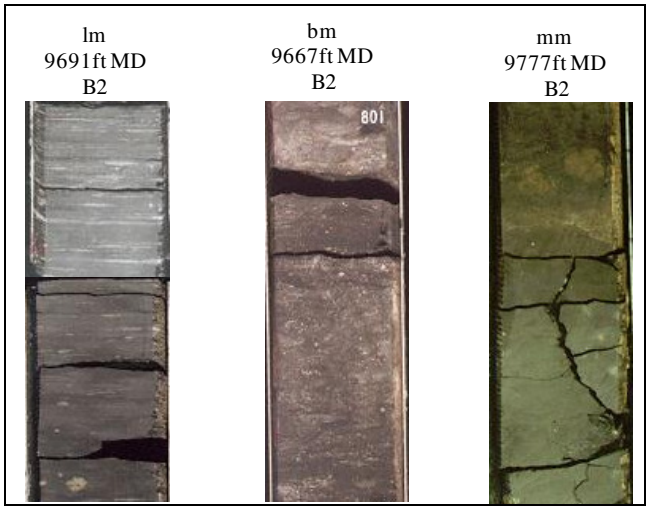

Figure 12. Photos of core from well B2 illustrating the siltstone-mudstones lithofacies.

3.2. MINERALOGY

The evaluation of whole rock and clay fraction mineralogy from 41 samples using x-ray diffraction (XRD) of seven lithofacies in average is presented in Table 7. Lithofacies ms and xls have quartz greater than 93% and total clays less than 4%. Kaolinite and illite are the clay major content.

The matrix-rich bioturbated sandstone lithofacies, sb3, has 82% quartz and 7% total clays. Illite and kaolinite are dominant in sb3 lithofacies. Lithofacies sb2 has chlorite content higher than other lithofacies in the unit. The mudstone and siltstone lithofacies, mm and bm, have the highest pyrite content.

Table 7. Bulk-fraction rock mineralogy and clay-fraction mineralogy from XRD in average.

Lithofacies	ms	sb1	sb2	sb3	xls	mm	bm
Mineralogy (%)							
Quartz	96.2	85.5	87.5	82.4	93.8	46.7	62.8
K-Feldspar	0.6	2.2	2.3	3.6	1.0	4.4	3.5
Plagioclase	0.1	0.2	0.5	1.0	0.3	3.2	1.0
Calcite	0.1	5.5	1.8	3.4	0.0	9.2	6.1
Fe-Dolomite	0.6	1.6	1.9	0.5	0.1	0.5	1.0
Siderite	0.0	0.5	0.4	0.8	0.2	0.0	0.6
Pyrite	0.3	0.6	0.1	1.4	0.5	3.5	4.2
Total Non-Clays	97.8	96.2	94.5	93.0	96.3	67.6	79.0
Illite/Smectite	0.4	0.9	0.4	1.0	0.4	14.8	3.5
Illite/Mica	0.6	0.9	0.9	2.8	1.0	14.2	8.4
Kaolinite	1.1	1.5	1.5	2.9	2.2	2.7	8.0
Chlorite	0.1	0.5	2.7	0.4	0.1	0.7	1.2
Total Clays	2.2	3.8	5.5	7.0	3.7	32.4	21.0

3.3. DIAGENESIS

Porosity in Roabiba Sandstones is depositional in origin, but diagenesis has affected it. The forms of diagenesis are mechanical compaction, cementation from quartz overgrowths, calcite cementation, grain-coating/pore lining clay development, and grain dissolution. Figure 13 shows the scanning electron microscopy (SEM) photomicrographs of lithofacies in selected wells.

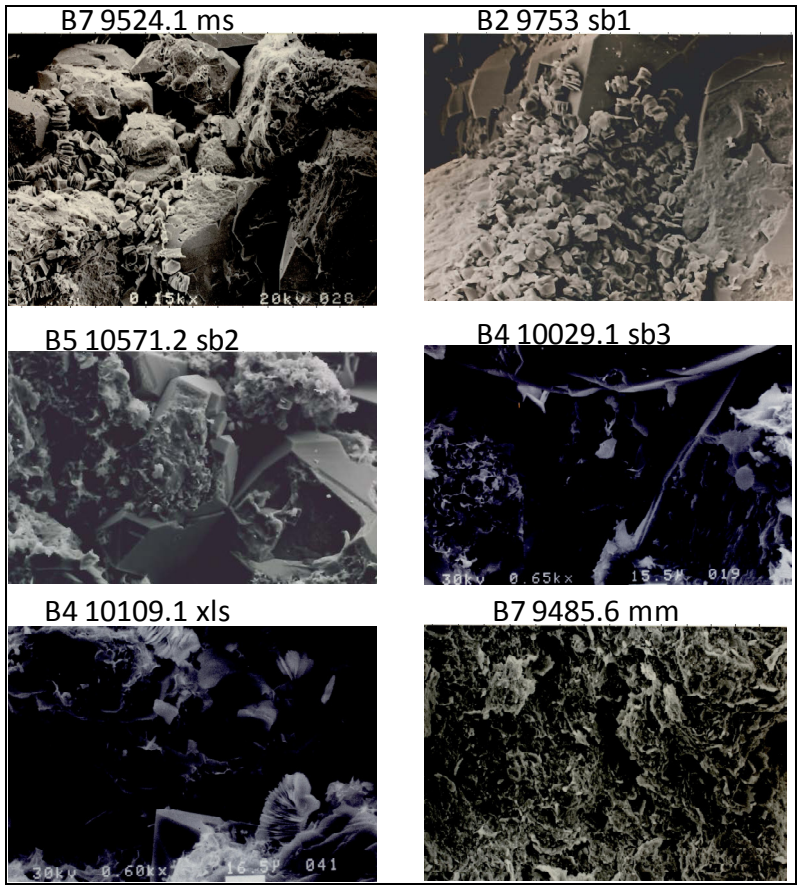

Figure 13. SEM photomicrographs of six lithofacies in selected wells.

Mechanical compaction is the most prevalent form of diagenesis. Contacts between more competent quartz grains tend to be elongated and slightly sutured which indicates grain rearrangement and a tighter packing configuration. Quartz cementation, in the form of overgrowths, is extensive in the sandstones that locally interlock, and it causes reduction of intergranular pore space. The rough surface of quartz grain is due to the irregular quartz overgrowth development (Figure 13 lithofacies sb1).

Minor amounts of diagenetic illite are present and occur primarily as thin coatings on portions of the grain surfaces. These appear to locally have inhibited the development of quartz overgrowths (Figure 13 lithofacies sb2 and sb3). Authigenic kaolinite precipitated at a late diagenetic stage and locally filled intergranular pores (Figure 13 lithofacies ms, sb1, sb3, and xls). Secondary kaolinite in lithofacies sb2 is widespread, occurring as clusters of crystallites where it is intergrown with minor fibrous illite.

Grain dissolution producing secondary porosity occurred at a late stage (Figure 13 lithofacies ms, sb2, and xls). Ankerite and pyrite represent only minor diagenetic components. Traces of ankerite and kaolinite occur in some intergranular pores, and traces of pyrite precipitated at an early diagenetic stage (Figure 13 lithofacies ms). Pyrite occurs in mudstone as framboids embedded in the detrital clay (Figure 13 lithofacies mm). Neither mineral significantly impacts the preservation or development of pore space.

3.4. DEPOSITIONAL ENVIRONMENT

The name Roabiba Sandstone was first used by Yoshino et al. (2003) to define the reservoir in the Lower Kembelangan Formation. Kasim et al. (2000) stated that Roabiba Sandstones appears to have been deposited in a shallow marine to shoreline environment during a rapidly subsiding basin with very close sedimentation rates to the subsidence rates.

The Lower Roabiba Sandstones was inferred to have been deposited in a tidal channel based on depositional structures, trace fossils, and facies analysis. Associated depositional facies include estuarine channels and marsh deposits. In this case, wireline log signatures and core studies indicate the presence of thin shales within the Lower Roabiba section that are interpreted to represent abandoned, low energy channels.

The Middle Roabiba Sandstones was deposited by a major flooding. The trace fossils assemblage of *Terrebelina sp.* suggests flooding and abandonment prior to the deposition of Upper Roabiba section. Brackish and offshore shale dominates the Middle Roabiba Sandstones.

The Upper Roabiba Sandstones represent tidal dominated shoreface delta as inferred from depositional structures, trace fossils, and facies analysis. Typical depositional facies include tidal channel and bar deposits interbedded with shoreface sandstones. Wireline log signatures and core description indicate the presence of poorer quality lower shoreface sandstones and thin shales within the Upper Roabiba section. The summary sedimentology of interpreted depositional environment in Bintuni field is presented in Table 8.

Table 8. Summary sedimentology of interpreted depositional environment in Bintuni field (modified after Salo, 2005).

Interpreted Depositional Environment	**Rock Interval Lithology**	**Description**	**Bioturbation**	**Gamma-ray Wireline Log Signature**
Upper Shoreface	Sandstone, minor argillaceous sandstone	Sands, fine to vey fine grained; moderately well sorted,;with tough cross-bedding and low angle (10-20°) tabular cross-bedding, load cast, scour surfaces.	Sparse to moderate *(Ophiomorpha, Thalassinoides, Planolites, Glossifungites)*	
Lower Shoreface	Sandstone, minor shale	Fine to very fine grained sands; moderate to well sorted; trough cross-bedding, low angle (10-20°) tabular cross-bedding, asymmetric ripple lamination, flaser bedding, mud drapes, convolute laminae, normally graded beds;	Moderate to intense *(Ophiomorpha, Thallasinoides, Planolites, Palaeophycus, Teichichnus, Diplocraterion)*	
Tidal Sand Bar	Massive clean sandstone, argillaceous sandstone, silty shale	Sands with occasional muds, medium to fine grained; moderate to well sorted, graded bedding, trough cross bedding, ripple laminae, flaser bedding; bivalve and gastropod tests	Common to rare *(Ophiomorpha, Palaeophycus, Skolithos, Planolites, Teichichnus)*	

Bay (Brackish shale)	Shale, silty shale, carbonaceous shale, sandstone	Muds, silts and very fine grained sands with parallel laminae, symmetric and asymmetric ripple laminae, wavy and lenticular bedding, load casts; siderite, pyrite, bivalve and gastropod tests	Rare to moderate *(Planolites, Thallasinoides, Asterosoma)*	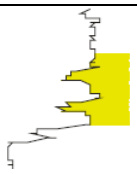
Offshore shelf	Shale, silty shale, sandstone	Mudstone and siltstone with beds of very fine to upper fine-grained sandstone; parallel lamination, wave, and current ripple cross-lamination; siderite, pyrite, bivalve and gastropod tests	Rare to moderate *(Planolites, Terrebelina, Teichichnus).*	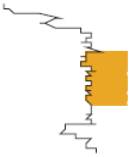
Marsh	Sandstone,silty sandstone, carbonaceous shale, coal	Muds, silts, and medium to very fine grained sandstone; moderately sorted; trough cross-bedding and low angle tabular cross-bedding, parallel and asymmetric ripple laminae; organic debris, clay clasts, root traces		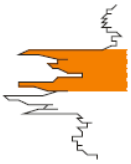
Estuarine channel	Sandstone, silty to argillaceous sandstone	Sands, medium to very fine grained; moderately well sorted; with trough cross-bedding and low angle tabular cross-bedding; parallel and asymmetric ripple laminae; organic debris, clay clasts	Rare to occasional *(Ophiomorpha, Skolithos, Palaeophycus)*	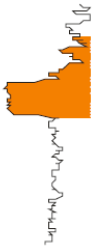

The depositional model of Roabiba Sandstone illustrates a tide-dominated shoreline setting with an active distributary system that supplies sand to a prograding, tide dominated delta (Figure 14). An example of the stratigraphic column and depositional environment of well B2 is shown in Figure 15. The stratigraphic column and depositional environment for other wells are attached in Appendix A.

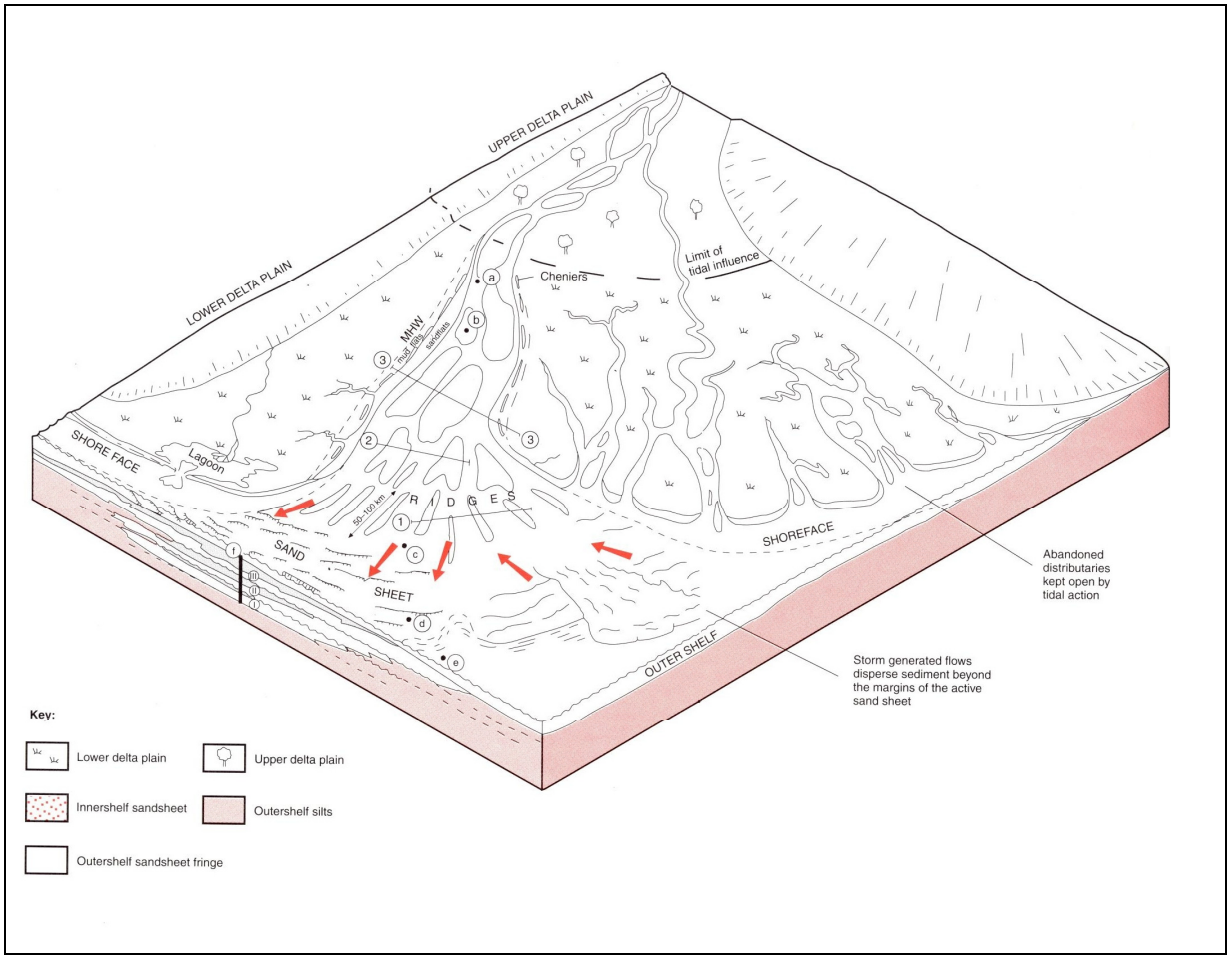

Figure 14. Model of a tide dominated shoreline setting (modified after Emery et.al, 1996).

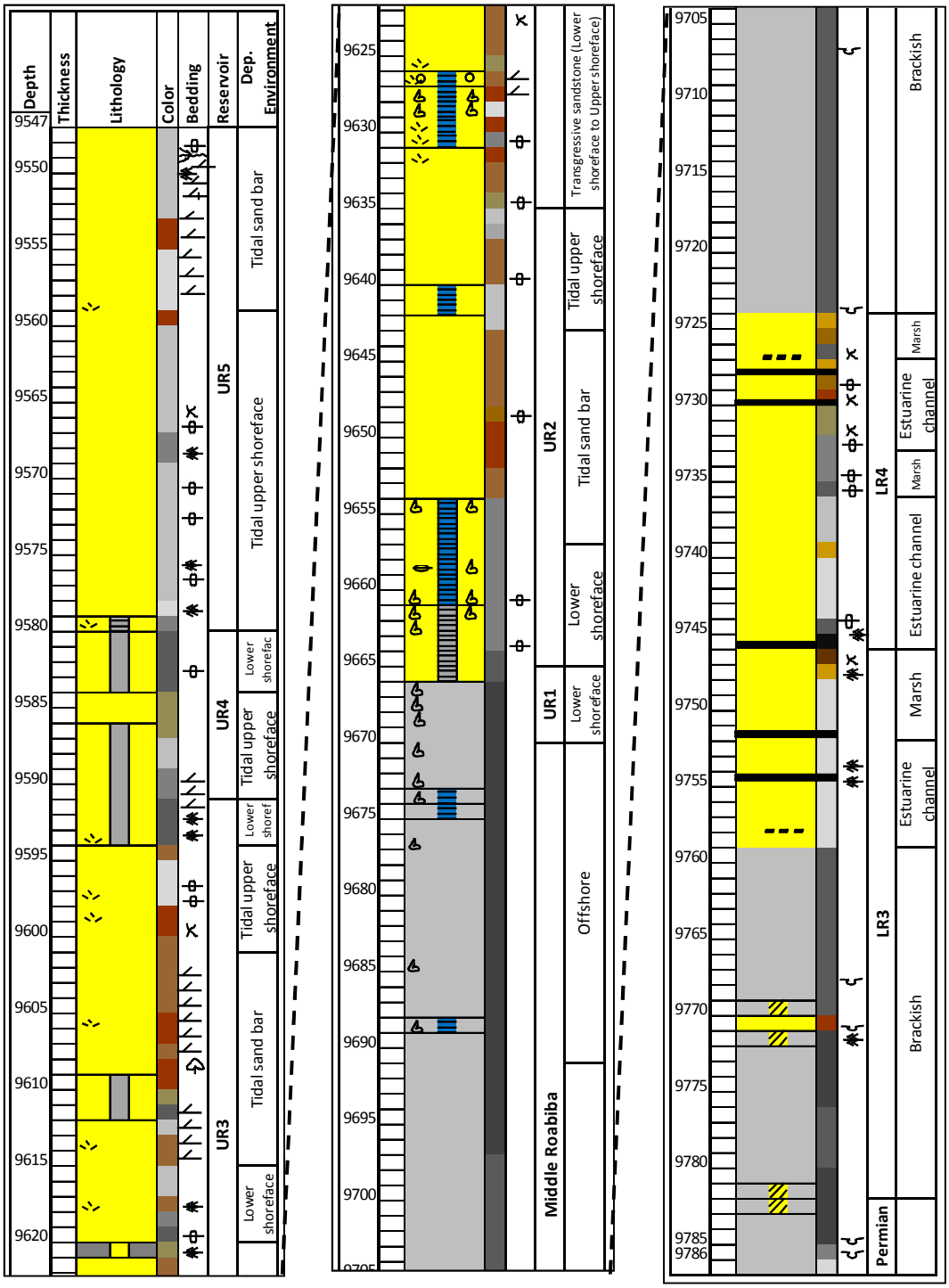

Figure 15. Stratigraphic column illustrating the subdivision of Roabiba Sandstones of B2 well.

3.5. DESCRIPTION OF STRATIGRAPHIC ZONES

Core of B2 well is the representative of the Bintuni field stratigraphy, since it contains a complete section of the Roabiba sandstone. Below are the interpretations of depositional environment for zones UR5 to UR1, MR, LR4, and LR3 based from core description well B2. Figure 16 shows the gamma ray log, lithofacies and the associated depositional environment.

3.5.1. ZONE UR5

Zone UR5 consists of lithofacies sb3 to xls. This interval is 38 ft thick and consists of massive, cross laminated, bioturbated sandstones interbedded with shales. Burrowing and bioturbation are abundant. Ichnofacies such as *Thallasinoides*, *Skolithos*, and *Planolites* are present. Constituents included lignite fragments and rip-up clasts. Texture, composition, and sedimentary structures indicate that UR5 interval represents a tidal sandbar in upper part and tidal upper shoreface in lower part.

3.5.2. ZONE UR4

Zone UR4 consists of lithofacies bs, sb3-2, and ms. The upper part is dominated by bioturbated and bioclastic sandstones while lower part is less bioturbated. Ichnofacies *Palaeophycus* and *Teichichnus* are present. The depositional environment is interpreted to be lower shoreface in the upper part of the zone and upper shoreface in the lower part.

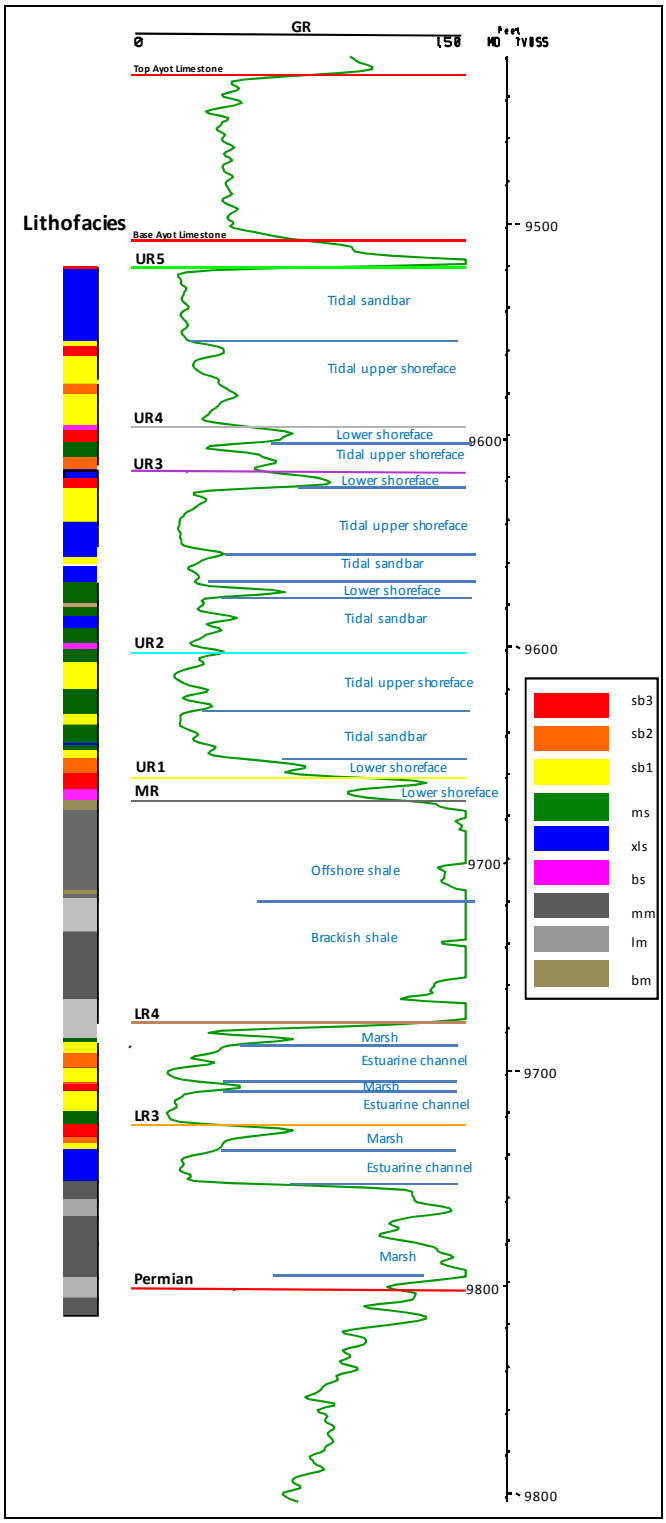

Figure 16. GR log of well B-2 showing the lithofacies and depositional environment.

3.5.3. ZONE UR3

Zone UR3 consists of lithofacies sb3, sb1, and xls. It is 43ft thick and consists of cross-laminated, massive, wavy, and parallel-bedded sandstones. Bioturbation is abundant in parts of the zone while graded bedding and stylolites are present in lower part. The lower part contains ammonites, roots, lithic grains, and shell fragments filled with calcite cement. Ichnofacies present are *Ophiomorpha*, *Skolithos*, and *Palaephycus*. The texture, composition, and sedimentary structures indicate that this interval represent lower to upper shoreface with a tidal sandbar in the middle.

3.5.4. ZONE UR2

Zone UR2 consists of lithofacies sb2 to xls. The upper 20 ft is dominated by massive sandstones, the lower part is bioturbated. Ichnofacies present are *Palaeophycus*, *Skolithos*, and *Teichichnus*. The lower 8 ft are calcite cemented and contain shell fragments. The depositional environment is interpreted to be tidal upper shoreface, tidal sandbar, and lower shoreface respectively from top to bottom.

3.5.5. ZONE UR1

Zone UR1 contains lithofacies bs and sb3. It is calcite cemented and contains shell fragments, siderite nodules, wavy, and mud drapes. The depositional environment is interpreted to be lower shoreface.

3.5.6. ZONE MR

Zone MR consists of massive, laminated, and bioturbated mudstones. The upper 24 ft contain abundant shell fragments, pyrite, and calcite cement while the lower 20 ft contains siderite nodules. The depositional environment is interpreted to be offshore in the upper part and estuarine in the lower part.

3.5.7. ZONE LR4

Zone LR4 consists of bioturbated sandstone lithofacies (sb3-sb1), minor massive sandstones in the lower 4 ft and mudstones in the top 3 ft. The interval is 24 ft thick in total include lignite layers, clasts, rootlets, and burrows. Ichnofacies present are *Ophiomorpha*, *Skolithos*, and *Palaeophycus*. The depositional environment is interpreted to be marsh and estuarine channels respectively.

3.5.8. ZONE LR3

Zone LR3 consists of bioturbated to cross laminated sandstones (sb3-xls) and laminated mudstones lithofacies. The upper 14 ft are dominated by bioturbated sandstones while the lower 21 ft are mudstones. Coal layers and rootlets are present in upper part. The depositional environment is interpreted as marsh and estuarine channels from top to bottom successively.

3.6. LITHOFACIES PROPORTIONS

Of the eight appraisal wells in Bintuni Field, five wells were cored in Upper Roabiba reservoir (B2, B3, B4, B5, and B6) and five wells were cored in Lower Roabiba reservoir (B2, B3, B4, B7, and B8). Below are the lithofacies proportions and porosity-permeability distribution for Upper Roabiba and Lower Roabiba Sandstones.

3.6.1. UPPER ROABIBA SANDSTONE RESERVOIR

The main lithofacies in the Upper Roabiba are sb1, sb3, xls, sb2, and ms with minor bs (<1%) as shown in Figure 7. Grain size ranges from lower fine to lower medium grained quartzarenites with variable amounts of lithic and feldspar grains. The proportion of lithofacies for each zone in Upper Roabiba (UR1-UR9) is shown in Figure 17.

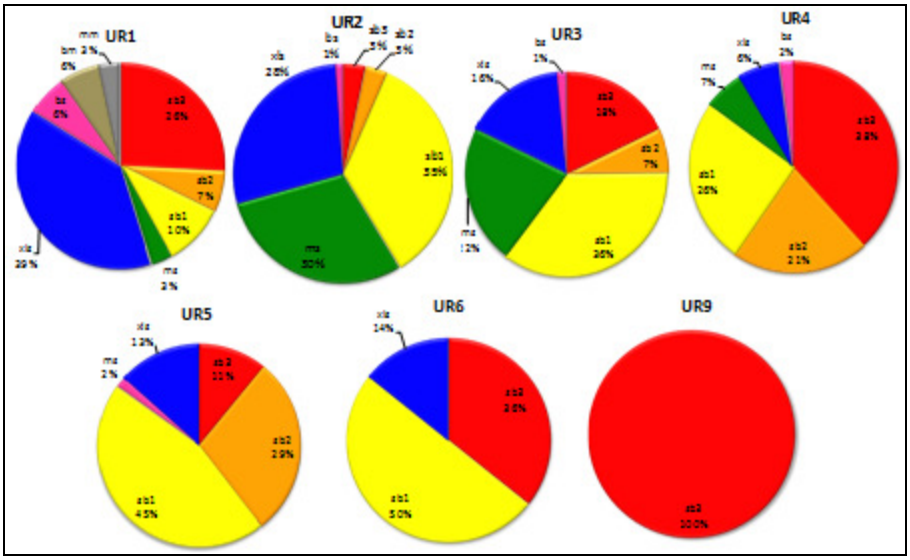

Figure 17. Lithofacies proportion of Upper Roabiba zones. The proportion of bioturbated sandstones increases and cross-laminated sandstones decrease from zones UR1 to UR9.

Note that the proportion of bioturbated sandstones increases while lithofacies xls decreases from zones UR1 toUR9. The greatest amounts of bioturbated sandstones occur in zones UR4 and UR9. The distribution of porosity-permeability by lithofacies and zones are shown in Figures 18 and 19. The lithofacies xls, ms, and sb1 mostly have permeability values >100 md and porosity >10%. The matrix-rich bioturbated sandstone lithofacies, sb3, mostly has permeability values <10md and porosity <13%. In the plot of porosity-permeability distribution by facies, zones UR2, UR4, and part of UR3 have permeability values >100 md and porosity >10%.

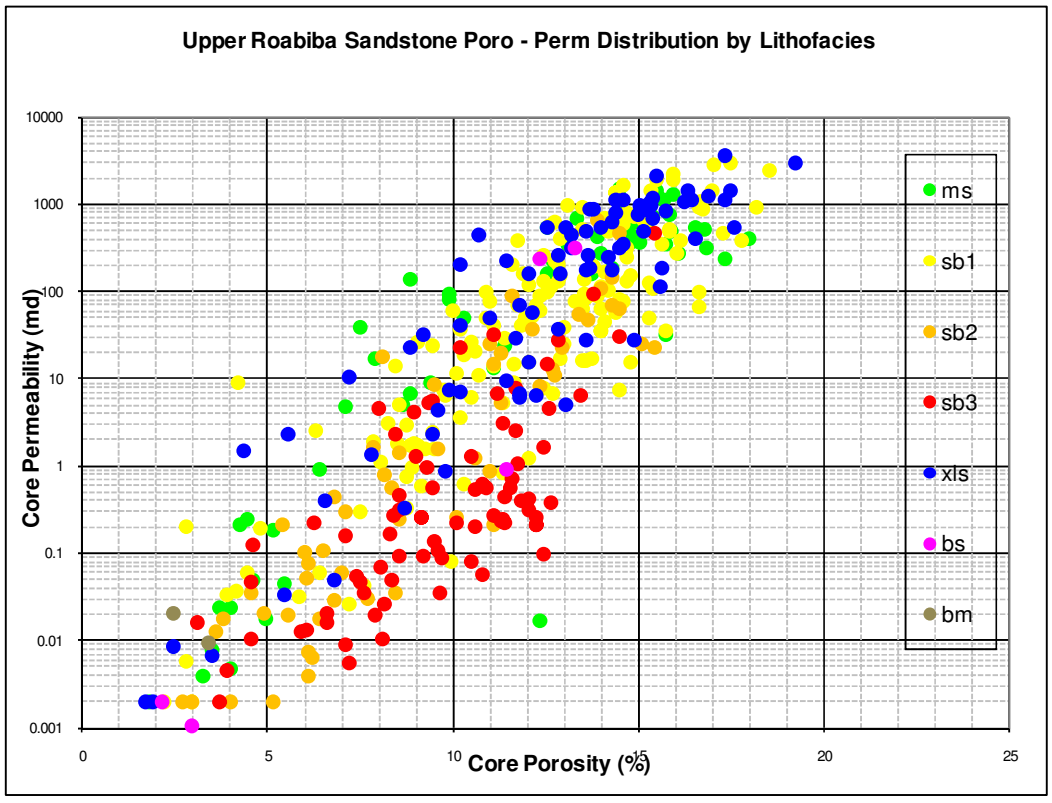

Figure 18. Distribution of Upper Roabiba Sandstone porosity-permeability by lithofacies.

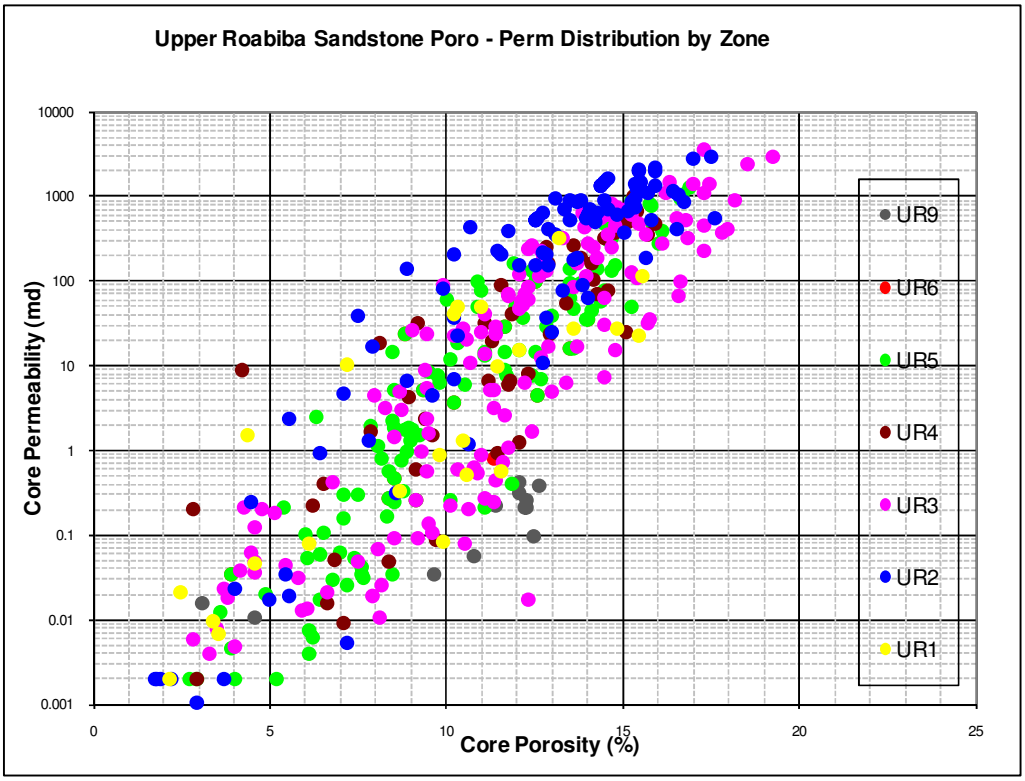

Figure 19. Distribution of Upper Roabiba Sandstone porosity-permeability by zones.

Figure 20 shows the average porosity for each zone in the Upper Roabiba Sandstone in the seven lithofacies. Lithofacies ms, xls, and sb1 have porosity average >10% and lithofacies sb3 has average <10%. Figure 21 illustrates the average permeability for each zone in the Upper Roabiba Sandstone in the seven lithofacies. The permeability values are in the log scale. Lithofacies ms, xls, and sb1 have average permeability > 100 md. Lithofacies sb3 has average permeability < 6 md. Zone UR2 has the highest average permeability (>300 md). Zones UR 1, UR 6, and UR 9 have low average permeability < 16 md.

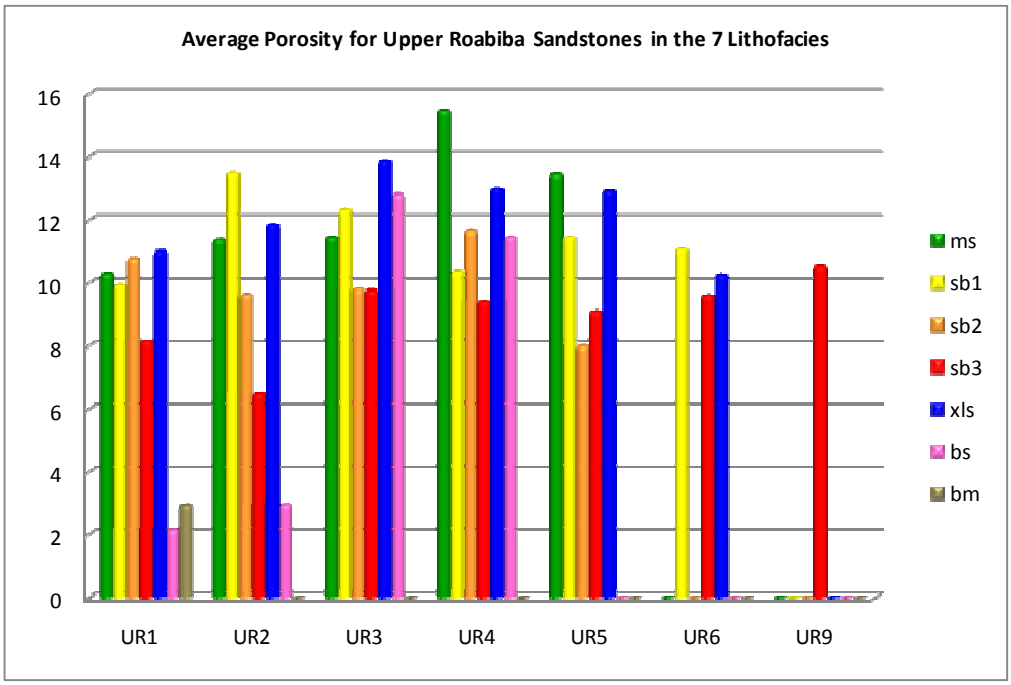

Figure 20. Average porosity values per zone for Upper Roabiba Sandstone in the seven lithofacies.

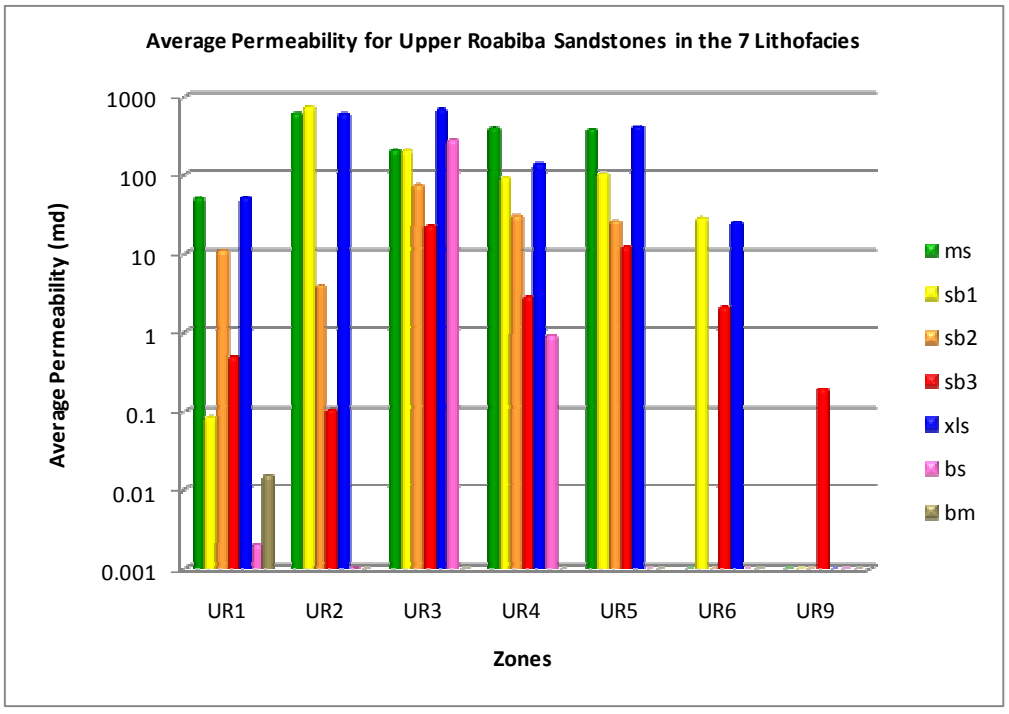

Figure 21. Average permeability values per zone for Upper Roabiba Sandstone in the seven lithofacies.

Figure 22 shows the porosity-permeability distribution by lithofacies of high calcite cement values for Upper Roabiba Sandstone. The densest permeability values population is below 0.1 md and porosity less than 8%. The cement does not correlate with any lithofacies.

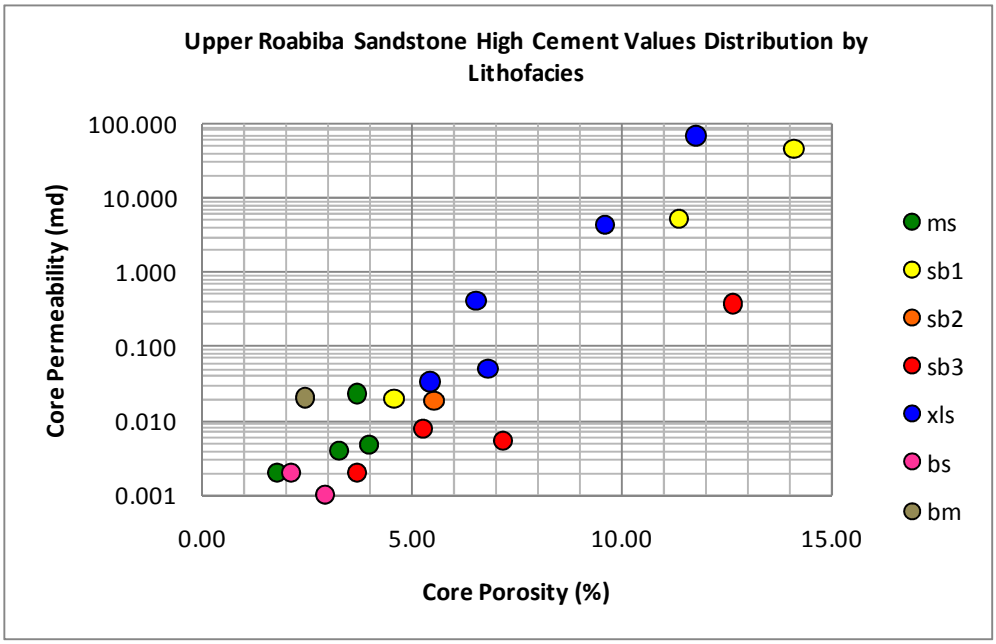

Figure 22. Porosity-permeability plot for high calcite cement values for Upper Roabiba in seven lithofacies.

High calcite cement value positions in the wells with datum of MR zone is shown in Figure 23. The positions of high calcite cement in well B2 spread over zones UR1 to UR5. The zone overlying MR relatively contains high calcite cement. Moreover, the position of high cement value in zone UR5 shows correlation between wells B2 and B4.

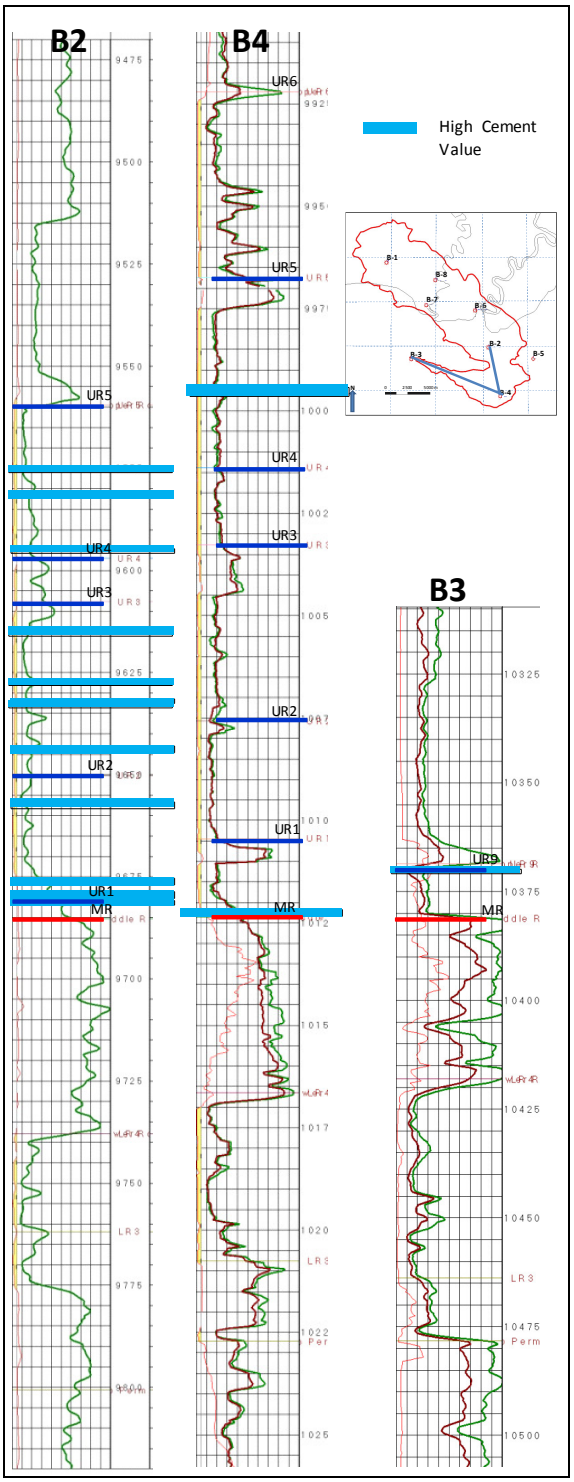

Figure 23. Logs plot showing the positions of high calcite cement value for Upper Roabiba.

3.6.2. LOWER ROABIBA SANDSTONE RESERVOIR

The main rock types in the Lower Roabiba Sandstone is bioturbated sandstone lithofacies designated as sb3, sb2, sb1, and ms. A nearly equal proportion of cross-laminated sandstone lithofacies xls, xls-m, and lls along with lesser amount of siltstone and mudstone (lithofacies bm and lm) are present. The lithofacies are shown in Figure 7. Grain size ranges from lower fine to lower coarse grained quartzarenites with variable amounts of lithic and feldspar grains.

The lithofacies proportions for each zone in Lower Roabiba Sandstone (LR3 and LR4) are shown in Figure 24. Note that siltstones, mudstones and bioturbated sandstones are more abundant in LR3 than in LR4. Reversely, cross-laminated sandstone lithofacies are more abundant in LR4. The grain sizes change upward since zone LR3 contains more shale (coarsening upward sequence).

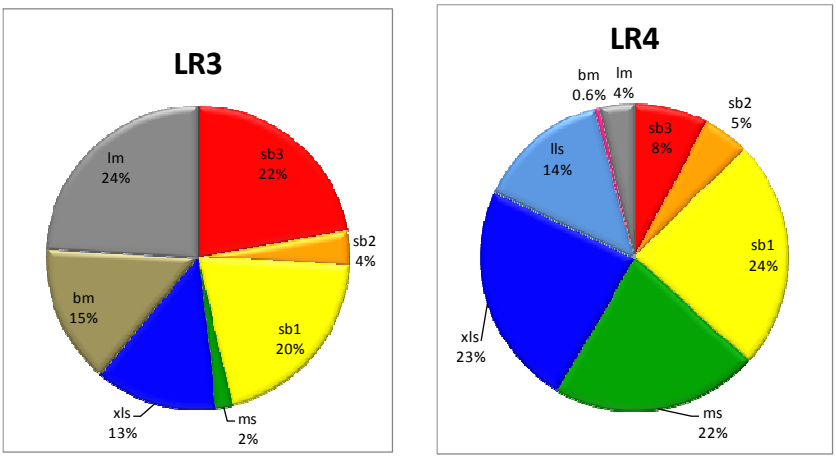

Figure 24. Proportion of lithofacies in the Lower Roabiba Sandstone. Siltstones, mudstones and bioturbated sandstones become less abundant in LR4. Cross-laminated sandstones are more abundant in LR4.

The distribution of porosity-permeability by lithofacies and zones is shown in Figures 25 and 26. Lithofacies xls, ms, and sb1 have porosity >10% and permeability >100 md. Lithofacies sb2, sb3, and lls have porosity <15% and permeability <10 md. Figure 26 shows that zone LR4 have major permeability values >100 md and porosity >10%. On the other way, zone LR3 have lower permeability (<100 md) and lower porosity values (<15%).

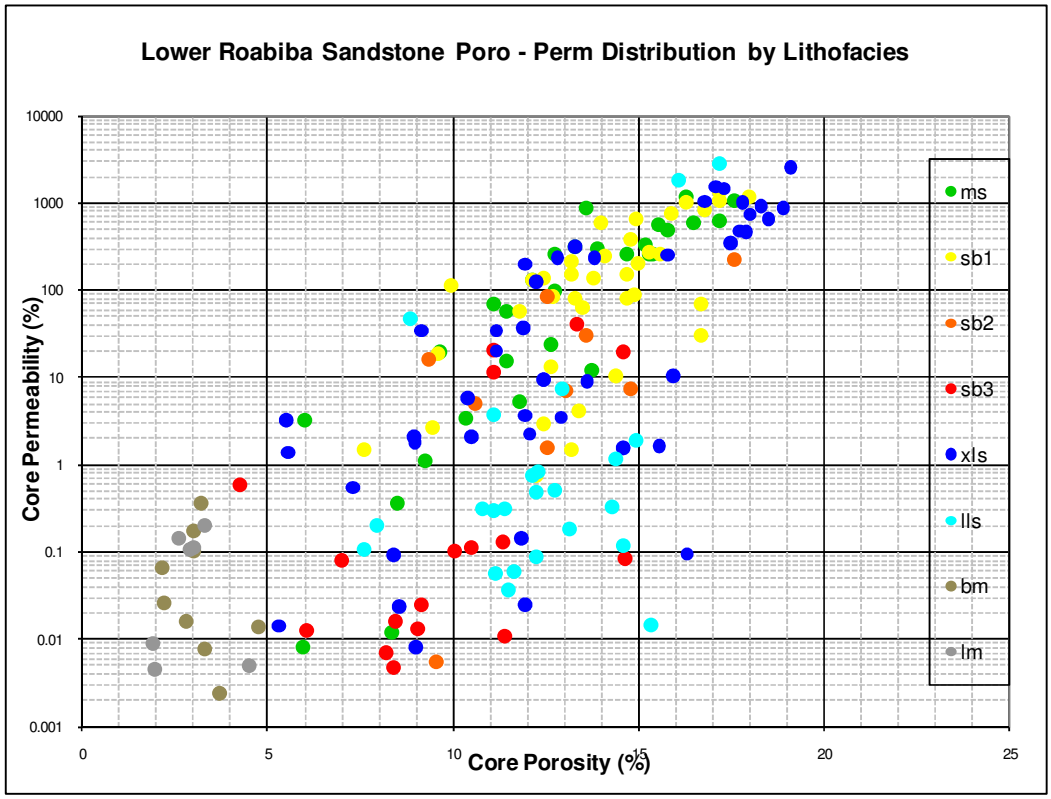

Figure 25. Lower Roabiba Sandstone porosity-permeability distributions by lithofacies.

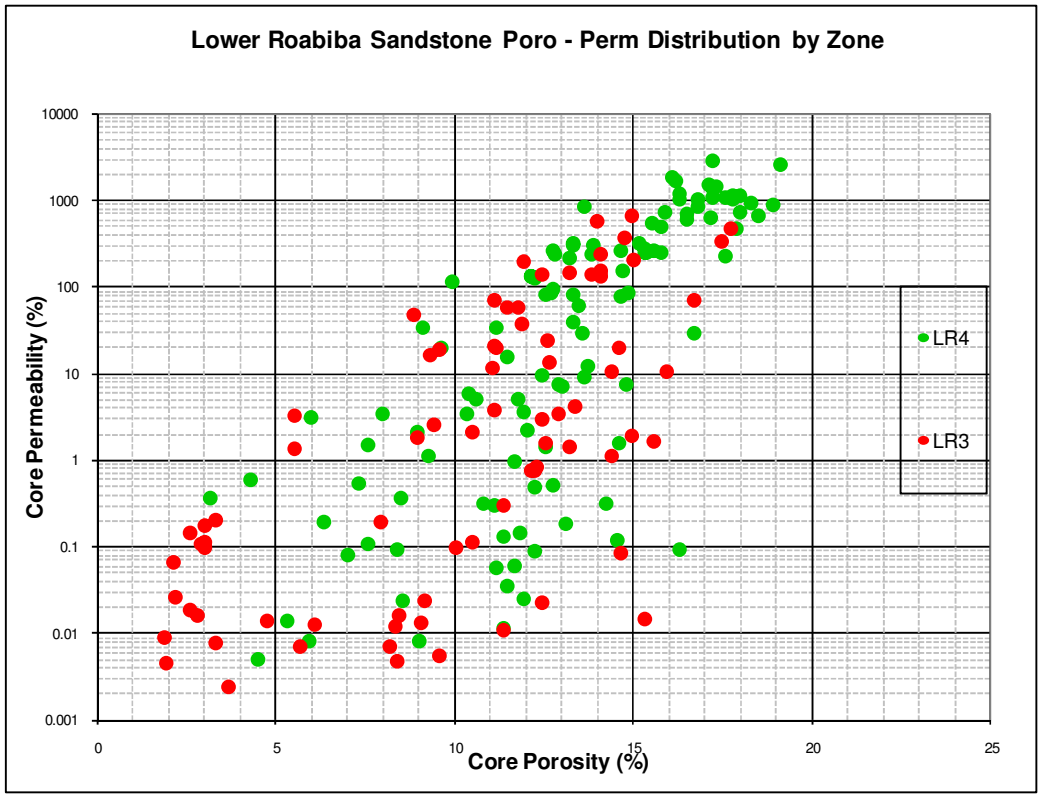

Figure 26. Lower Roabiba Sandstone porosity-permeability distributions by zones.

Figure 27 shows the average porosity for each zone in the Lower Roabiba Sandstone in the seven lithofacies. Lithofacies ms, sb1, and xls have porosity average >13% and lithofacies sb3 has average <10%. Figure 28 illustrates the average permeability for each zone in the Lower Roabiba Sandstone in the seven lithofacies. The permeability values are in the log scale. Lithofacies ms, sb1 and xls have average permeability >200 md. Lithofacies sb3 has average permeability <5 md. Zone LR4 has the highest average permeability (>150 md) and zone LR3 has average permeability <80 md.

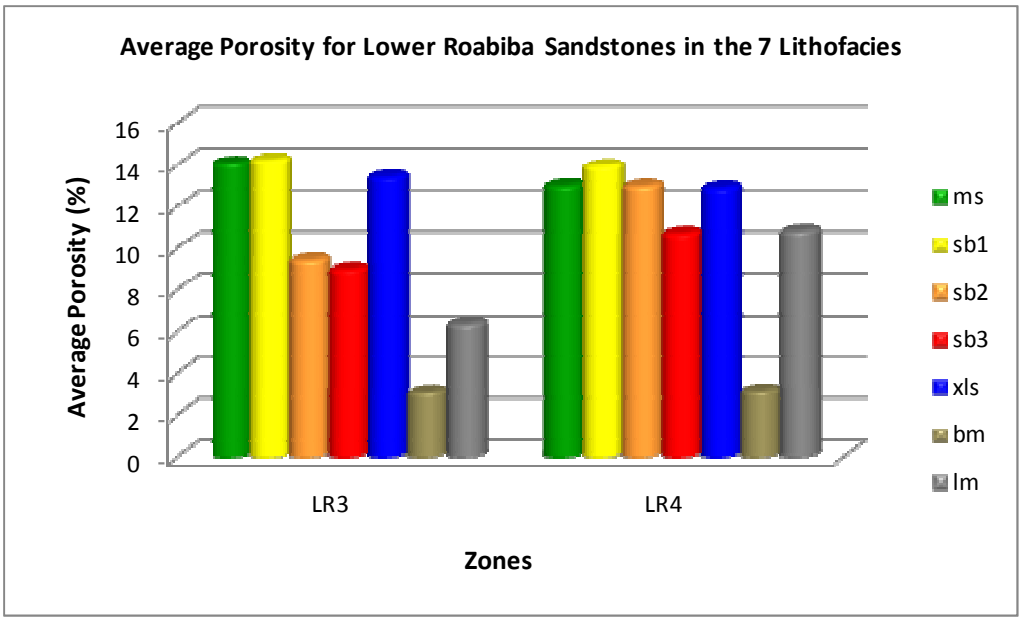

Figure 27. Average porosity values per zone for Lower Roabiba Sandstone in the seven lithofacies.

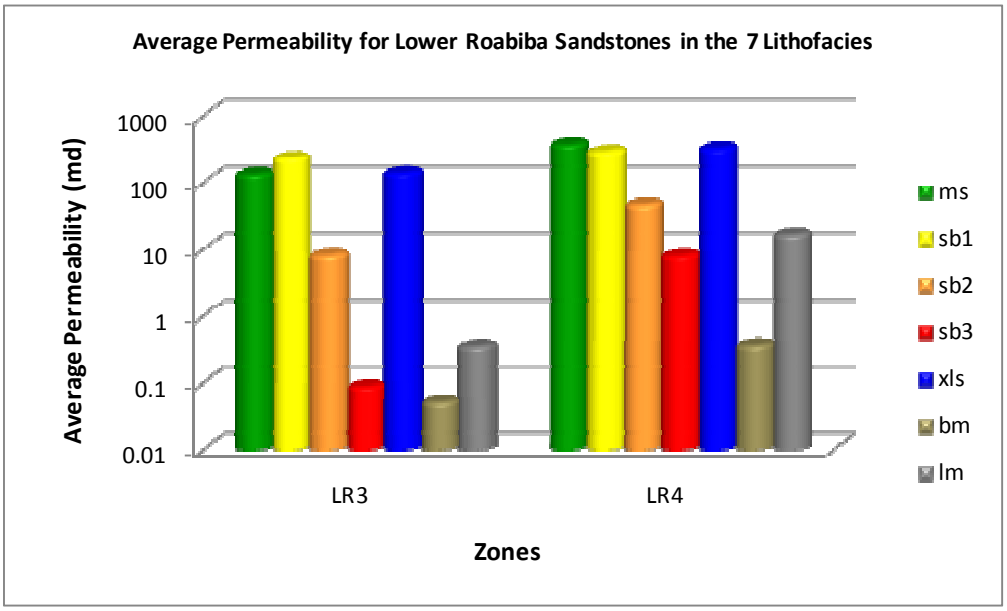

Figure 28. Average permeability values per zone for Lower Roabiba Sandstone in the seven lithofacies.

4. RESERVOIR ARCHITECTURE

The study area covers an area of 205 km² with approximately 50% of the field onshore. The structure is a four-way dip closure sitting on the crest of a NW-SE oriented anticline that is modified by east-west trending left-lateral strike-slip faults.

The structural trap of Bintuni field is a plunging anticline (Figure 29).The isopach map of the Upper Roabiba sediments indicate that the sandstone was deposited on a south-southwest dipping shelf, with progressively thicker section predicted towards the south of the field (Figure 30). Figure 31 shows an isopach of the Lower Roabiba Sandstone indicating deposition on a westward to southwestward dipping shelf. No Lower Roabiba section was encountered in the B1, B7, and B8 wells in the north part of the study area. Like the Lower Roabiba Sandstone, the Upper Roabiba Sandstone is thickest in the B4 well. Naar et al. (2008) interpreted the wells B3 and B8 as both being on horst blocks with a Permian graben between them. As a response to local uplift on horst block, the Lower Roabiba Sandstone is anomalously thin in B3 well. The thickest portions of the Lower Roabiba Sandstone occur in the B4 well (105 ft) and 119 ft in the B5 well. This represents the thickest part of the Upper Roabiba Sandstone also. Upper Roabiba Sandstones is thickening to the southern part (Figure 32) and in the northern part of the study area (Figure 33).

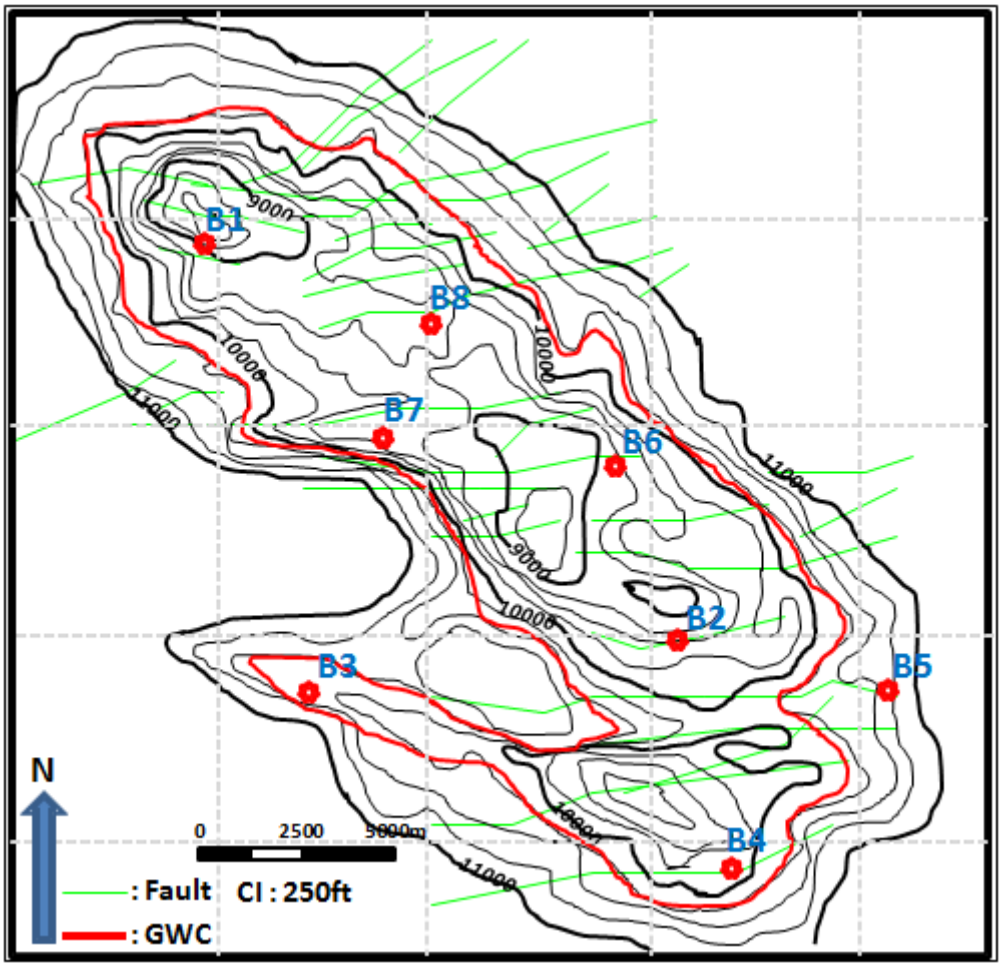

Figure 29. Structure map of the Upper Roabiba Sandstone reservoir showing the NW-SE oriented anticline, east-west strike-slip faults, and GWC at 10175 ftTVD subsea in the study area except at B3 well which is 10425 ftTVDss .

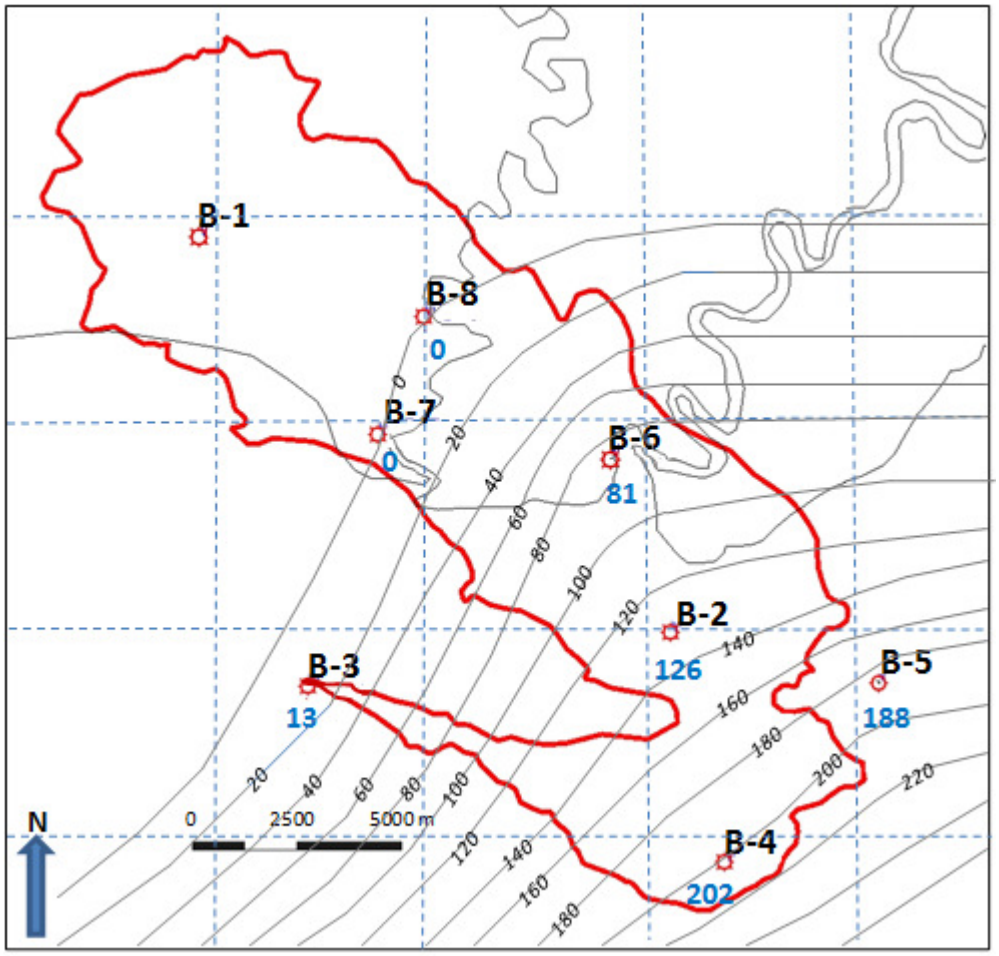

Figure 30. Isopach map of the top of Upper Roabiba Sandstone reservoir showing the thickest sand is in the southern part.

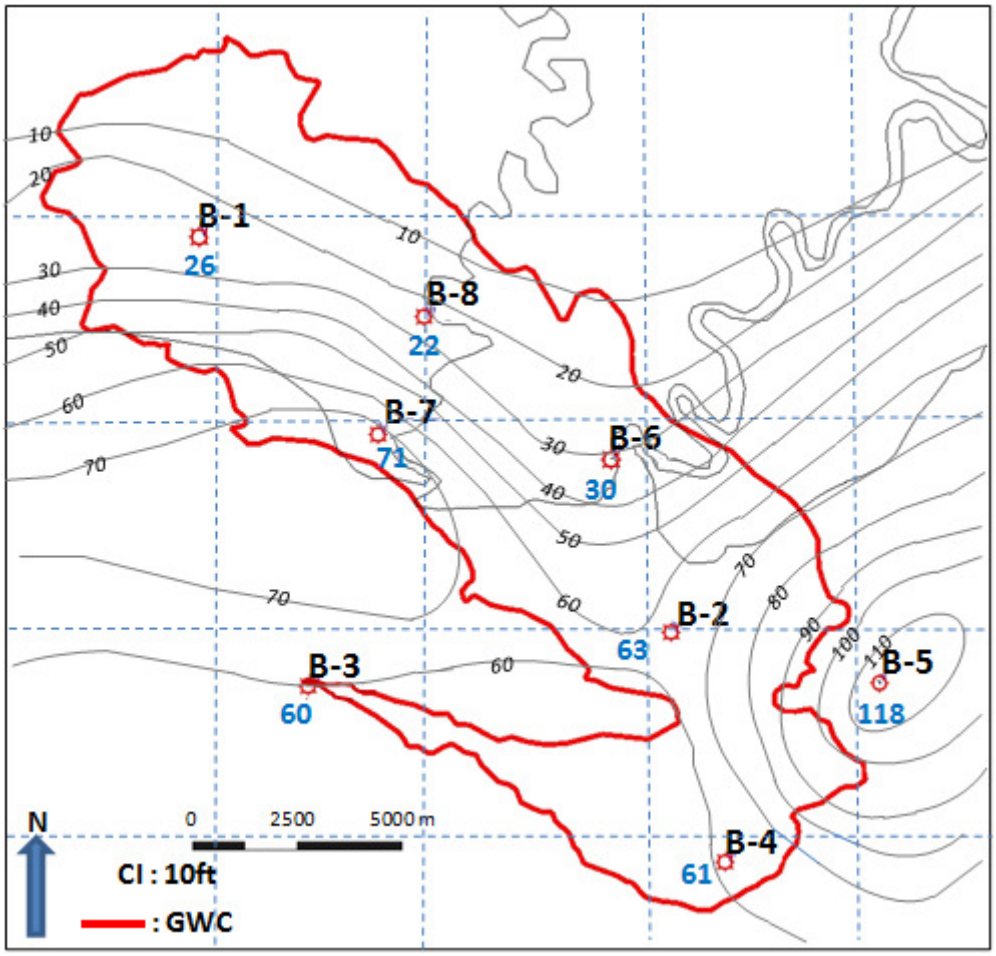

Figure 31. Isopach map of the Lower Roabiba Sandstone reservoir showing the thickest sand is in the southern part.

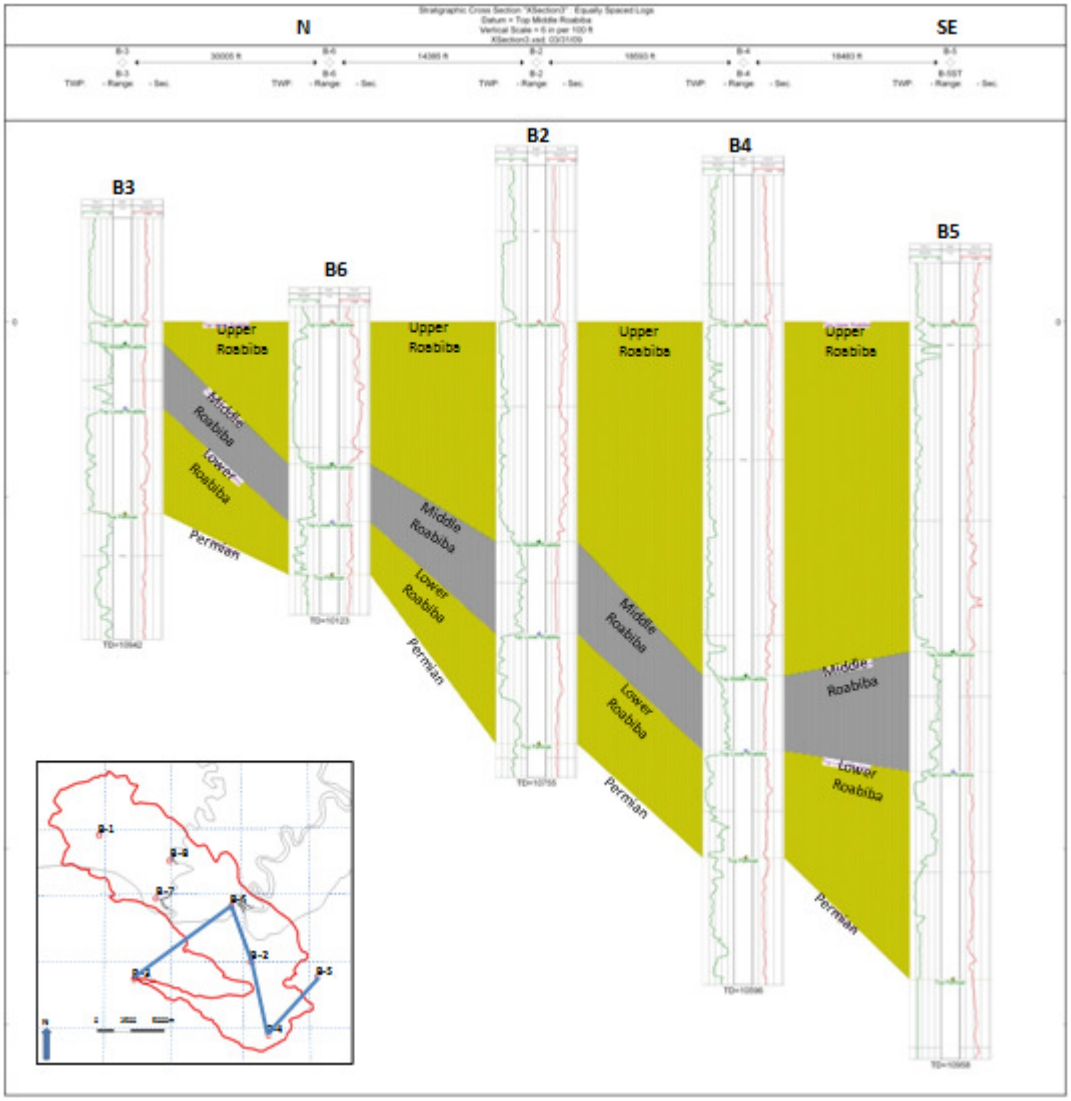

Figure 32. A stratigraphic cross section in the southern part of the field illustrating the distribution of Roabiba Sandstones (datum is Upper Roabiba Sandstone).

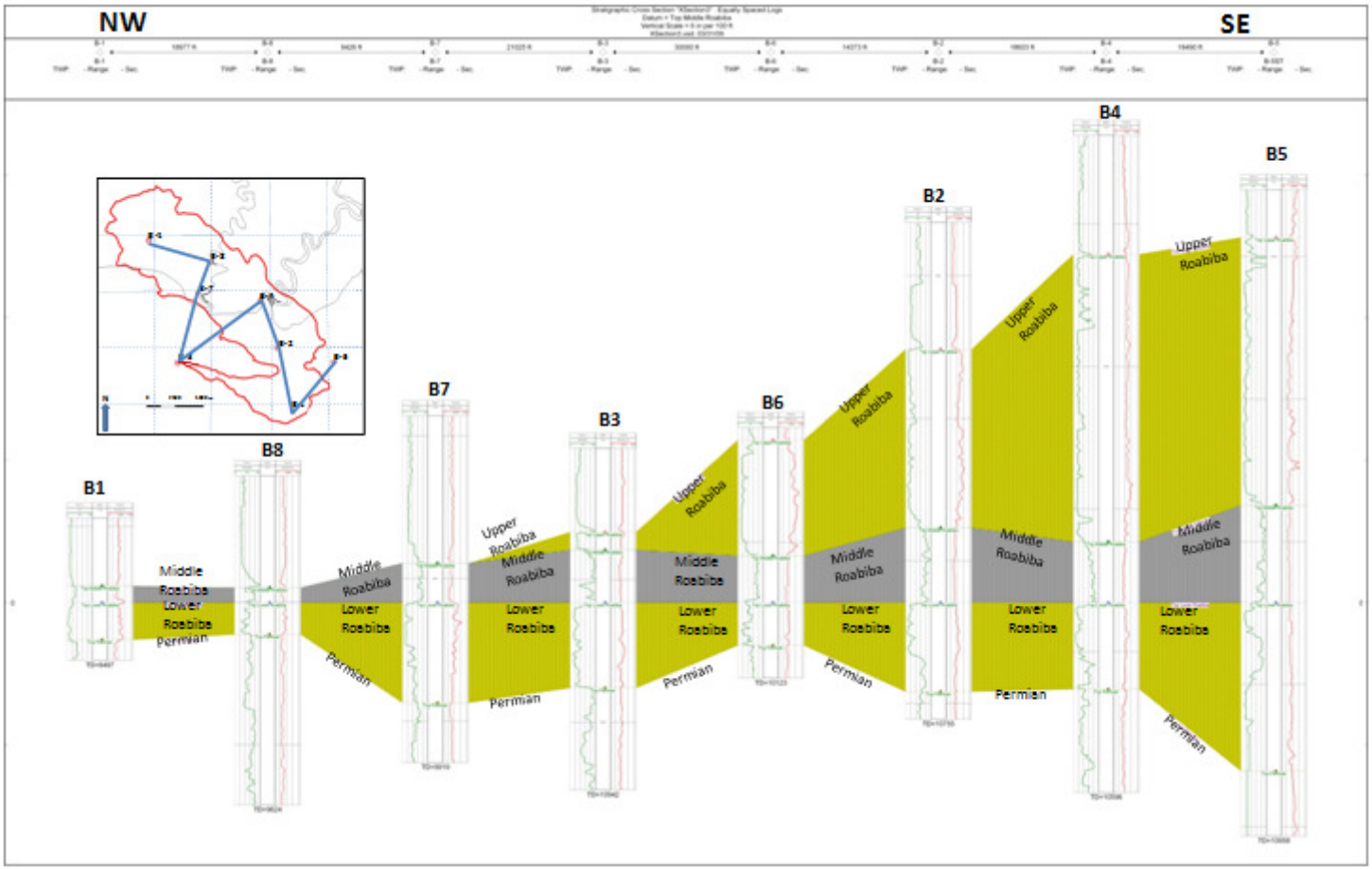

Figure 33. A stratigraphic cross section in strike direction illustrating the distribution of Roabiba Sandstones (datum is Lower Roabiba Sandstone).

5. PETROPHYSICAL ANALYSIS

Several reservoir properties were measured to better understand the petrophysics of Roabiba Sandstones. For example, porosity and permeability values were obtained from core analyses and from density/neutron logs calculation. Sw was obtained from core analyses and Archie calculation. Additionally, capillary pressure measurements were done as part of special core analysis (SCAL) in selected wells.

5.1. PERMEABILITY

Permeability is one of the important characteristics in hydrocarbon reservoirs, therefore it is important to estimate permeability for logged but uncored wells. A predictive function using x in y linear regression to minimize uncertainties in the predicted permeability can be applied routinely on uncored wells, and test on cored wells.

Porosity-permeability data from core analyses were plotted to determine a permeability equation for the uncored wells in the study area (Figure 34). The equation for is:

$$y = 0.0001 *(e^{(1.05*x)})$$

where x is porosity, y is permeability, and e values 2.718282.

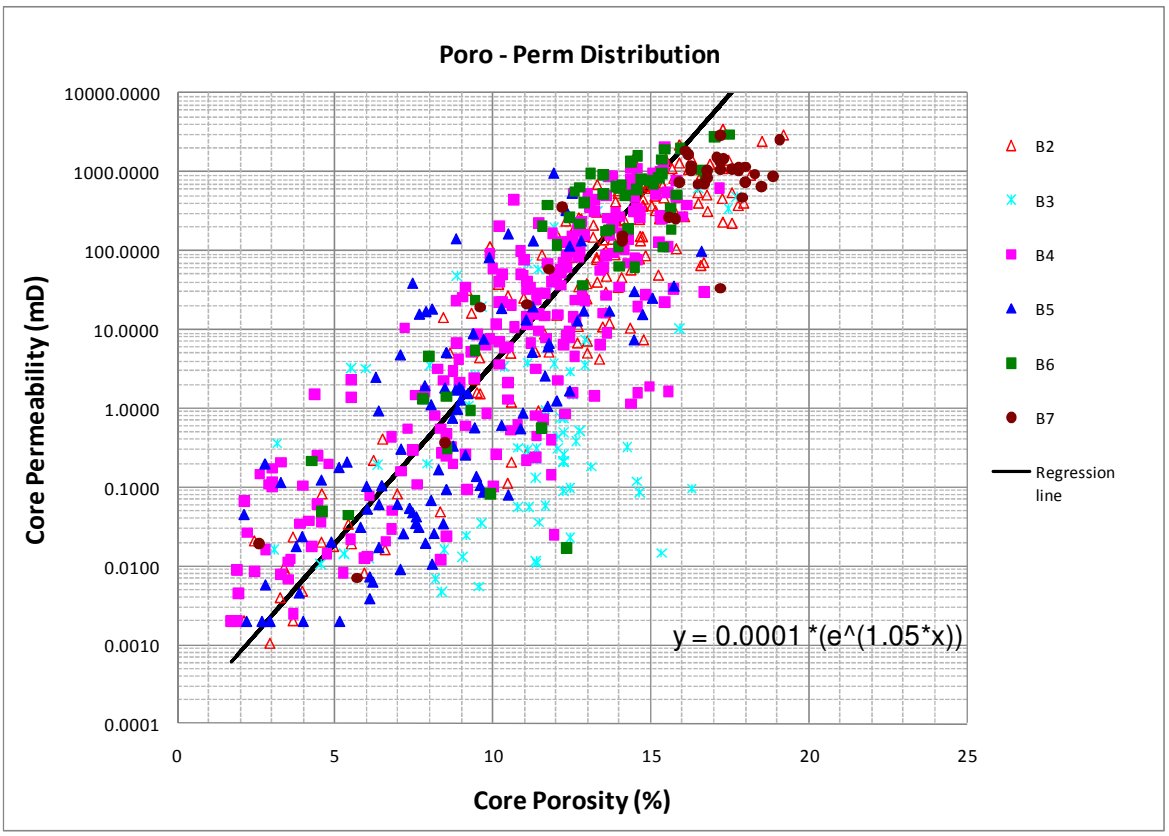

Figure 34. Cross plot of core permeability and porosity.

An example of log interpretation with cores permeability versus calculated permeability on the same scale is shown in the next figure which is also included core and calculated porosity, S_w, and V_{sh} (Figure 35). Log analyses for other wells are shown in Appendix B. Overall the core permeability points match the calculated data from log permeability. An average permeability value in the Lower Roabiba Sandstone is 183 md and 260 md in the Upper Roabiba Sandstone.

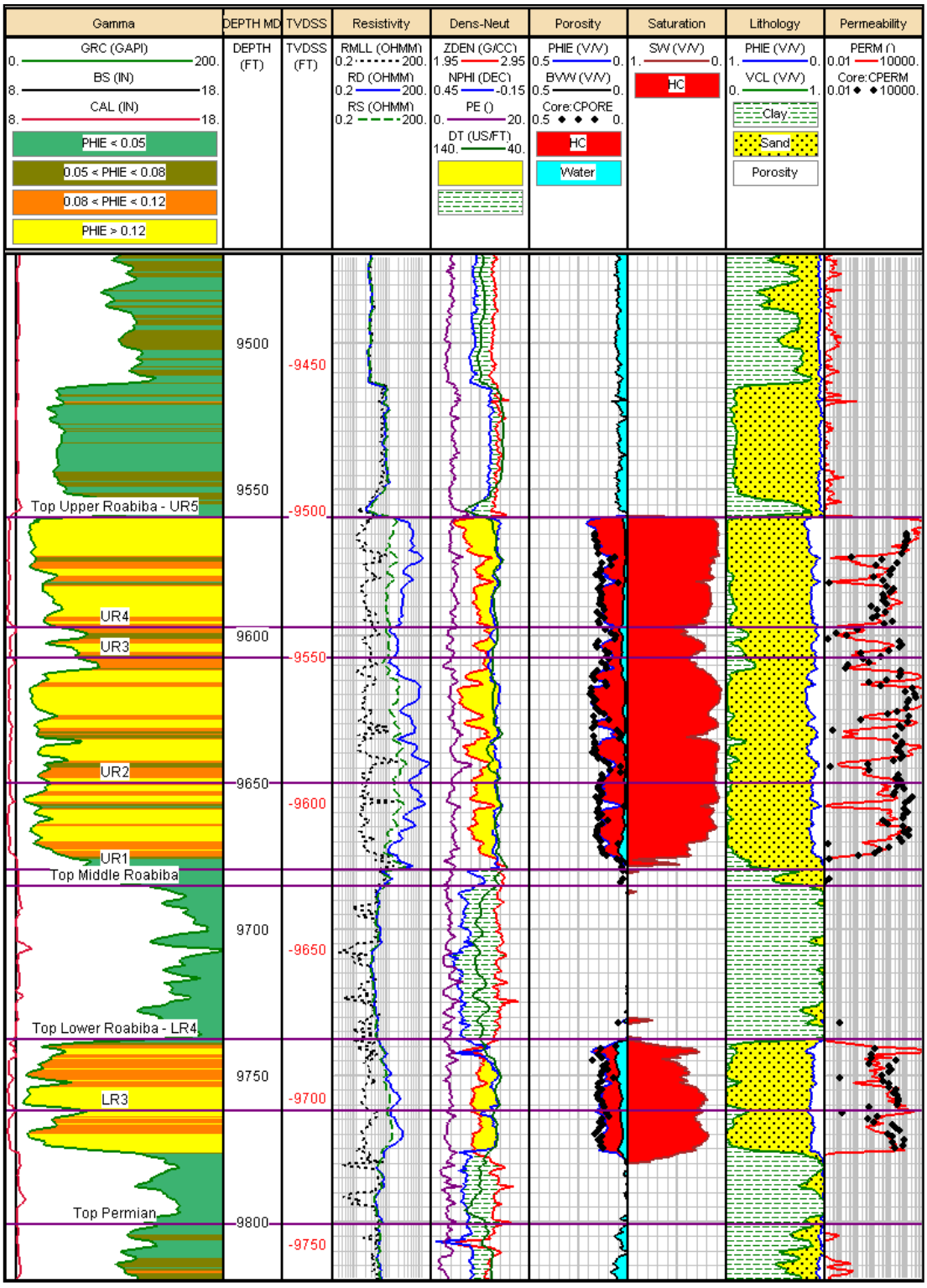

Figure 35. Log analysis of B2 well showing core porosity and permeability, calculated porosity and permeability, S_w, V_{sh}, and porosity values in color.

In order to show the permeability value in the entire well, the permeability value greater than 200 md is colored yellow, orange for permeability between 50 to 200 md, and green for less than 50 md (Figure 36). These color bands are illustrated in the GR log. Another cross section in SW-NE dip direction is displayed in the Appendix C.

From the cross sections it can be inferred that Upper Roabiba Sandstone has the higher permeability compared to Lower Roabiba. Comparatively high permeability is present in the Lower Roabiba Sandstone particularly in wells B3 and B7. Highest permeability values occur in lithofacies ms, xls and sb1.

5.2. POROSITY

Porosity influences the calculated S_w from Archie equation. The best source of porosity is direct measurements on core. For the uncored intervals, porosity can be estimated from logs. In this field, density and neutron logs were run on wells; sonic logs were run on wells B2 through B7. Cross plot of core porosity versus log porosity is shown below (Figure 37).

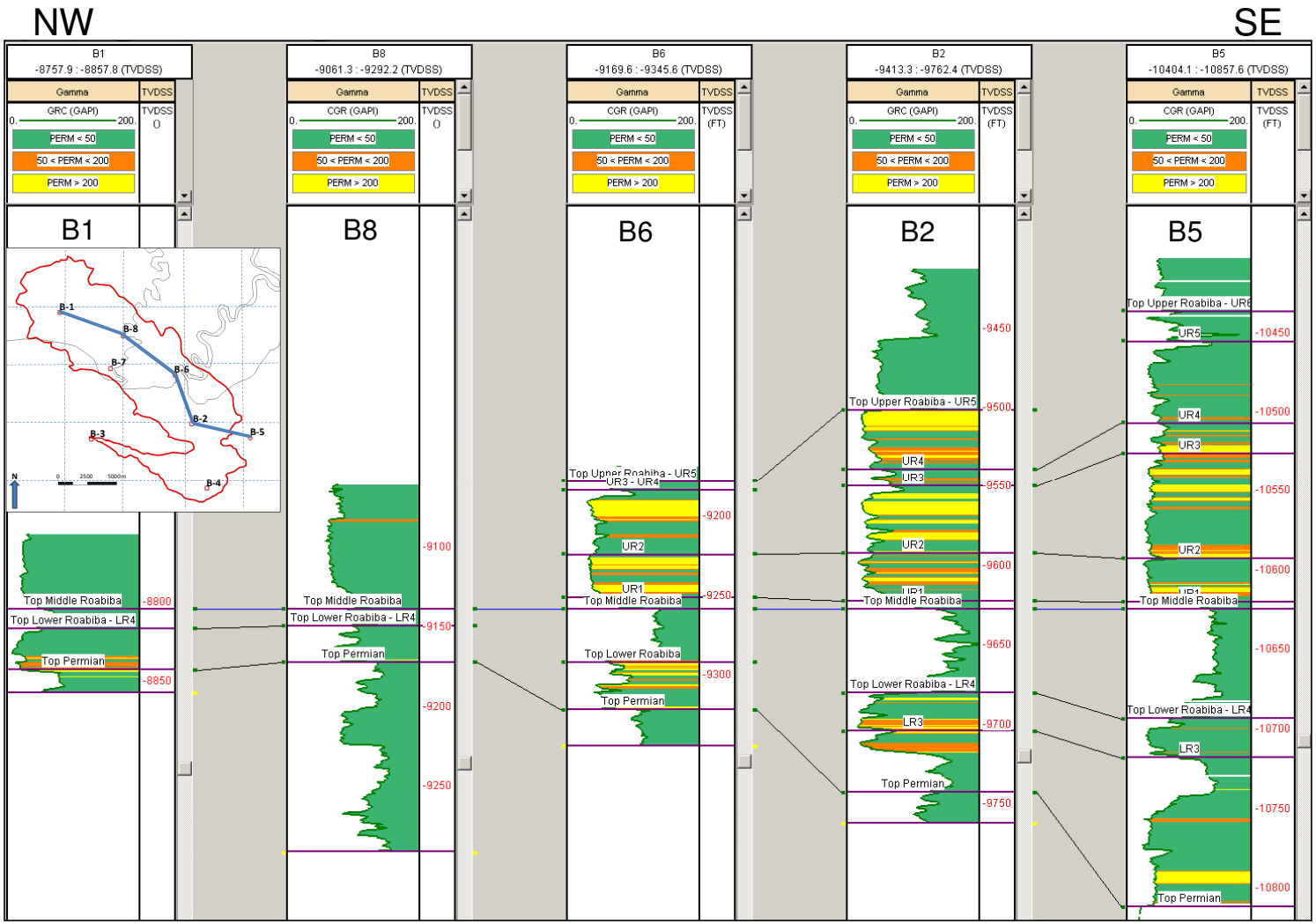

Figure 36. Permeability values along strike. Datum is top of Middle Roabiba Formation.

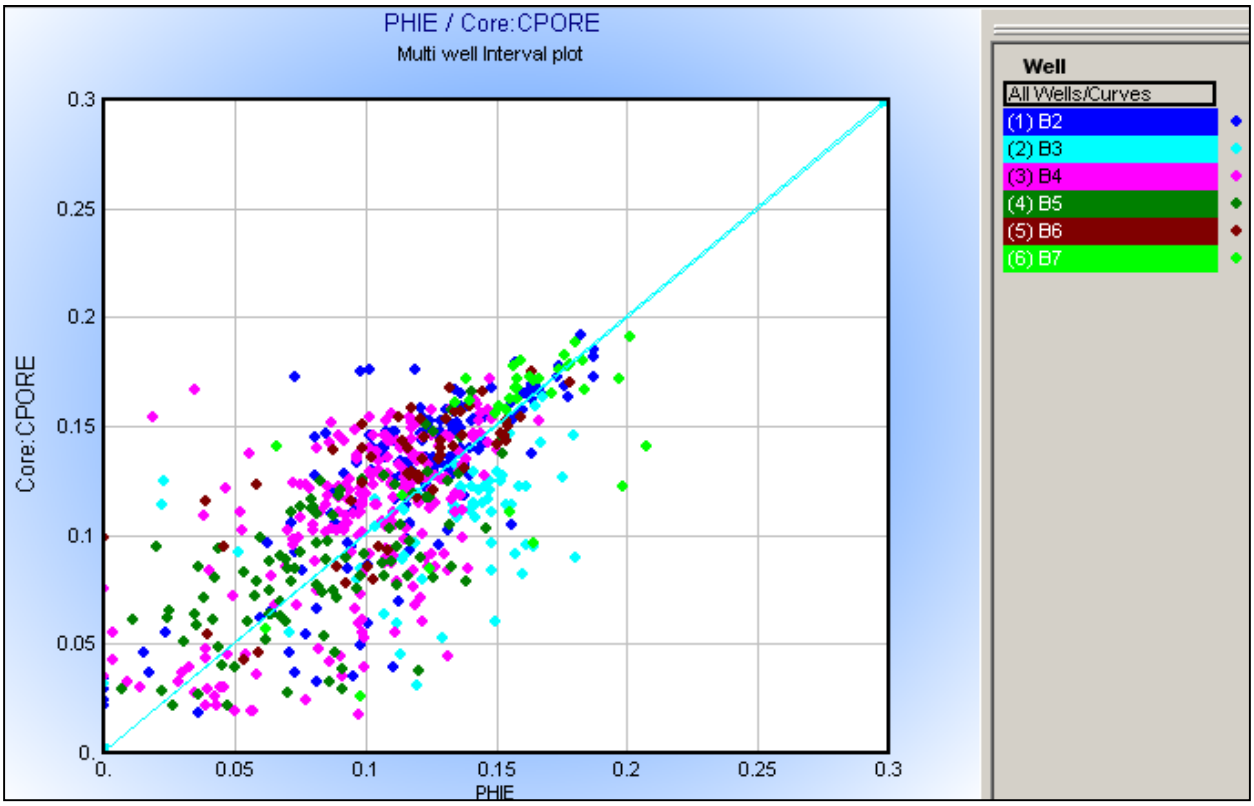

Figure 37. Cross plot of core porosity and log porosity.

A cross section of the strike direction across the field with designated color code to differentiate the porosity values is shown in the next figure (Figure 38). The porosity greater than10% is yellow and porosity less than 5% is green. The cross section shows that porosity values greater than 5% are related to low GR values or sandstones lithology and porosity values less than 5% are related to high GR values or shale. In the northern field area around wells B1 and B8, porosity in the Lower Roabiba Sandstone is lower than in wells to the south. The SW-NE cross section (Appendix C) shows that well B8 has lower porosity in the Lower Roabiba section than in wells to the west. The range of porosity in Lower Roabiba Sandstone is 9-16% while it is 11-14% in the Upper Roabiba. The high permeability values occur in lithofacies ms, xls, sb1, and sb2.

5.3. WATER SATURATION

Water saturation (S_w) is defined as the proportion of the porosity that contains water (Darling, 2005). S_w can be determined from direct Sw measurement on cores, saturation estimates from MICP and S_w calculated from resistivity logs using the Archie or Simandoux equation.

A formation water resistivity (R_w) value was obtained by generating a Pickett plot (Figure 39). It is inferred from the plot that Rw is 0.043 Ωm. Archie's equation is used to obtain Sw. Additionally, the cementation factor (m) and saturation exponent (n) from SCAL analysis are applied in the equation. Values of m=1.83 and n=1.85. The average S_w in the Upper Roabiba ranges from 15 to 70 percent while it is 30 to 80 percent in Lower Roabiba. Well B5 is wet and contains only residual gas. All log analyses are displayed in Appendix B.

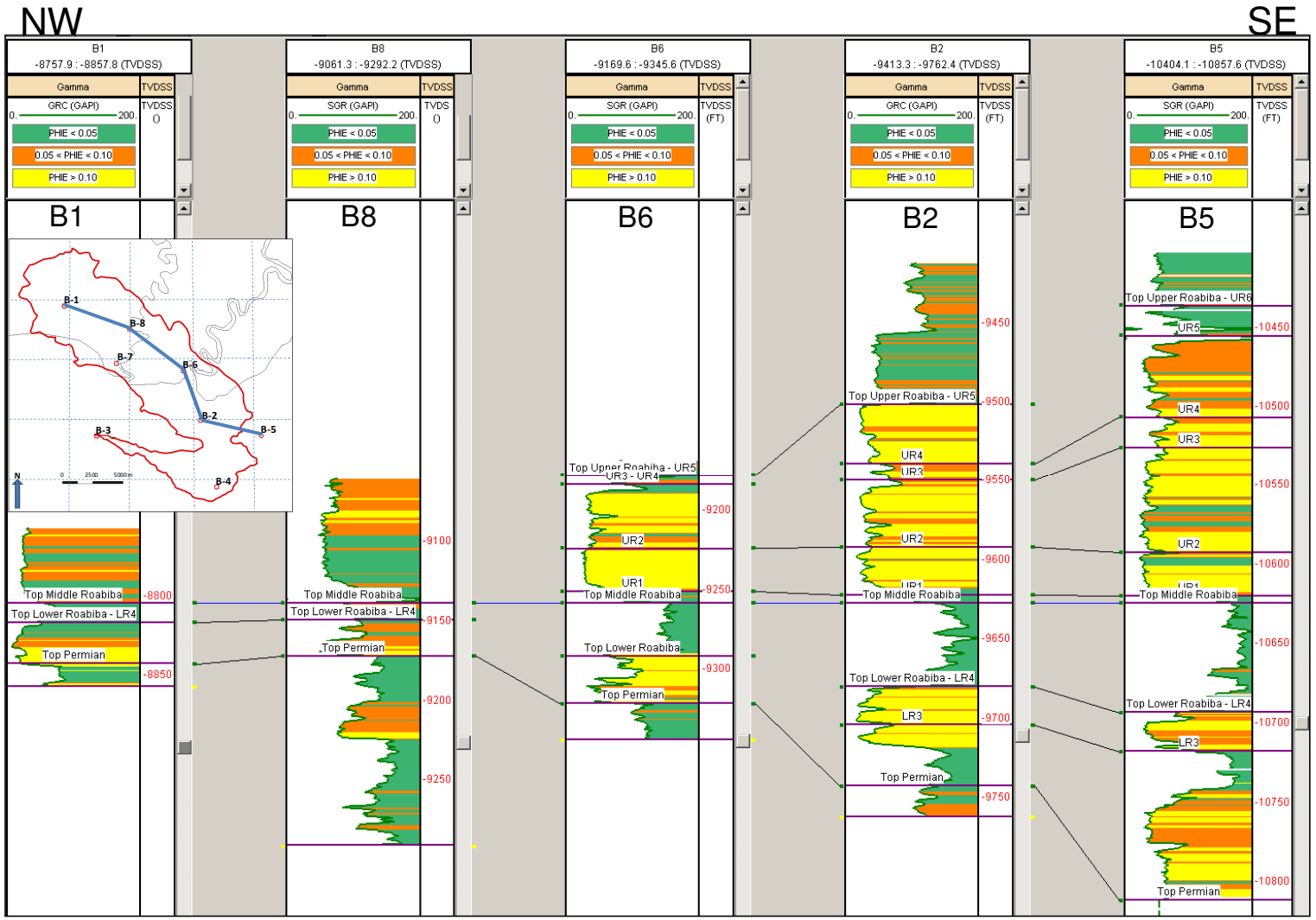

Figure 38. Porosity values along strike. Datum is top of Middle Roabiba section.

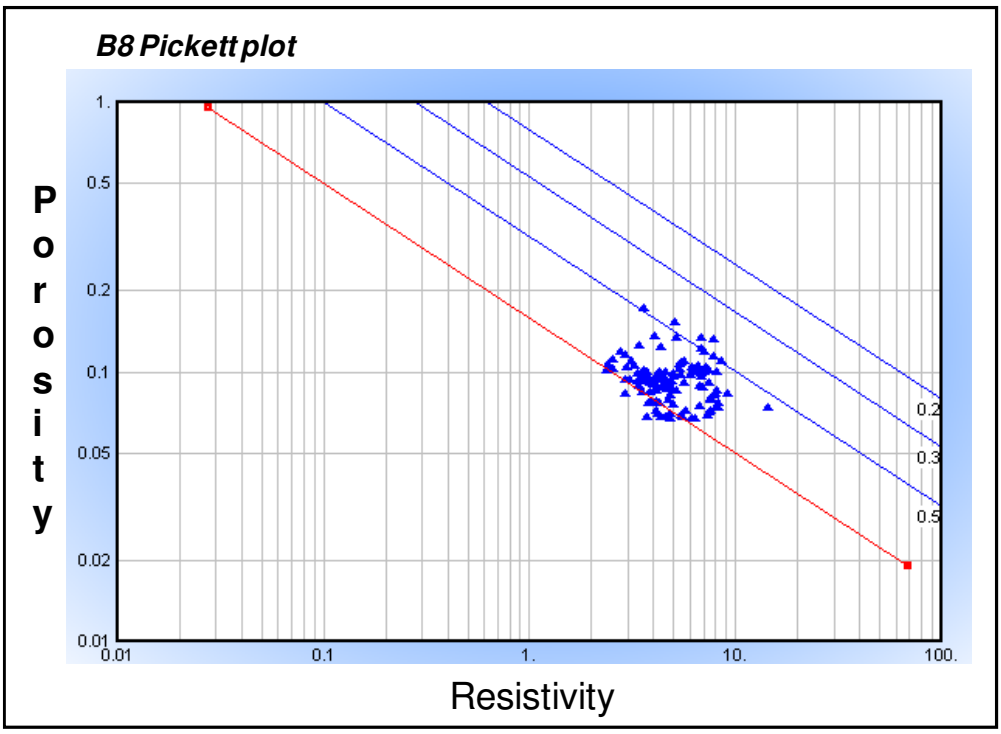

Figure 39. Example of a Pickett plot taken from B8 well.

5.4. NET PAY

The net reservoir and net pay cut offs were set based on the porosity, V_{sh}, and S_w. The log model that was used in the petrophysical evaluation has been calibrated to core with a reasonable match. A minimum porosity of 5% and a maximum shale volume of 50% have been used to determine net pay cut offs. Based on the porosity-permeability crossplot, the 5% effective porosity (PHIE) corresponds to permeability of more or less 0.01 md, which is the limit of the reservoir to contribute to the flow for the gas reservoir. Moreover, the previous figure (Figure 38) shows that PHIE values greater than 5% correspond to low GR values (sandstones lithology) and below PHIE values less than 5% correspond to high GR values (shales lithology).

Since the effective porosity was used as the net reservoir cut off, in theory, the clay effects have been removed. However, the V_{sh} cut off was set at 50% to avoid

imperfection on the log analysis computation. A water saturation cut off of 65% has been applied in net pay calculation refer to S_w cut off used in adjacent field which is determined from salinity measurement and log S_w matching to capillary pressure data.

The sensitivity analyses were run to PHIE, V_{sh} and S_w. The results indicated that the models are most sensitive to the V_{sh} and PHIE. The 5% porosity cut off, 50% clay volume cut off and 65% water saturation cut off were picked to include nearly all the potential hydrocarbon present in the reservoir (Figure 40).

Petrophysical evaluation of the Upper and Lower Roabiba Sandstone generated average values for petrophysical properties shown in Tables 9 and 10. Net pay maps for each reservoir are shown in Appendix D. Total net pay for Upper Roabiba Sandstone reservoir is 381 ft and total net pay for Lower Roabiba Sandstone reservoir is 230 ft. Cumulative net pay is 611 ft.

B4 well has the thickest net pay in Upper Roabiba Sandstone, which also has the greatest net reservoir thickness in the field. The net reservoir is anomalously thin in the B3 well where 12 ft of net pay was found. In Lower Roabiba Sandstone reservoir, B5 well has the greatest net reservoir thickness which may reflect topography at the time of deposition.

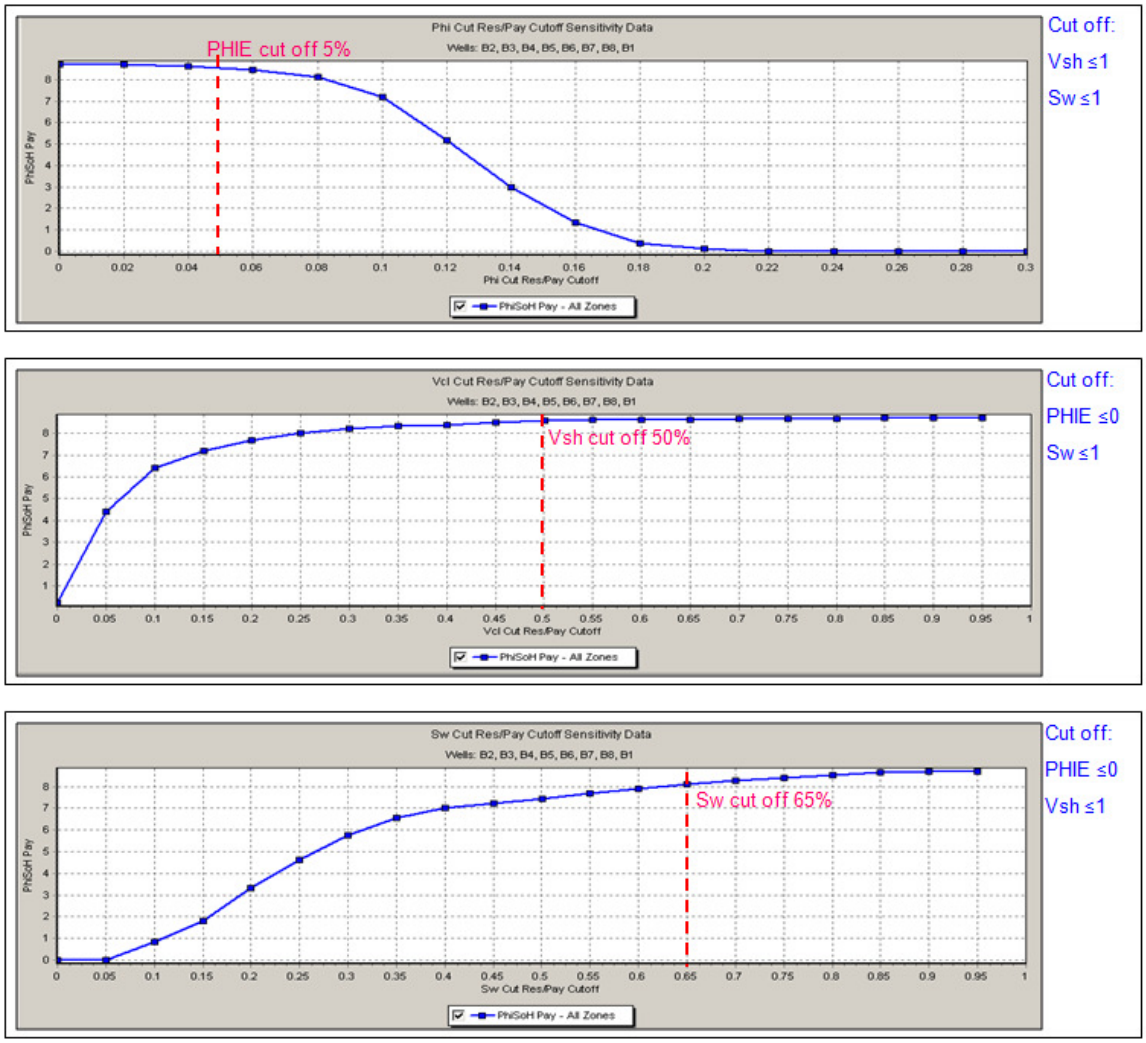

Figure 40. The sensitivity analyses to PHIE, V_{sh}, and S_{w}.

Table 9. Summary table of Upper Roabiba petrophysical properties.

Well	Reservoir	Gross TVT ft	Net Reservoir TVT ft	N/G decimal	Net Pay TVT ft	Av Phi frac	Av Sw decimal	Av Vsh decimal	Av Perm md
B2	UR	125.47	114.98	0.92	114.98	0.13	0.16	0.06	1335.34
B3	UR	12.48	12.08	0.97	12.08	0.14	0.33	0.08	1443.89
B4	UR	201.51	193.28	0.96	192.78	0.11	0.23	0.09	30.13
B5	UR	187.96	148.54	0.79	0.00	0.11	0.69	0.05	192.52
B6	UR	81.16	63.98	0.79	61.48	0.12	0.19	0.04	863.84

Table 10. Summary table of Lower Roabiba petrophysical properties.

Well	Reservoir	Gross TVT ft	Net Reservoir TVT ft	N/G decimal	Net Pay TVT ft	Av Phi frac	Av Sw decimal	Av Vsh decimal	Av Perm md
B1	LR	25.97	17.73	0.68	16.73	0.11	0.28	0.05	268.92
B2	LR	62.64	37.40	0.60	35.40	0.12	0.33	0.06	545.23
B3	LR	60.06	57.88	0.96	55.39	0.14	0.33	0.07	1207.84
B4	LR	60.87	45.98	0.76	43.48	0.12	0.32	0.07	208.82
B5	LR	118.22	88.11	0.75	0.00	0.10	0.80	0.09	331.62
B6	LR	30.36	27.86	0.92	23.86	0.13	0.41	0.21	1799.35
B7	LR	70.22	48.26	0.69	42.79	0.15	0.31	0.20	3372.58
B8	LR	22.32	16.99	0.76	11.99	0.09	0.60	0.21	27.58

5.5. HIGH PRESSURE MERCURY INJECTION CAPILLARY MEASUREMENTS

37 samples from wells B2, B3, and B4 were examined with MICP in order to quantify pore to pore throat relationships. The samples represent Upper and Lower Roabiba Sandstone reservoirs.

Results from the MICP provide 1) drainage curves for each sample based on mercury saturation at each incremental pressure point, 2) pore throat sizes. MICP curves contain useful information about reservoir rock characteristics. In addition to providing data on pore throat geometry, pore throat size sorting, and pore-pore throat connectivity, MICP analysis can be used to estimate permeability and recovery efficiency (Ahr, 2008). Table 11 summarizes the MICP values. The column of R_{35}, calculated using the Winland equation, is the pore aperture radius corresponding to the 35^{th} percentile of mercury saturation in a mercury porosimetry test.

Table 11. Summary table of MICP samples for B2, B3 and B4.

Well ID	Depth	Lithofacies	Core PHI (%)	Core K (md)	HPMI PHI (%)	HPMI K air (md)	Theshold Pressure (psia)	R35 (µm)
B2	9550	xls	15.7	835.547	16.08	582	3.7	20.680
B2	9651	ms	15.4	721.554	16.5	765.6	3.1	23.762
B2	9742	ms	15.2	324.386	16.06	305	6.3	14.158
B2	9680	mm			2.4	0.16	1523.3	0.862
B2	9689.5	bm			3.2	0.004	1248.9	0.077
B2	9703.4	lm			1.9	3.5	2508.5	6.472
B2	9721.5	lm			2.2	1.1	1515.2	2.887
B2	9759.8	lm			2.4	9.6	2492.2	9.574
B2	9776.5	mm			3.1	0.61	2500.3	1.518
B3	10370.1	sb3	12.3	0.258	15.51	2.46	59.6	0.857
B3	10453.1	ms	11.1	68.975	12.71	72.8	6.3	7.464
B3	10362.1	sb3	4.5	0.01	4.3	0.04	151.4	0.231
B3	10366.1	sb3	12.6	0.38	13.4	0.51	49.9	0.386
B3	10374.1	sb3	12.5	0.098	11.2	0.29	89.6	0.323
B3	10383.5	bm			2.9	0.008	401.1	0.126
B3	10393.6	lm			2.1	N/A	1986.7	
B3	10413.1	lls	16.3	0.095	16	0.267	150.3	0.226
B3	10416.9	lls	12.9	7.362	11.8	6.6	19.9	1.940
B3	10420.2	ms	13.6	861.274	13.3	821	2.0	29.828
B3	10423	xls-m	13.1	0.18	11.6	0.37	89.8	0.362
B3	10429.1	lls	11.1	0.298	9.4	0.12	173.9	0.224
B3	10441.2	sb2	12.3	0.742	11.9	0.86	50.1	0.581
B3	10448	xls	11.9	37.054	11.4	40.4	11.9	5.799
B3	10457.1	xls	17.5	342.606	16.8	404	2.0	16.065
B3	10462.1	sb3	12.5	0.023	12.3	0.058	150.2	0.116
B3	10470.1	xls	5.5	3.225	5.3	9.45	32.4	4.784
B3	10475.4	mm			3.6	N/A	1991.2	
B4	9999.1	sb1	16.1	382.783	16.13	351.4	4.0	15.330
B4	10033.1	sb3	11.4	0.445	12.48	1.4	34.8	0.743
B4	10079.2	xls	15.5	2104.418	15.8	2543	2.6	49.969
B4	10090.1	xls	14.4	1132.04	14.38	1180	2.4	34.511
B4	10192.1	ms	12.7	96.608	13.31	102.61	8.3	8.776
B4	10036.1	sb3	5.9	0.013	5.6	0.1	124.9	0.314
B4	10146	lm			1.8	N/A	1768.5	
B4	10129.8	bm			2.5	0.004	1754.9	0.095
B4	10161	lm			3.6	0.008	3493.8	0.104
B4	10221	lm	1.9	0.005	2	0.003	610.0	0.097

5.5.1. UPPER ROABIBA SANDSTONE MICP ANALYSIS

A drainage curves categorized by facies of the Upper Roabiba Sandstone are given for well B2, B3, and B4 samples (Figure 41). Characteristic capillary pressure curves for bioclastic mudstone lithofacies, bm, exhibit entry pressure typically above 400 psi.

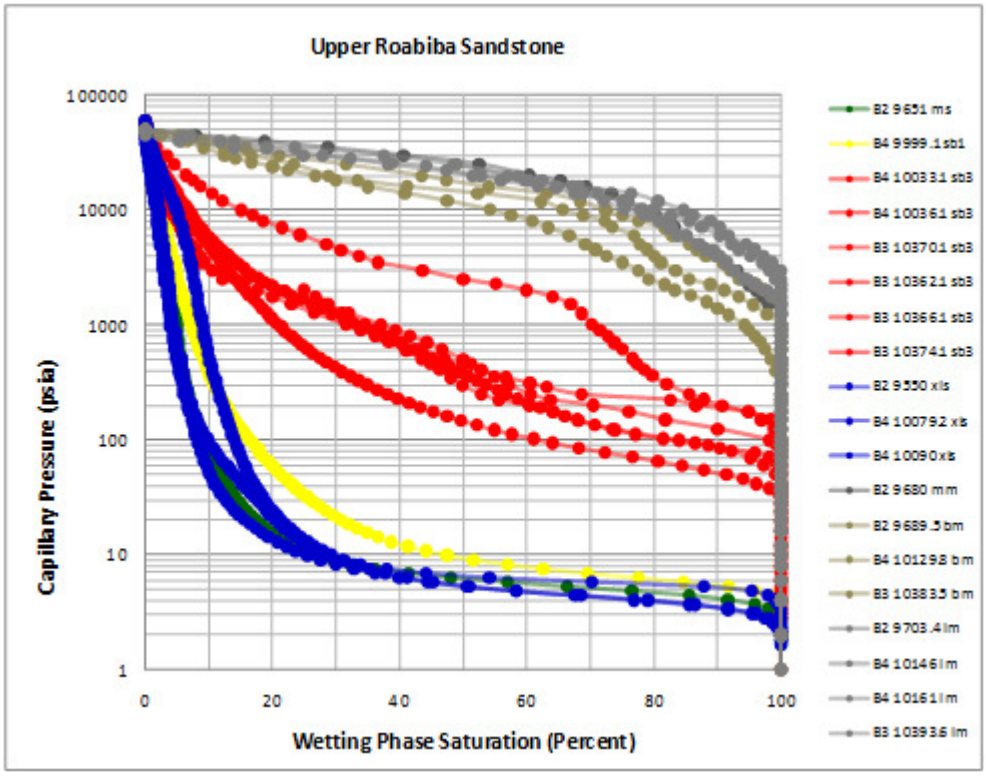

Figure 41. Mercury injection capillary pressure data for Upper Roabiba categorized by facies.

The massive and laminated mudstone lithofacies, mm and lm, have very high entry pressures above 1700 psi. Matrix-rich bioturbated sandstones, sb3, have variable threshold pressures ranging from 34 to 151 psi. The cleaner sandstone lithofacies, sb1, ms, and xls have lowest entry pressure, best aperture sorting, and greatest non-wetting

saturation at low pressure. To quantify the dominant pore throat dimension, pore throat radius were plotted against incremental mercury saturation (Figure 42).

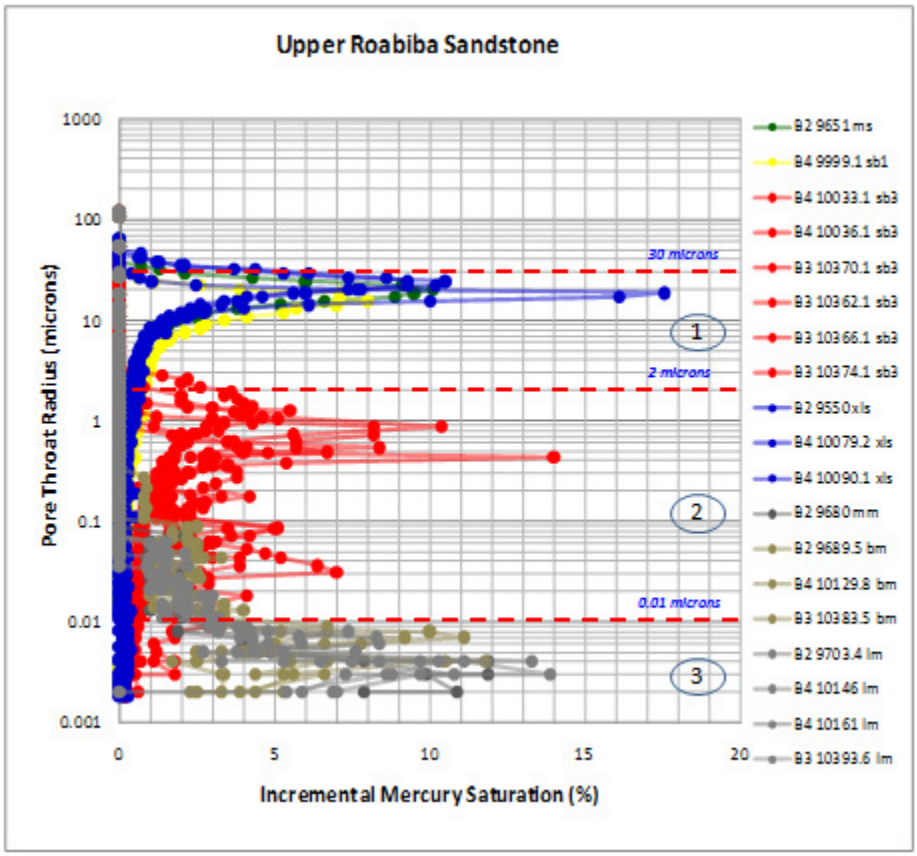

Figure 42. Identification of rock types from dominant pore throat dimensions.

Using the plot, three different rock types can be grouped according to the following pore throat radius:

- Rock type 1: r > 10 microns (best reservoir rock)
- Rock type 2: 0.01 microns < r ≤2 micron (low-quality reservoir rock)
- Rock type 3: 0.01 microns ≤ r microns (non reservoir rock)

The best reservoir rock or rock type 1 includes lithofacies ms, sb1, and xls. Rock type 2 consists of lithofacies sb3. Rock type 3 is mudstone and siltstone lithofacies.

A semilog plot of porosity-permeability and Winland R_{35} lines for dominant pore throat radii of 0.1, 0.5, 2, 5, 20, and 30 microns is shown below (Figure 43). Note that rock type 3 is not plotted since it is a non-reservoir rock.

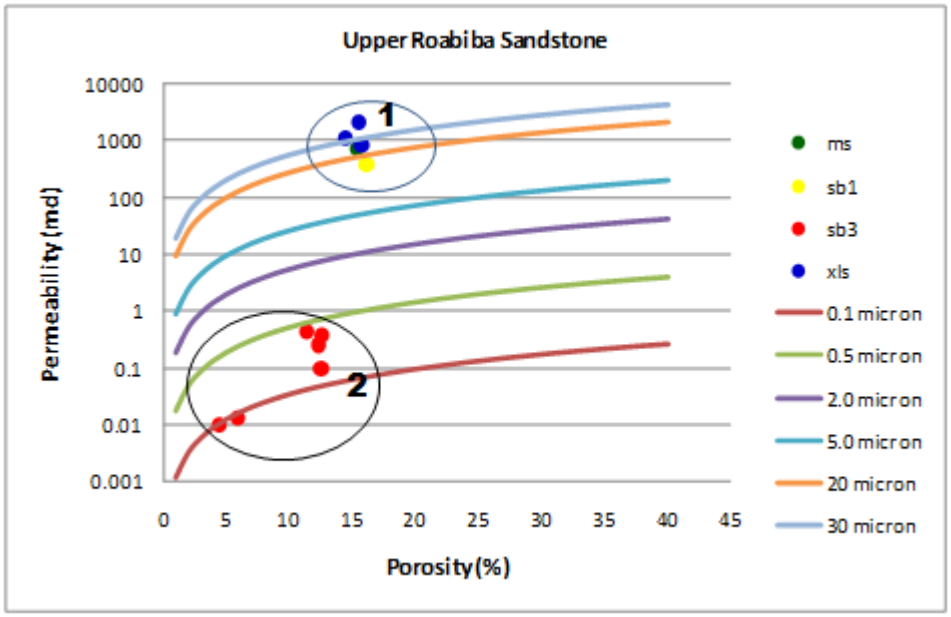

Figure 43. Winland's plot of permeability against porosity for various rock types in Upper Roabiba Sandstone.

The grouping of data points located within each ellipse represents the range of permeability and porosity for each rock type. According to the plot, two different rock types can be grouped as follows:

- Rock type 1: ms, xls, and sb1 lithofacies (high-quality reservoir rock)
- Rock type 2: sb3 lithofacies (low-quality reservoir rock)

5.5.2. LOWER ROABIBA SANDSTONE MICP ANALYSIS

A drainage curves categorized by facies of the Lower Roabiba Sandstone in wells B2, B3, and B4 is shown below (Figure 44). Mudstones and siltstones lithofacies (mm and lm) exhibit very high displacement pressure (greater than 600 psi). Lithofacies sb3 shows displacement pressure at 150 psi. Lithofacies sb2, lls, and xls-m exhibit displacement pressures ranging from 20 to 174 psi. The cleaner sandstone lithofacies, xls and ms, show the lowest entry pressures ranging from 2 to 32 psi.

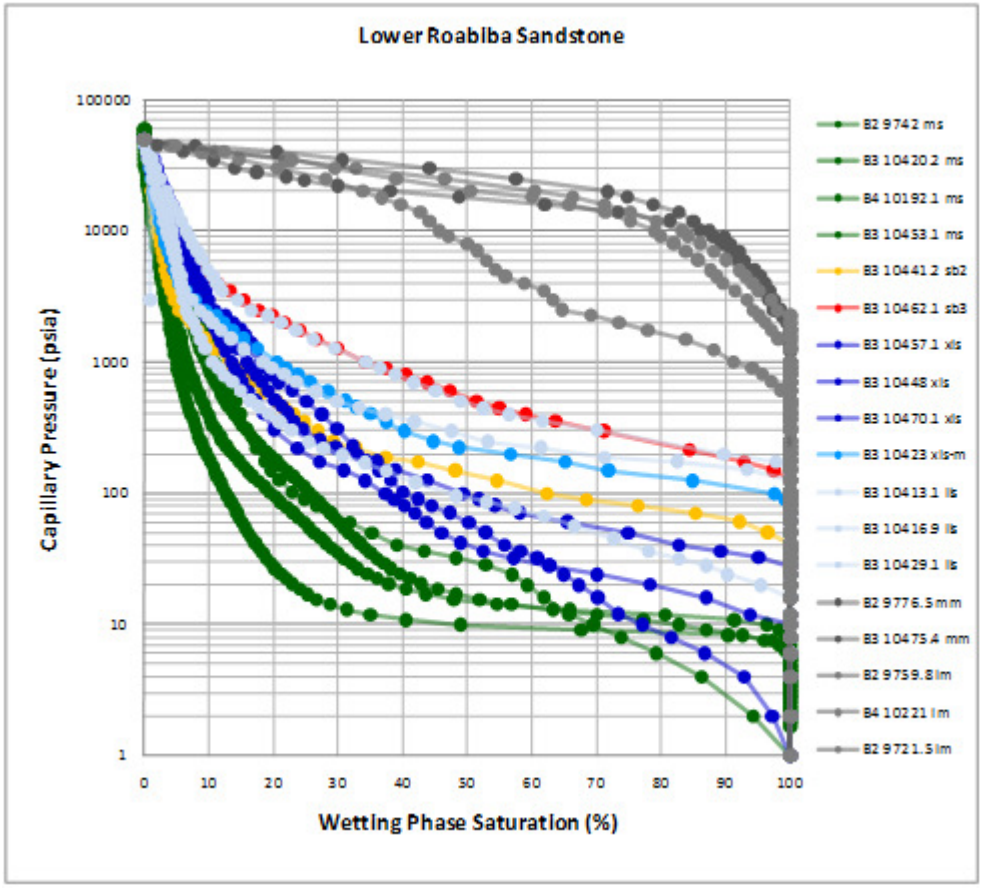

Figure 44. Mercury injection capillary pressure data for Lower Roabiba categorized by facies.

Next, to quantify the dominant pore throat dimension, pore throat radius was plotted against incremental mercury saturation (Figure 45).

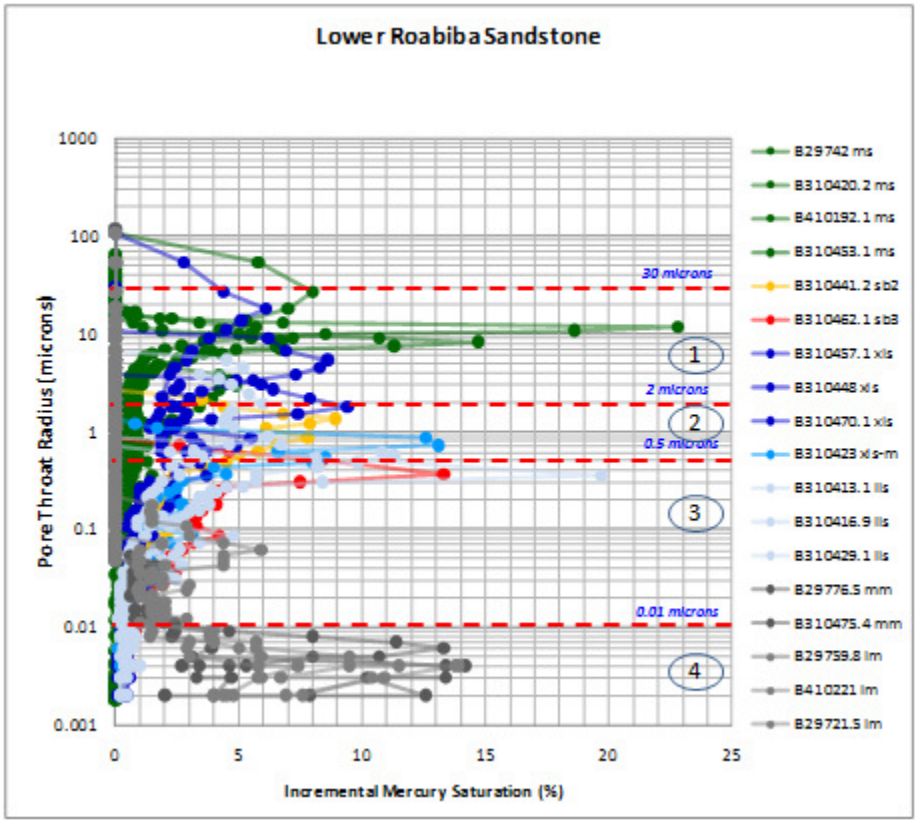

Figure 45.Identification of rock types from dominant pore throat dimensions in Lower Roabiba Sandstone.

Using the plot, four different rock types can be grouped according to the following pore throat radius:

- Rock type 1: $r > 2$ microns (best reservoir rock)
- Rock type 2: 0.5 microns $< r \leq 2$ microns (medium-quality reservoir rock)
- Rock type 3: 0.01 microns $< r \leq 0.5$ microns (low-quality reservoir rock)
- Rock type 4: 0.01 microns $\leq r$ microns (non-reservoir rock)

Rock type 4 is mudstone-siltstone lithofacies. The best reservoir or rock type 1 includes lithofacies ms and xls. Rock type 2 consists of lithofacies sb2, lls, and xls-m. Rock type 3 consists of sb3 lithofacies.

A semilog plot of porosity-permeability and Winland R_{35} lines for dominant pore throat radii of 0.1, 0.5, 2, 5, 20, and 30 microns is shown below (Figure 46). Note that rock type 4 is not plotted since it is a non-reservoir rock.

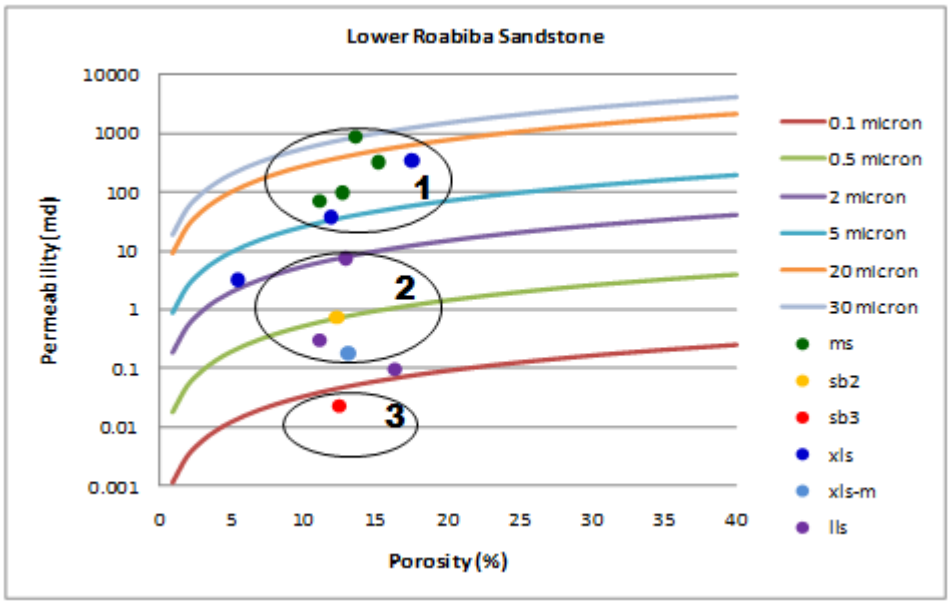

Figure 46. Winland's plot of permeability against porosity for various rock types in Upper Roabiba Sandstone.

The grouping of data points located within each ellipse represents the range of permeability and porosity for each rock type. According to the plot, three different rock types can be grouped as follows:

- Rock type 1: ms and xls lithofacies (best reservoir rock)
- Rock type 2: sb2, lls, and xls-m lithofacies (medium-quality reservoir rock)
- Rock type 3: sb3 lithofacies (low-quality reservoir rock)

Rock type 3 is the same as rock type 2 of Upper Roabiba Sandstone.

Based on Winland's plot in Upper and Lower Roabiba Sandstones, totally four rock types could be identified as follows:

1. Rock type 1: ms, xls, and sb1 (best reservoir rock)
2. Rock type 2: sb2, lls, and xls-m (medium-quality reservoir rock)
3. Rock type 3: sb3 (low-quality reservoir rock)
4. Rock type 4: mm, lm, bm (non reservoir rock)

6. DISCUSSION AND INTERPRETATION

Results of this study show that there is a strong relationship between lithofacies and reservoir performance characteristics in Bintuni field. The illustrations of the relationship between lithofacies and porosity-permeability values for 632 core samples in chapter 3 show that the lithofacies ms, xls, and sb1 have the highest porosity-permeability values.

From data trends in both Upper and Lower Roabiba capillary pressure measurement plots, four distinct petrophysical rock types can be assigned in this field. Table 12 summarizes the attributes of each petrophysical rock type.

Table 12. Summary table of typical attributes of petrophysical rock types.

Petrophysical Rock Type	Lithofacies	Porosity Range (%)	Permeability range (md)
1	ms, xls, sb1	6 - 18	70 – 2100
2	sb2, lls, xls-m, bs	11-16	0.1 -383
3	sb3	5 - 13	0.01 - 10
4	mm, lm, bm	2 - 4	0.003 - 1

Petrophysical rock type 1 (R1) is the best reservoir rock and is dominated by ms, xls, and sb1 lithofacies with the average permeability values over 100 md and porosity greater than 10%. R2 exhibits the average porosity up to 16% and permeability less than 400 md. R3 is found to have the least favorable petrophysical flow properties. R4 is a non-reservoir rock. A cross-section of the NW-SE area along the strike direction displays the distribution of R1 (Figure 47).

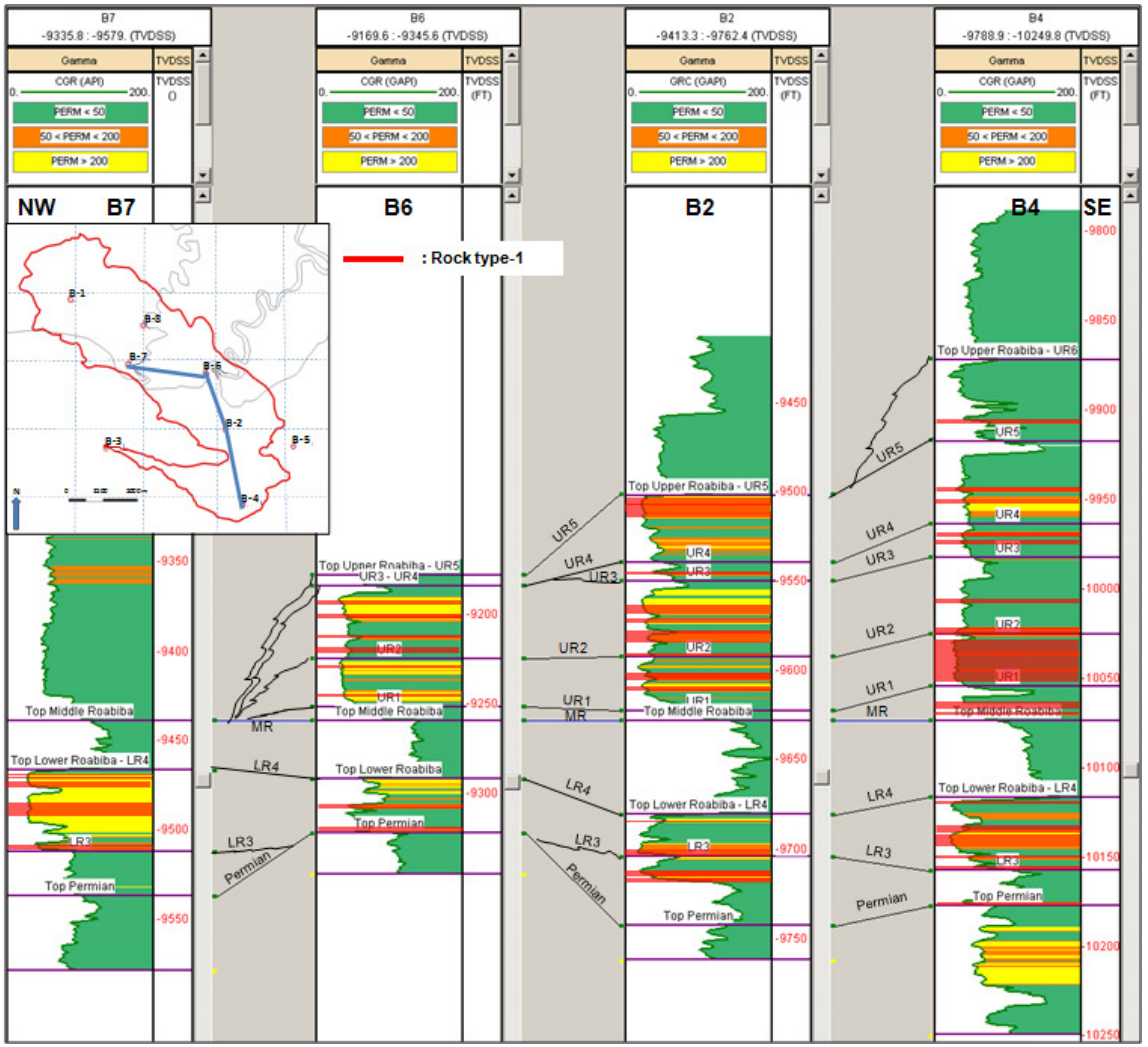

Figure 47. Cross-section in NW-SE direction showing distribution of rock type-1.

The interpretation of the R1 location is based on the distribution of lithofacies in this rock type found in the well and is limited by the permeability value greater than 50 md. R1 accounts for nearly 67% of Upper Roabiba Sandstone lithofacies and 53% of Lower Roabiba Sandstone lithofacies. R1 is found in almost every zone and concentrated most in zone UR2 in Upper Roabiba Sandstone reservoir and LR4 in Lower Roabiba Sandstone reservoir. R1 has average grain size lower medium, moderately well sorted, and low clay content (<4%). The associated lithofacies depositions are tidal sandbar and upper shoreface in Upper Roabiba Sandstone and estuarine channel in Lower Roabiba Sandstone. Accumulations appear to thin in the north since the Upper Roabiba Sandstone is truncated in this direction, and it also needs to be taken into account that the down-dip distribution is limited by GWC.

R3 accounts for nearly 18% of Upper Roabiba Sandstone lithofacies and 10% of Lower Roabiba Sandstone lithofacies. R3 is found in almost every zone and concentrated most in zone UR9 in Upper Roabiba Sandstone reservoir and zone LR3 in Lower Roabiba Sandstone reservoir. R3 has average grain size upper fine, moderate to well sorted, and high clay content (7%). The grain-coating/pore lining clay development is a common diagenesis in this rock type. The associated lithofacies depositions are lower shoreface and marsh. The cross-sections of the NW-SE area along the strike direction display the distribution of R3 and R2 and are attached in the Appendix E.

7. SUMMARY AND CONCLUSIONS

7.1. SUMMARY

Core analysis led to identification of two reservoirs divided into seven zones in the Upper Roabiba Sandstone reservoir and two zones in the Lower Roabiba Sandstone reservoir based on palynostratigraphy study. Ten lithofacies were identified from core descriptions: massive sandstone (ms), bioturbated sandstone (sb1), matrix-rich moderately to intensely bioturbated sandstone (sb2-sb3), cross-laminated sandstone to matrix rich cross-laminated sandstone (xls- xls-m), low-angle laminated sandstone (lls), bioclastic sandstone (bs), laminated mudstone (lm), bioturbated mudstone (bm), and massive mudstone (mm). The associated depositional facies are upper shoreface, lower shoreface, tidal sandbar, estuarine channel, marsh, and offshore.

Diagenesis, including mechanical compaction, cementation from quartz overgrowths, calcite cementation, grain-coating/pore lining clay development, and grain dissolution, has altered rocks in the study area. Porosity and permeability were enhanced by dissolution and reduced by cementation and compaction.

Petrophysical evaluation of the Upper and Lower Roabiba Sandstones generated average values for petrophysical properties. The average Sw in the Upper Roabiba ranges from 15 to 70 percent while it is 30 to 80 percent in Lower Roabiba. B5well is wet and contains only residual gas. B4 well has the thickest net pay (193ft) in the Upper Roabiba Sandstone, which also has the greatest net reservoir thickness (193ft) in the field. Total net pay from both reservoirs is 611ft.

Based on porosity-permeability plots, lithofacies ms, xls, and sb1 have the highest average permeability (>100md) and porosity greater than 10%. They are found mostly in zones UR2 and LR4. Zone UR2 is associated to depositional environment of tidal upper shoreface and zone LR4 to estuarine channel.

Lithofacies sb3 has low average permeability (<10md) and porosity (<10%) and it is found almost in every zone. Lithofacies sb3 is associated to depositional environments lower shoreface, marsh, and estuarine.

High pressure mercury injection capillary data and the Winland method illustrated that petrophysical properties have a strong relationship with lithofacies. From this development, four petrophysical rock types were defined and characterized. Petrographic rock type 1 (the best reservoir rock) consists of lithofacies ms, xls, and sb1. Therefore, these lithofacies may be used as a pore-proxy rock property for the determination of best reservoir rock and corresponding flow units at the reservoir scale.

7.2. CONCLUSIONS

- Lithofacies were the basis for recognition and discrimination of facies on the core and logs. The study has recognized three major unit lithofacies that comprise bioturbated sandstones, cross-bedded sandstones, and siltstones-mudstones.
- The facies were associated with depositional environment tidal dominated shoreface delta to shoreline.
- The reservoir thickness found related to the depositional strike NW-SE and getting thicker to the south. GWC limits the field area.

- The average S_{hc} value in Upper and Lower Roabiba reservoirs varies from 20 to 84 percent.
- By plotting the lithofacies-based petrophysical properties, it can be inferred that porosity has no unique relationship for any lithofacies. On the other hand, permeability shows a strong relationship with the lithofacies. Therefore, porosity is not necessarily a good indicator of reservoir quality.
- The best reservoir rock is associated with lithofacies ms, xls, and sb1 based on porosity-permeability plots.
- When grouped according to the dominant pore throat dimension, distinct collections or grouping of rocks and their associated lithofacies were observed.
- Winland plot was engaged to do clustering of rock types since Winland $_{R35}$ pore port sizes represent 'cut off values' for good and bad flow unit quality. It is confirmed with Winland plots that the best reservoir rock (rock type 1) consists of lithofacies ms, xls, and sb1.
- Rock types 1 is found mostly in zones UR2 and LR4 Therefore, the associated lithofacies (ms, xls, and sb1) may be used as a pore-proxy rock property for the determination of best reservoir rock and corresponding flow units at the reservoir scale. The distribution of rock type 1 was defined by locating the associated lithofacies and high porosity-permeability values.
- The connectivity between layers is still unknown. To investigate pressure communications, perforating different parts of the stratigraphic sections in different wells should be integral part of the initial development.

- As a suggestion to characterize the same field as this case, a detail lithofacies defined from core should be developed instead of electrofacies and depositional facies, followed by petrophysical rock typing to guide field development activities.

REFERENCES CITED

Ahr, W. M., 2008, Geology of Carbonate Reservoirs: The Identification, Description, and Characterization of Hydrocarbon Reservoirs in Carbonate Rocks, New Jersey, John Wiley & Sons, Inc., Publication, p. 66-69.

Casarta, L.J., J.P.Salo, S. Tisnawidjaja, S. Sampurno, 2004, Wiriagar Deep: The discovery that triggered Tangguh LNG, Proceedings of the 2004 Deepwater and Frontier Exploration in Asia and Australasia Symposium, Indonesian Petroleum Association and American Association of Petroleum Geologists, DFE04-OR-016, p. 137-157.

Darling, T, 2005, Well Logging and Formation Evaluation, Oxford, Elsevier, p. 1.

Dolan, P. J., and Hermany, 1988, The Geology of the Wiriagar Field, Proceedings Seventeenth Annual Convention, Indonesian Petroleum Association, v. 1, p.53-87.

Emery, D., K. Myers, and G.T. Bertram, 1996, Sequence Stratigraphy, Massachusetts, Blackwell Publishing Company, p. 238-258.

Hamilton, W., 1979, Tectonics of Indonesian Region, US Geological Survey Professional Paper, 1078, 345 pp.

Kasim, A. T., I. Titus, J.W. Roberts, and T.P. Bulling, 2000, The Tangguh LNG gas fields: conceptual development overview. Paper SPE 64706 presented at the SPE International Oil and Gas Conference and Exhibition, Beijing, China, 7-10 November.

Livsey, A.R., N. Duxbury, F. Richards, 1992, The geochemistry of tertiary and pre-tertiary source rocks and associated oils in eastern Indonesia, Proceedings of the Twenty First Annual Indonesian Petroleum Association Convention, v. 1, p. 500-520.

Marcou, J. A., D. Samsu, A.T. Kasim, Meizarwin, N. Davis, 2004, Tangguh LNG's gas resource: discovery, appraisal and certification, Proceedings of the 2004 Deepwater and Frontier Exploration in Asia and Australasia Symposium, Indonesian Petroleum Association and American Association of Petroleum Geologists, DFE04-OR-021, p.159-176.

Naar, J., A.T. Kasim, M.S. Hendrawati, J.S. Petler, Zulfikri, 2008, Jurassic Reservoir Description – an internal presentation and discussion of BP Tangguh Reservoir and Well Team in Jakarta, Indonesia, on the field development project report (unpublished).

Perez,H.H., A. Datta-Gupta, and S. Mishra, 2003, The Role of electrofacies, lithofacies, and hydraulic flow units in permeability predictions from well logs: A comparative analysis using classification trees. Paper SPE 84301 presented at the SPE Annual Conference and Exhibition, Denver, Colorado, 5-8 October.

Perkins, T.W. and A.R. Livsey, 1993, Geology of the Jurassic gas discoveries in Bintuni Bay, Western Irian Jaya, Proceedings of the 1993 Twenty Second Annual, Indonesian Petroleum Association, v.1, IPA93-1.1-023, p. 793-830.

Porras, J.C., Barbato, R., and Khazen, L., 1999, Reservoir flow units: A comparison between three different models in the Santa Barbara and Pirital Fields, North Monagas Area, Eastern Venezuela Basin. Paper SPE 53671 presented at the SPE Latin American and Caribbean Petroleum Engineering Conference, Caracas, Venezuela, 21-23 April.

Purcell, W.R., 1949, Capillary pressure-their measurement using mercury and the calculation of permeability therefrom, American Institute of Mechanical Engineers, Petroleum Transaction, v. 186, p. 39-48.

Rushing, J.A., K.E. Newsham, and T.A. Blasingame, 2008, Rock typing: keys to understanding productivity in tight gas sands. Paper SPE 114164 presented at the SPE Unconventional Reservoirs Conference, Colorado, USA, 10-12 February.

Salo, J.P., 2005, Evaluating sites for subsurface CO2 injection/sequestration: Tangguh, Bintuni Basins, Papua, Indonesia, a doctoral thesis, The University of Adelaide, Australia, p.108-113.

Scheihing, M. H. and C.D. Atkinson, 1992, Lithofacies and environmental analysis of clastic depositional systems in development geology reference manual, AAPG Methods in Exploration Series, no.10, p. 263.

Soeder, D.J., 1986, Laboratory drying procedures and the permeability of tight sandstone core, SPE Formation Evaluation, v.1, p. 16-25.

Winland, H.D., 1972, Oil accumulation in response to pore size changes, Weyburn field, Saskatchewan: Amoco Production Company Report F72-G-25, 20 p. (unpublished).

Yoshino, H., T. Tanaka, H. Yamaguchi, 2003, Petroleum geology in Bintuni Basin in East Indonesia – A case study of exploration and evaluation of giant gas fields, Journal of the Japanese Association for Petroleum Technology, v. 68, no.2-3, p. 200-210.

SUPPLEMENTAL SOURCES CONSULTED

Archie, G.E., 1950, Introduction to petrophysics of reservoir rocks, AAPG Bulletin, v. 34, p. 943-961.

Hartmann, D.J. and Beaumont, E.A., 1999, Chapter 9: Prediction reservoir system quality and performance, Volume Treatise of Petroleum Geology/Handbook of Petroleum Geology: Exploring for Oil and Gas Traps, p. 1-154.

Keho, T., and Samsu, D., 2002, Depth Conversion of Tangguh Gas Fields, in Society of Exploration Geophysicists Journal, The Leading Edge, October 2002, p. 966-971.

Newsham, K.E. and J.A. Rushing, 2001, An integrated work-flow process to characterize unconventional gas resources: part geological assessment and petrophysical evaluation. Paper SPE 71351 presented at the SPE Annual Technical Conference and Exhibition, New Orleans, Lousiana, 30 Sept.-3 Oct.

Swanson, R.G., 1981, Sample examination manual: AAPG Special Publication no.92, p. 1-35.

APPENDIX A

CORE DESCRIPTION and STRATIGRAPHIC COLUMN

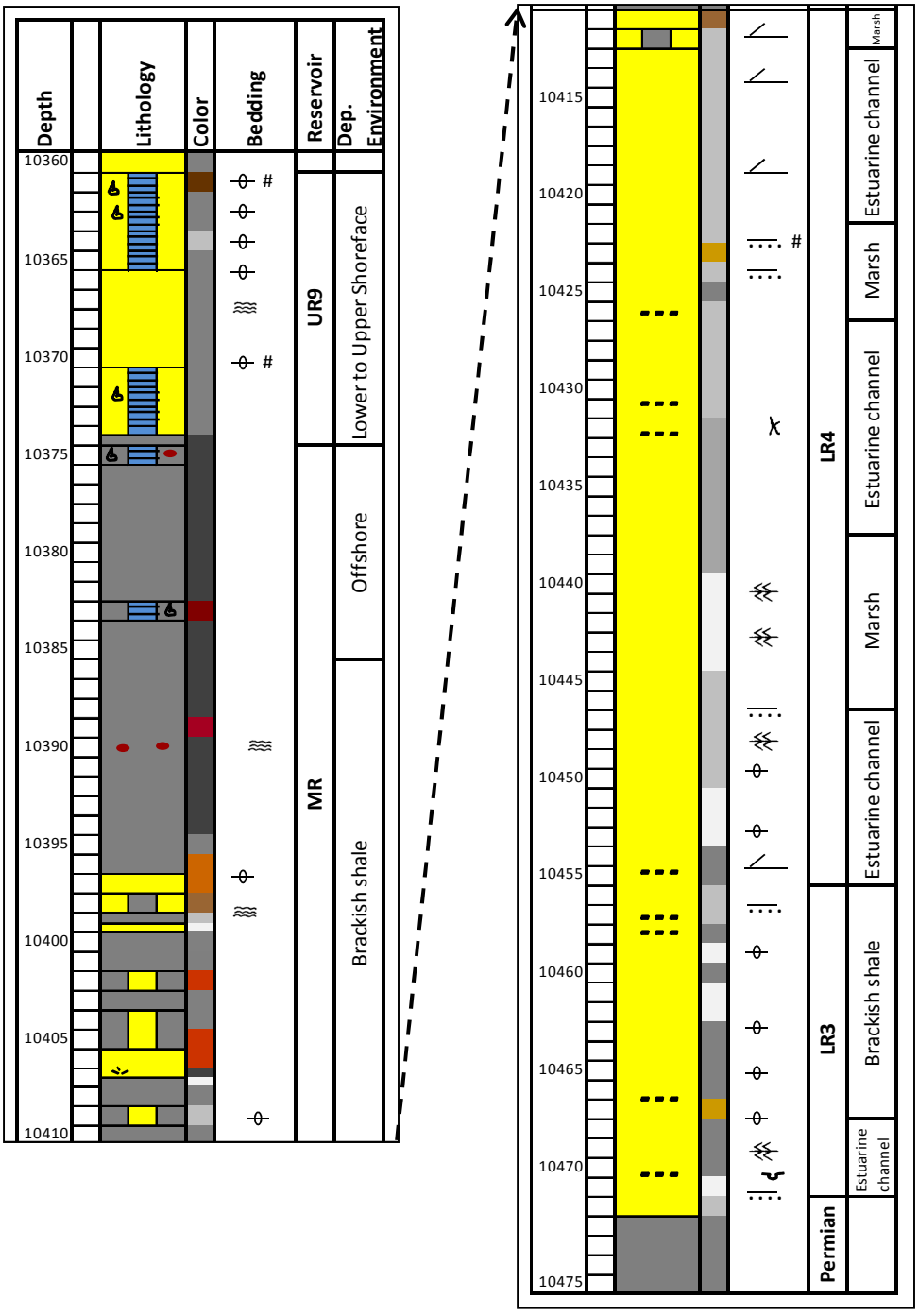

B3 well core description and stratigraphic column

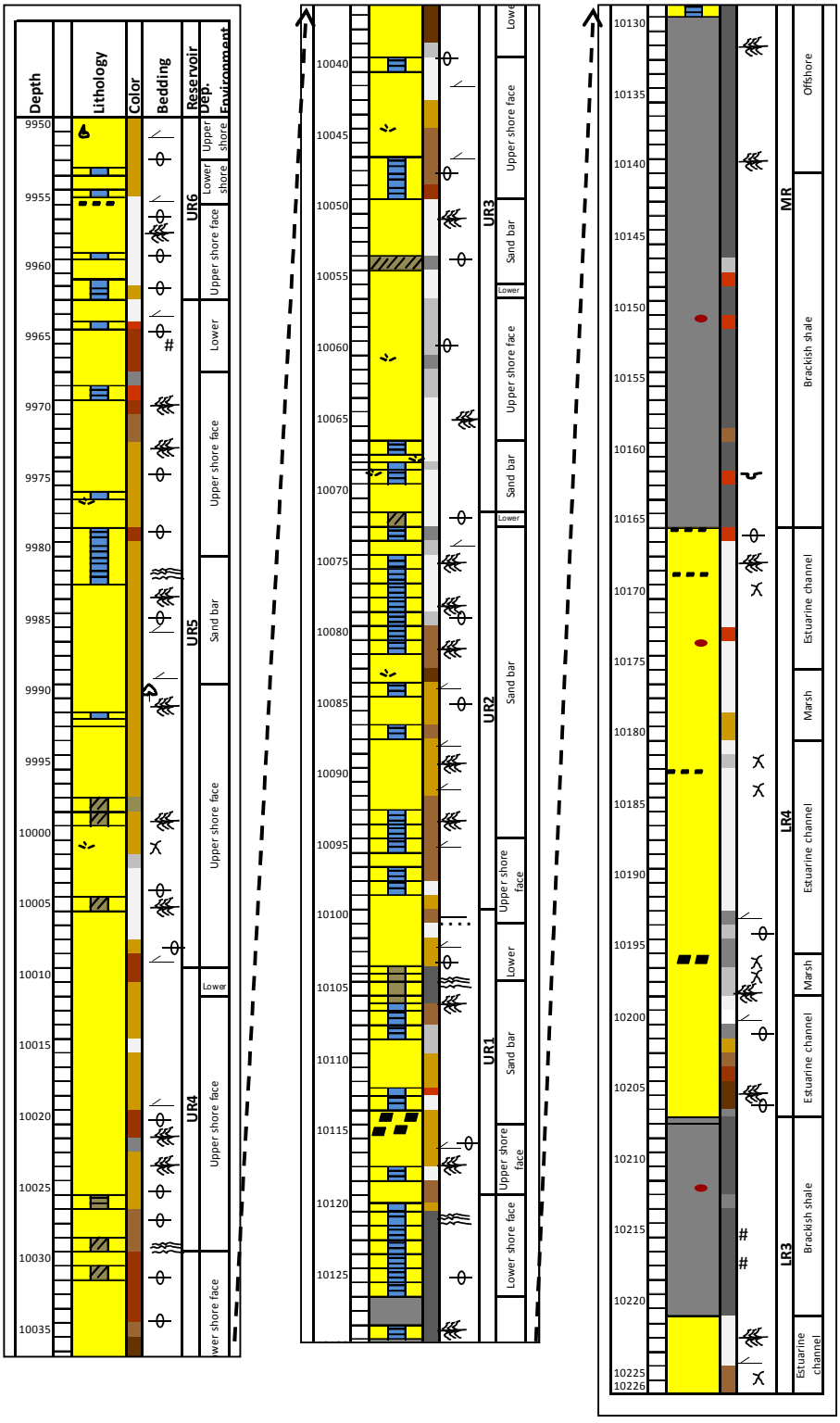

B4 well core description and stratigraphic column

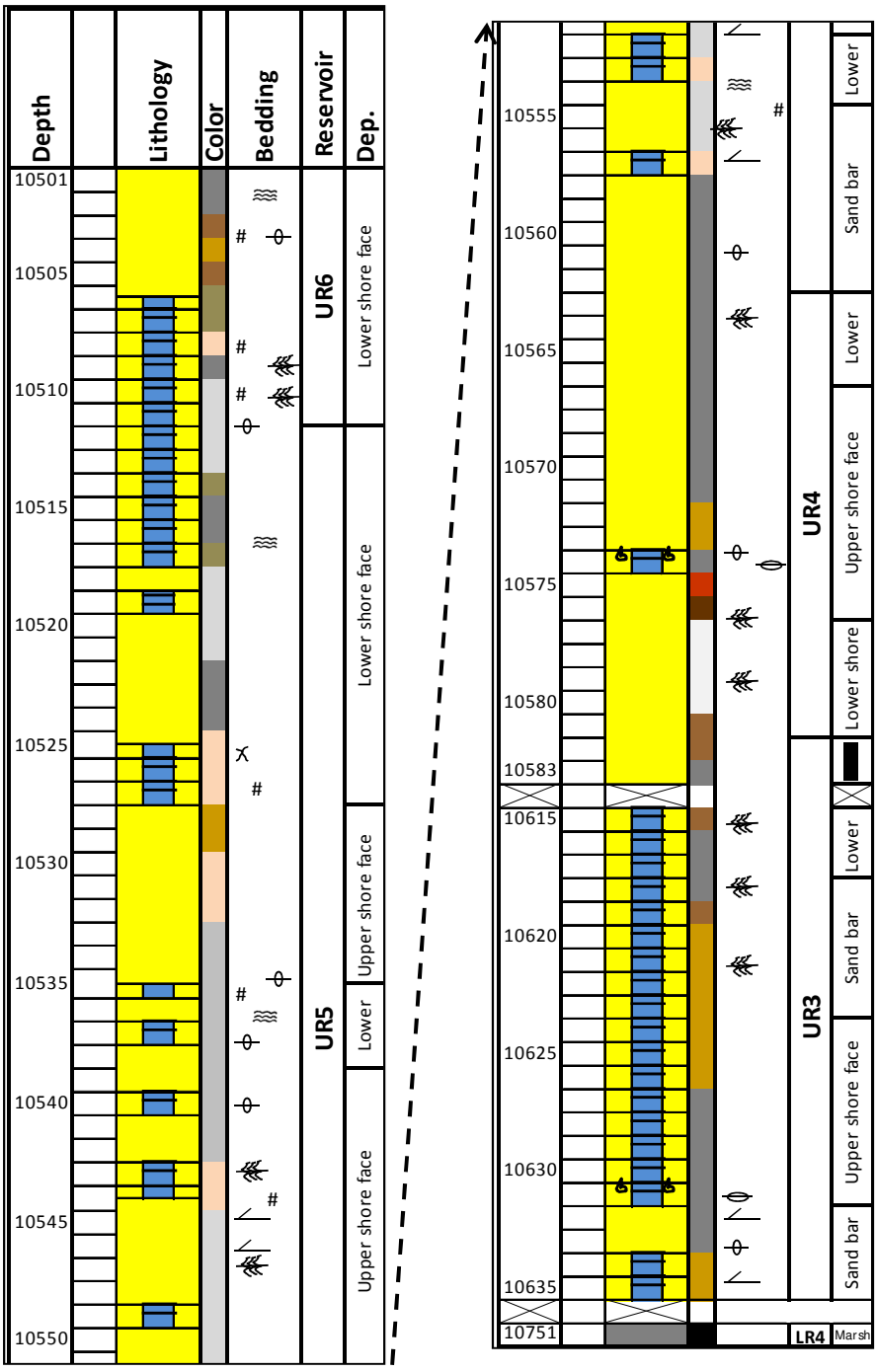

B5 well core description and stratigraphic column

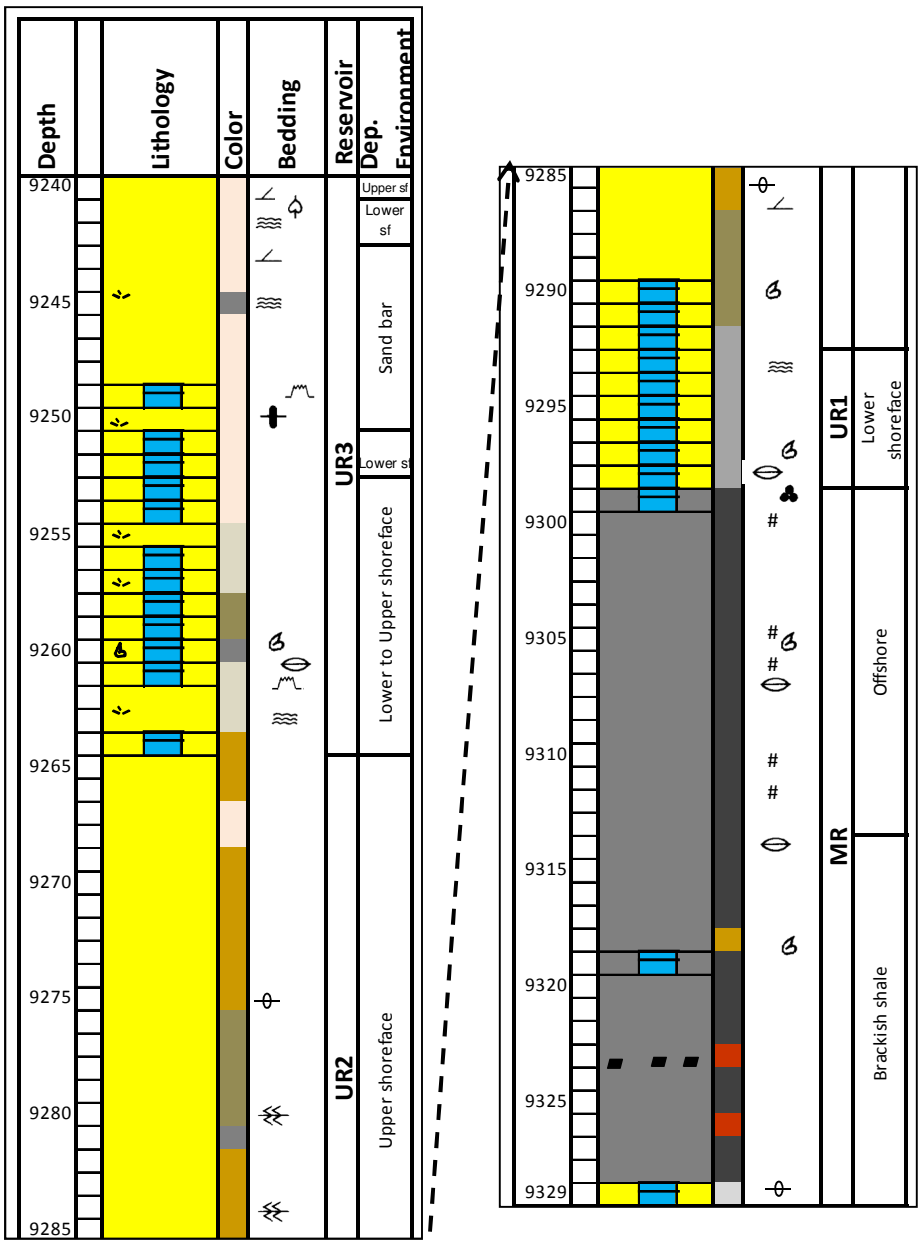

B6 well core description and stratigraphic column

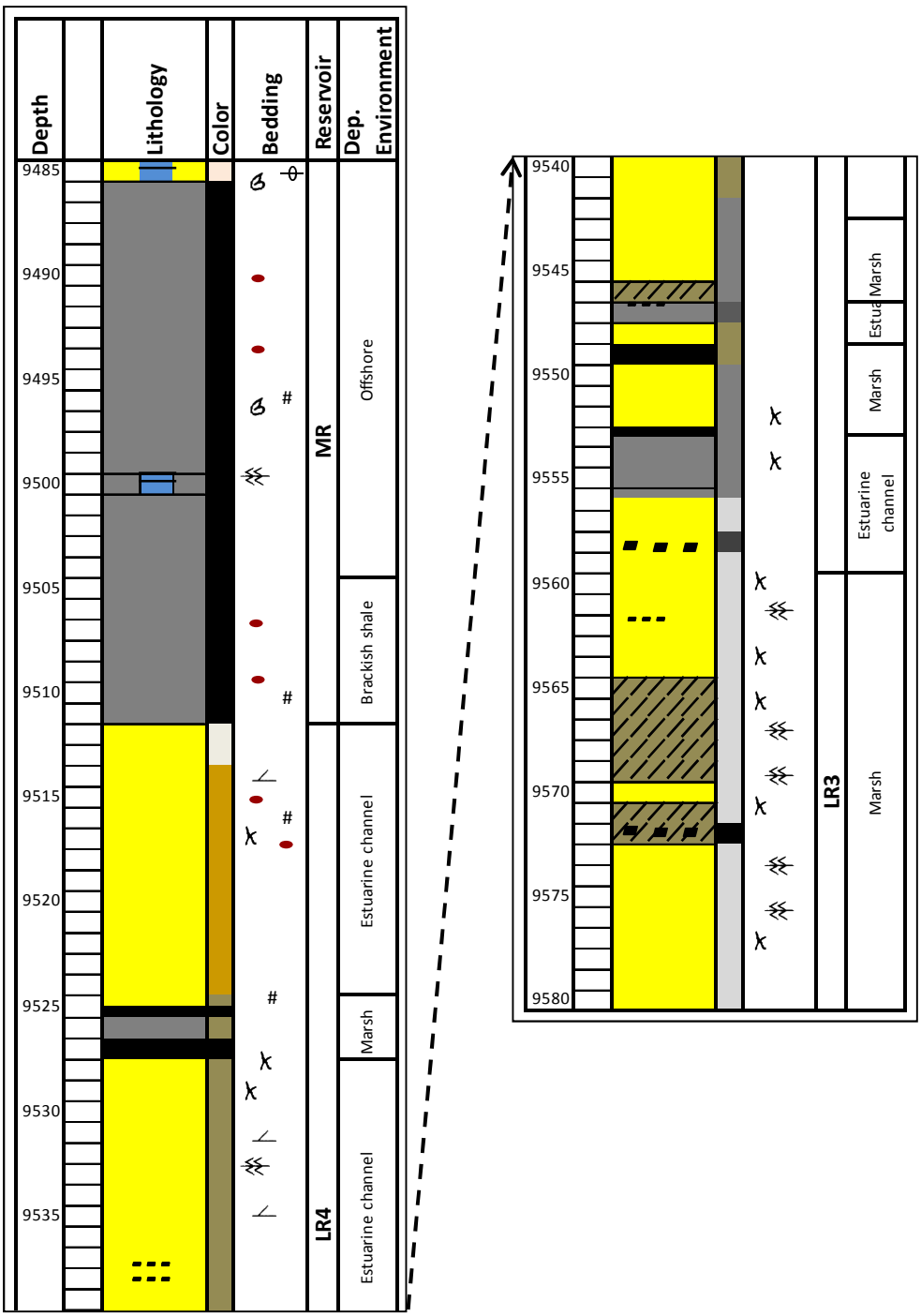

B7 well core description and stratigraphic column

Legends

Lithology

 : Mudstone / shale

 : Sandstone

 : Coal

 : Siltstone

 : Calcite cement

Symbol

 : Macrofossil fragments, undifferentiated

 : Molluscs, undifferentiated

 : Foraminifera, undifferentiated

 : Sublithic

 : Lignite / carbonaceous matter

 : Plant remains

 : Plant root tubes

 : Pyrite

 : Nodules

 : Bored

 : Burrowed

 : Irregular bedding

 : Cross bedding

 : Graded bedding

 : Load cast

 : Fractures

 : Dissolution-compaction

 : Stylolite

APPENDIX B

WELL LOG ANALYSES

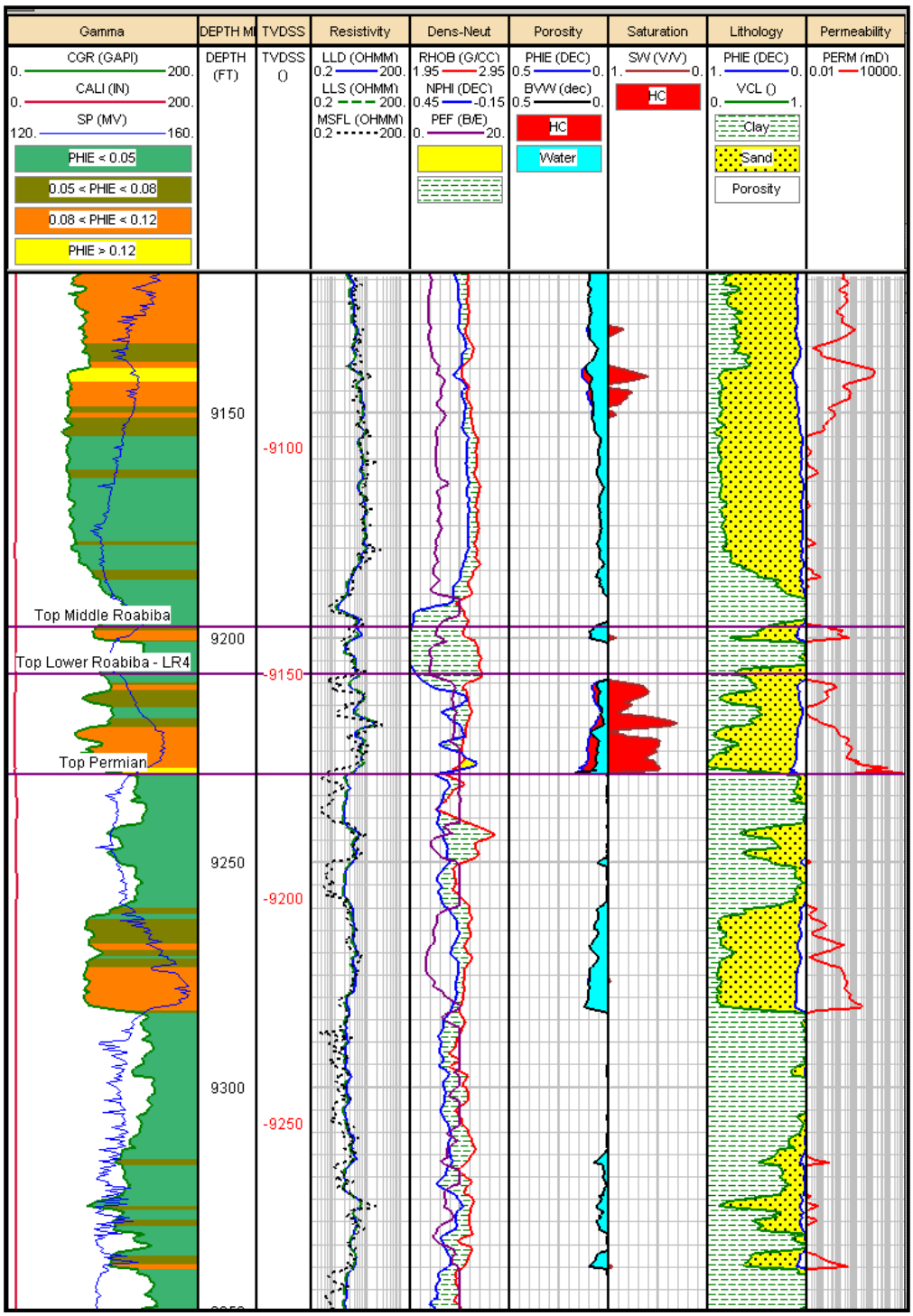

B1 well log analysis

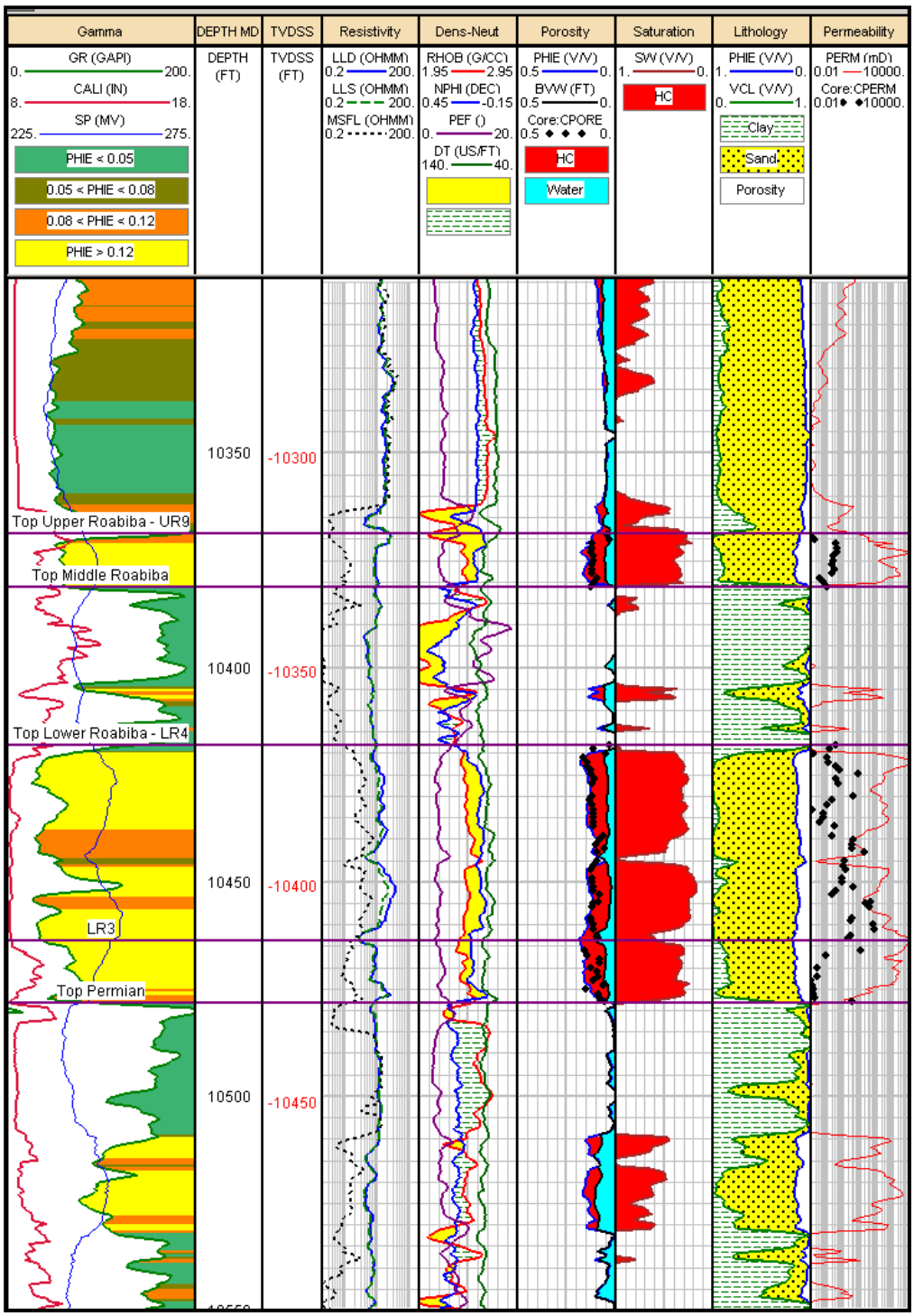

B3 well log analysis

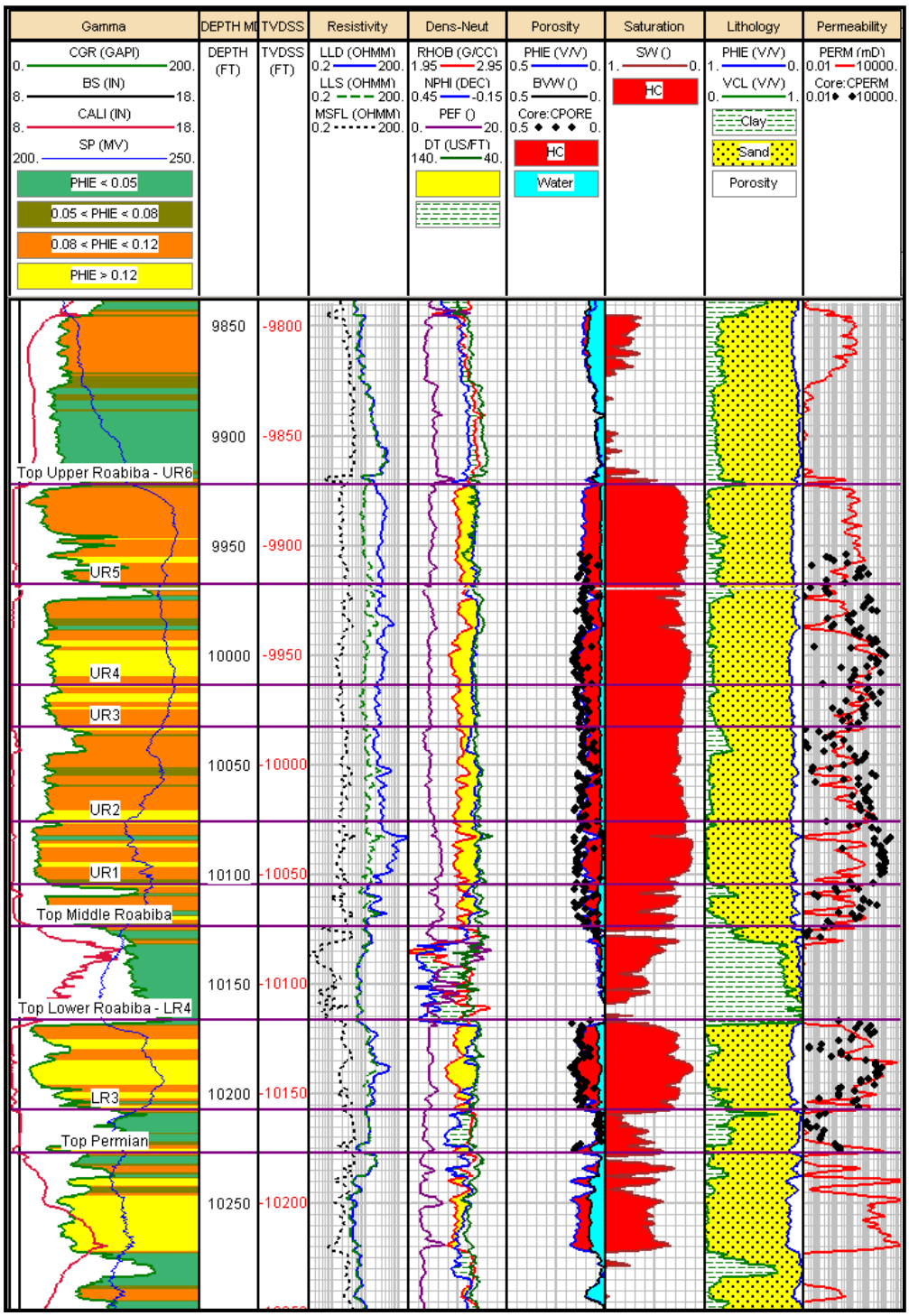

B4 well log analysis

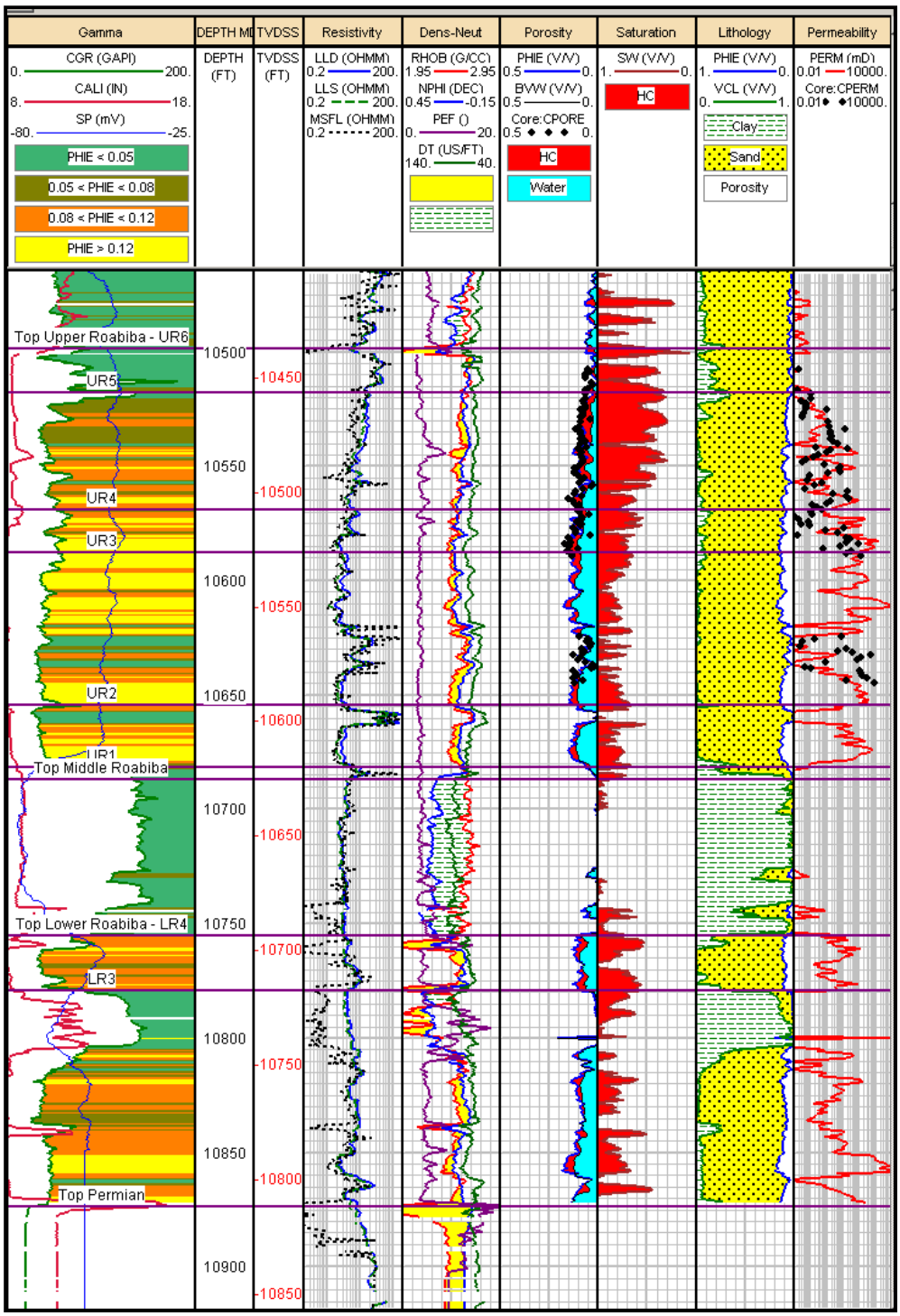

B5 well log analysis

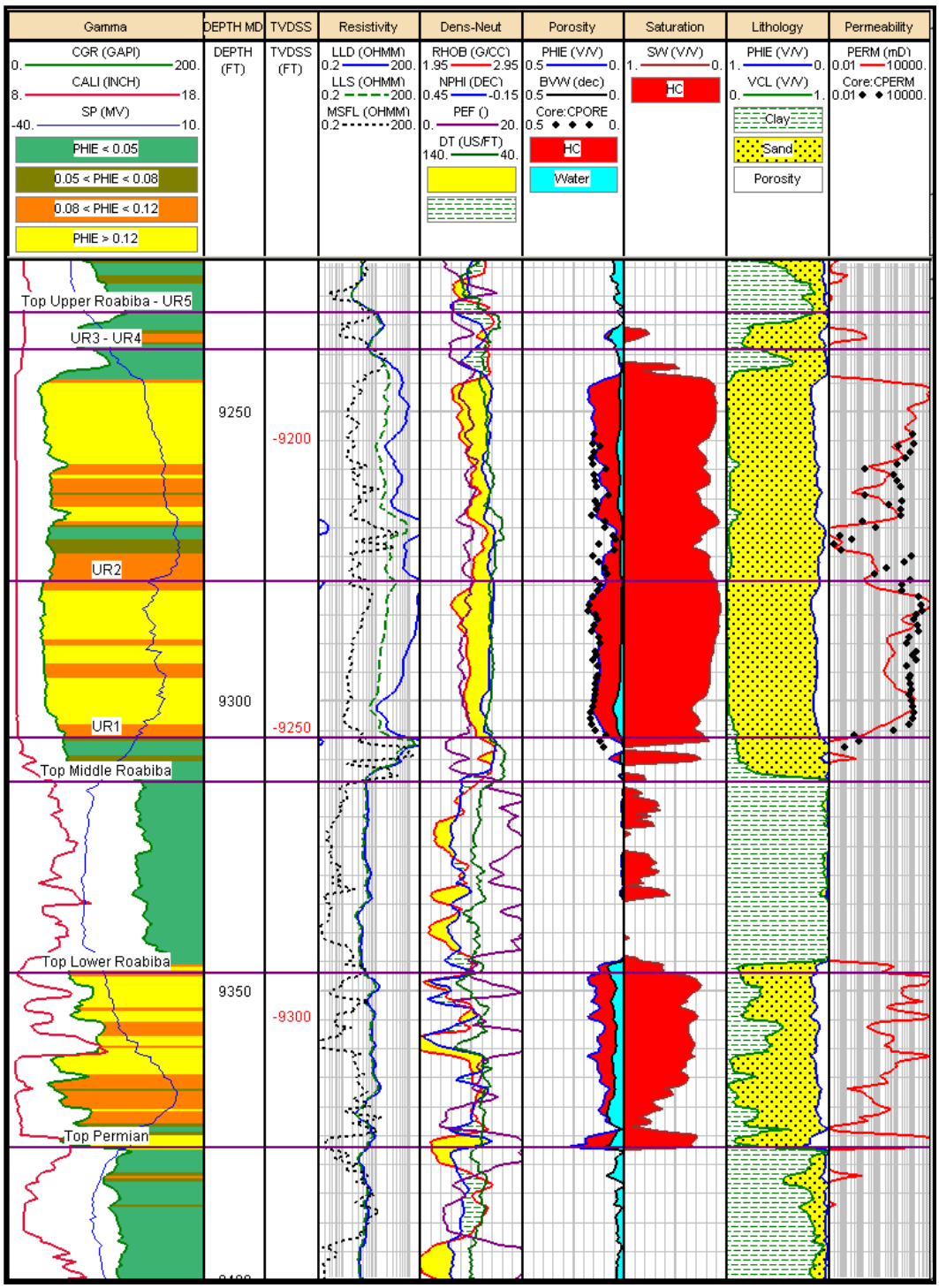

B6 well log analysis

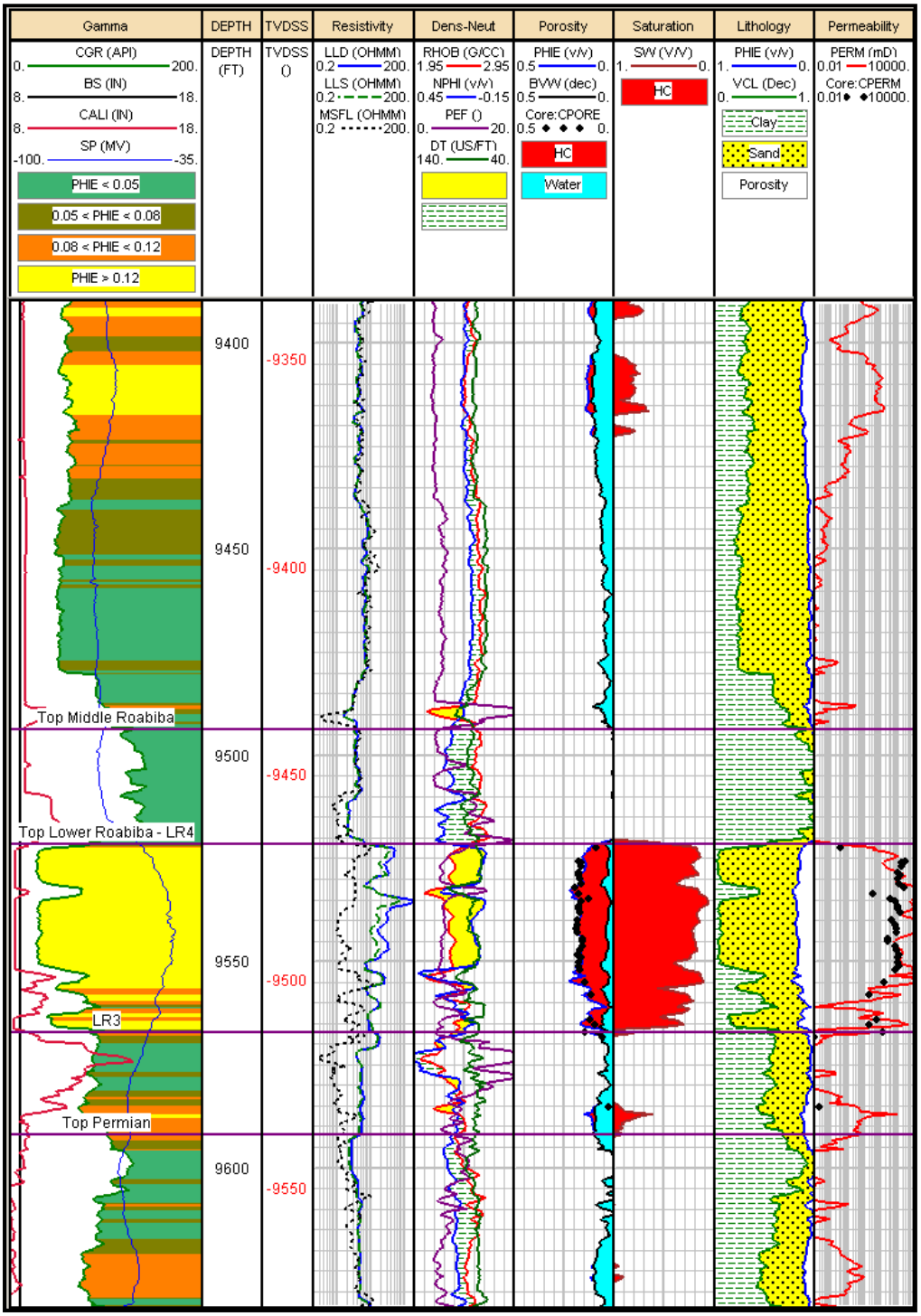

B7 well log analysis

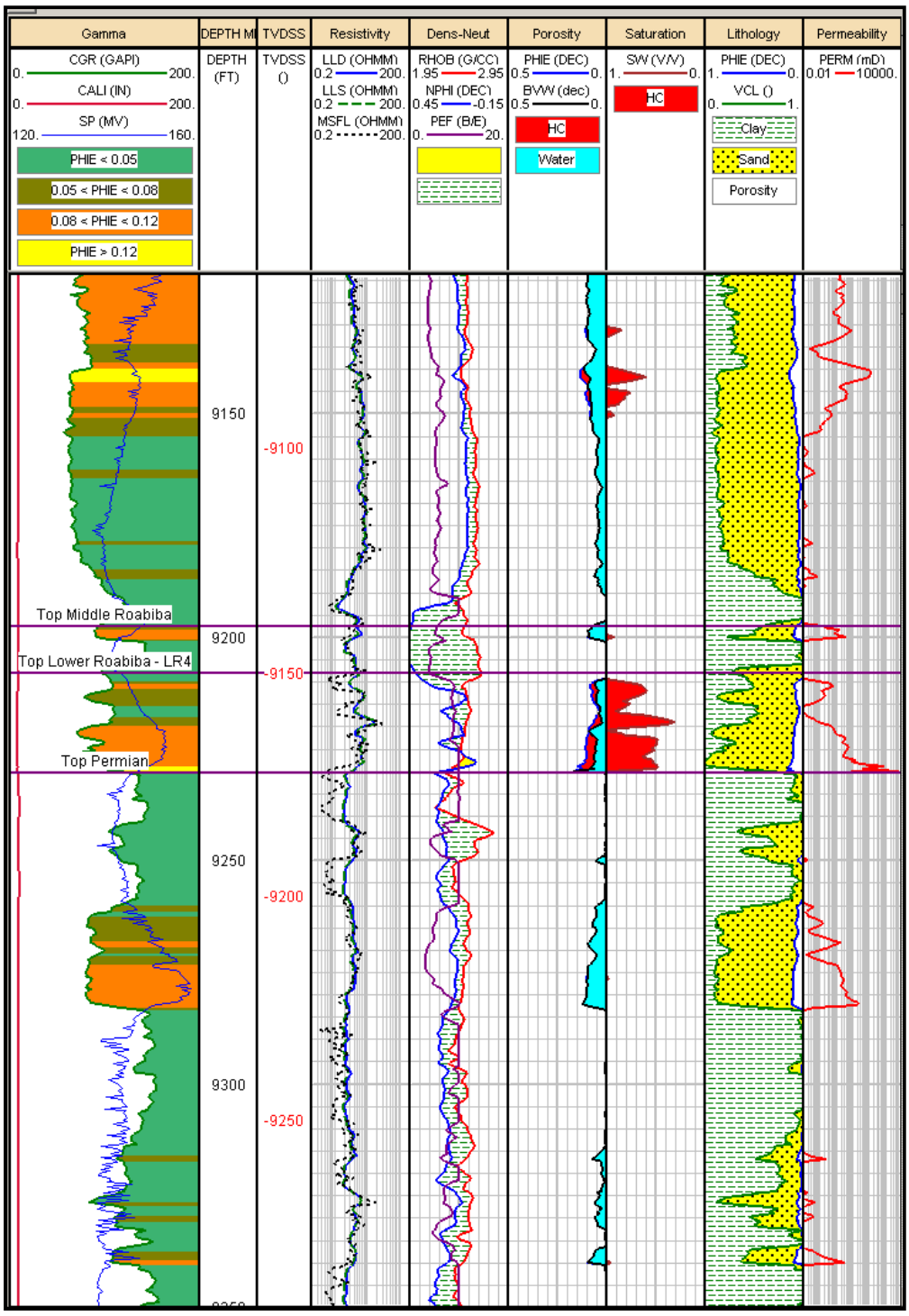

B8 well log analysis

APPENDIX C

CROSS SECTIONS

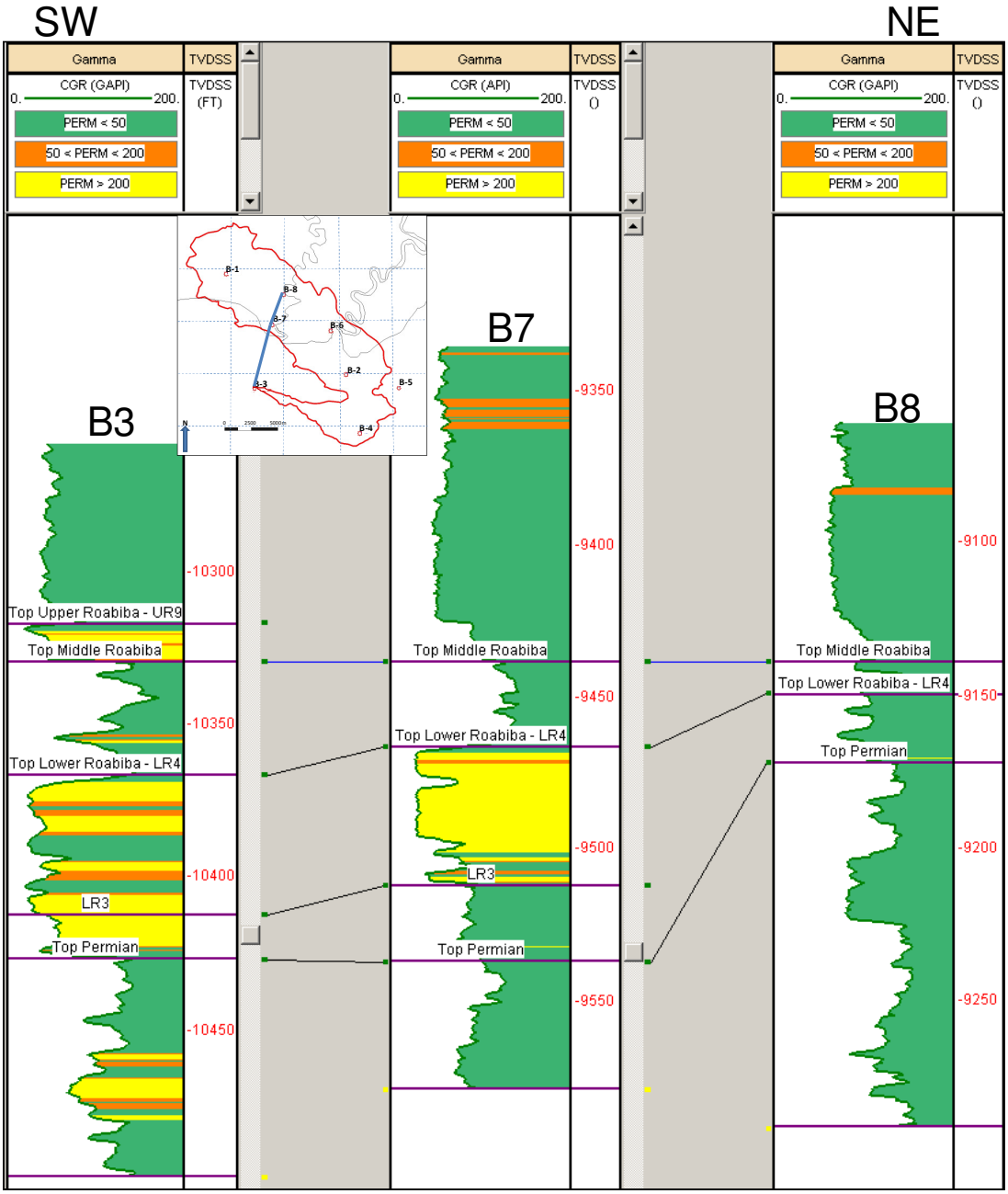

Permeability values along dip. Datum is top of Middle Roabiba Formation.

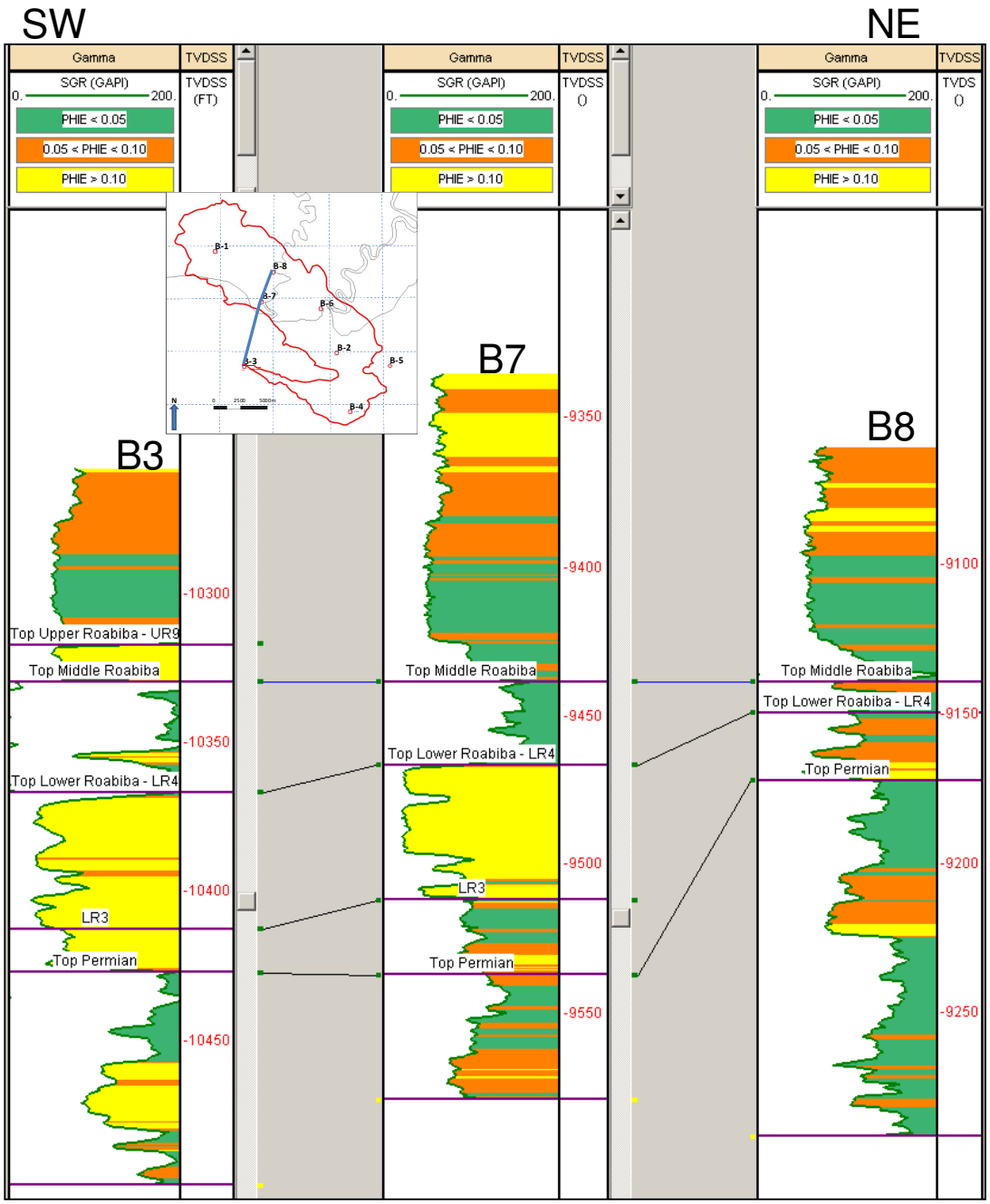

Porosity values along dip. Datum is top of Middle Roabiba Formation.

APPENDIX D

NET PAY MAPS

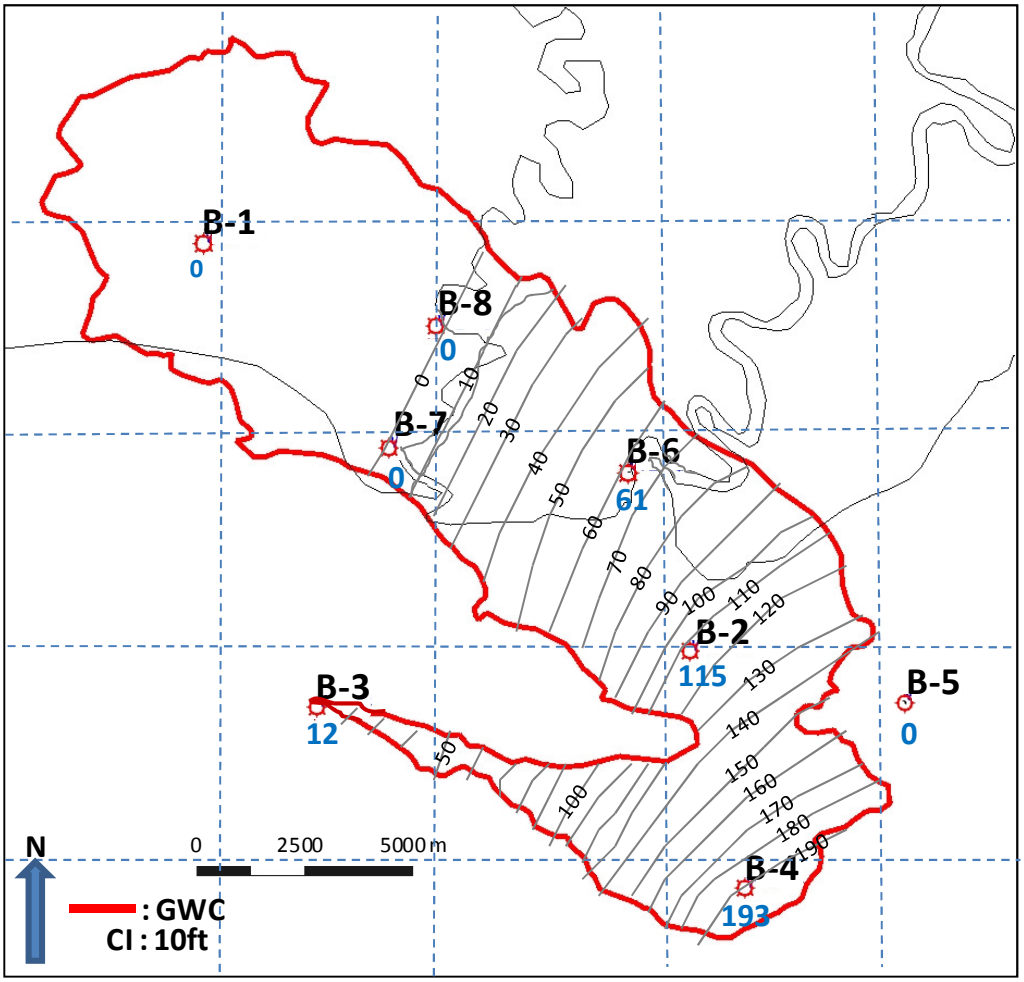

Net pay map of Upper Roabiba Sandstone reservoir

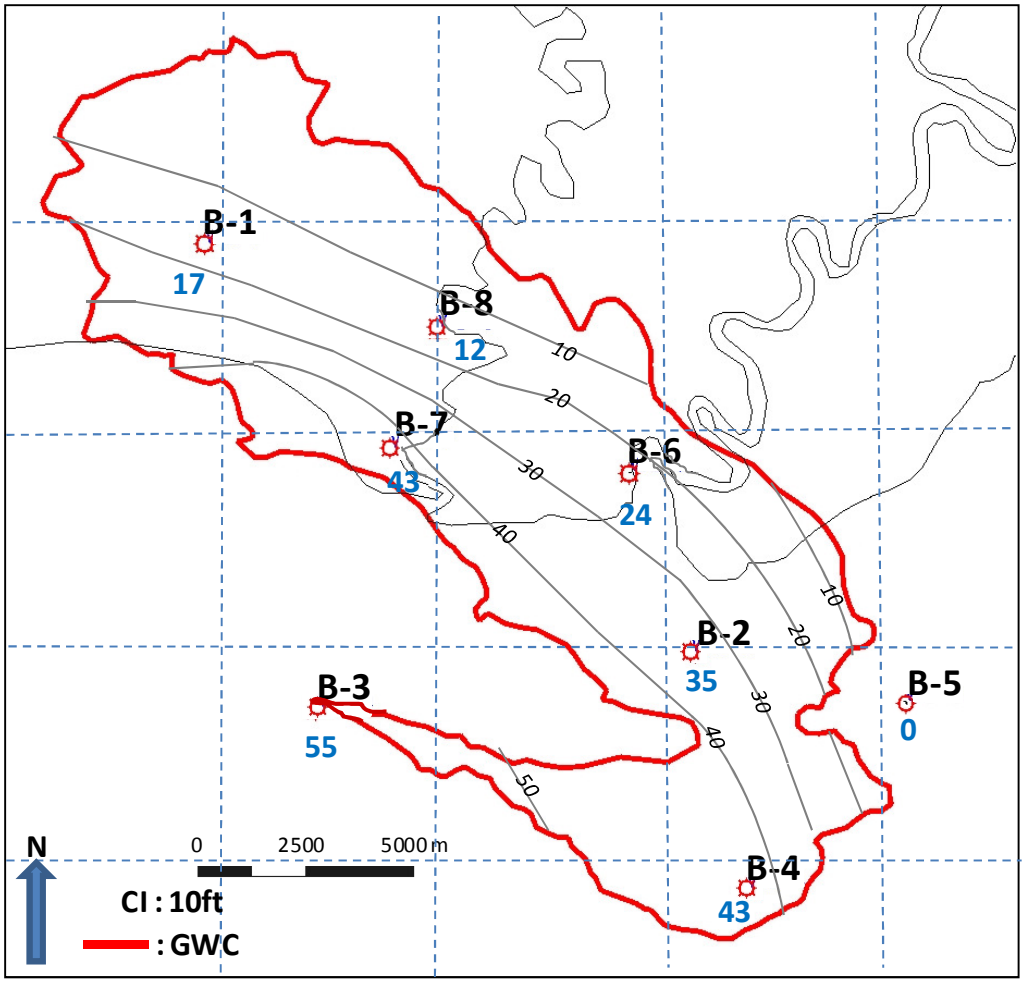

Net pay map of Lower Roabiba Sandstone reservoir

APPENDIX E

ROCK TYPE DISTRIBUTIONS

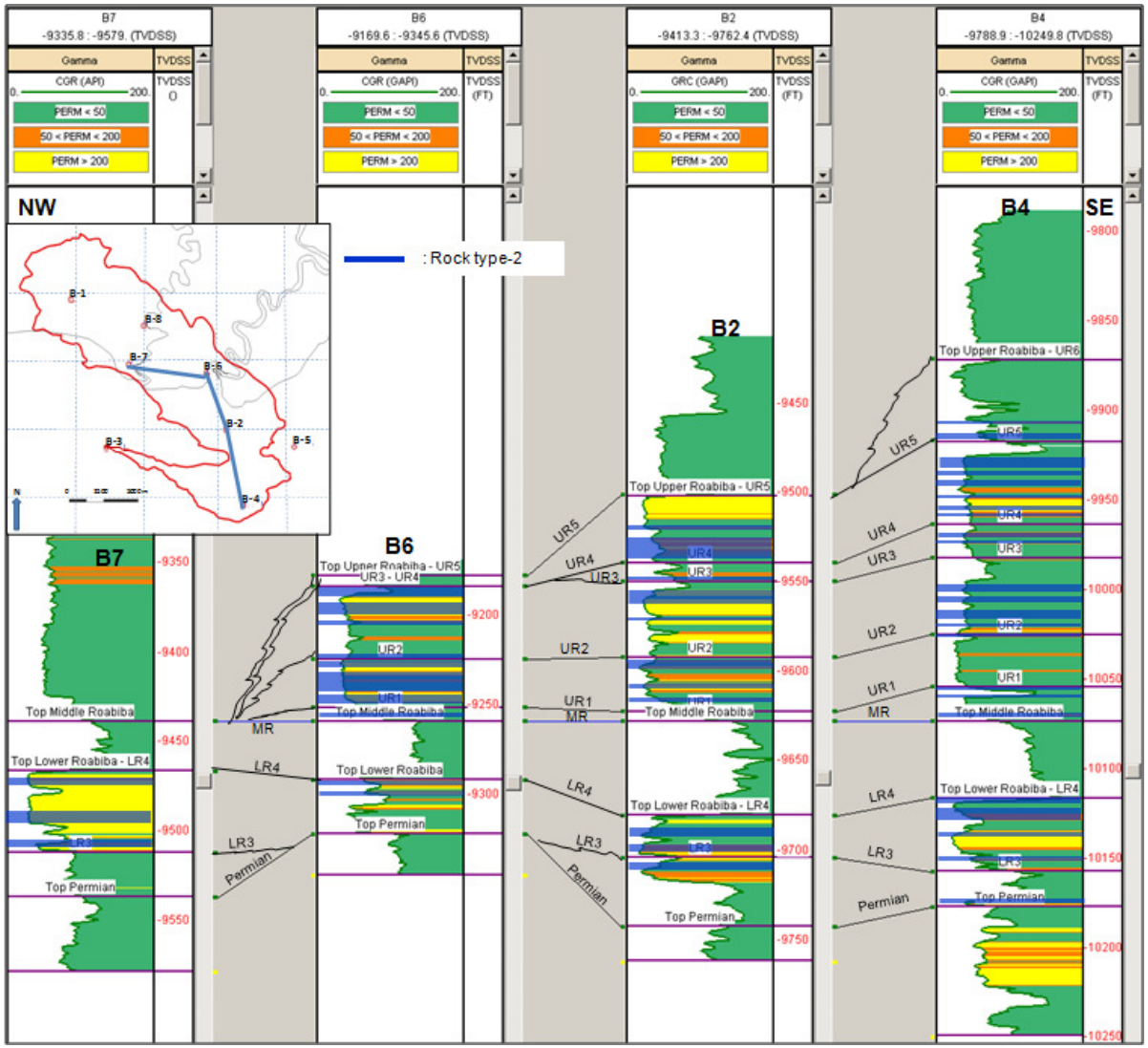

Cross-section in NW-SE direction showing distribution of rock type-2

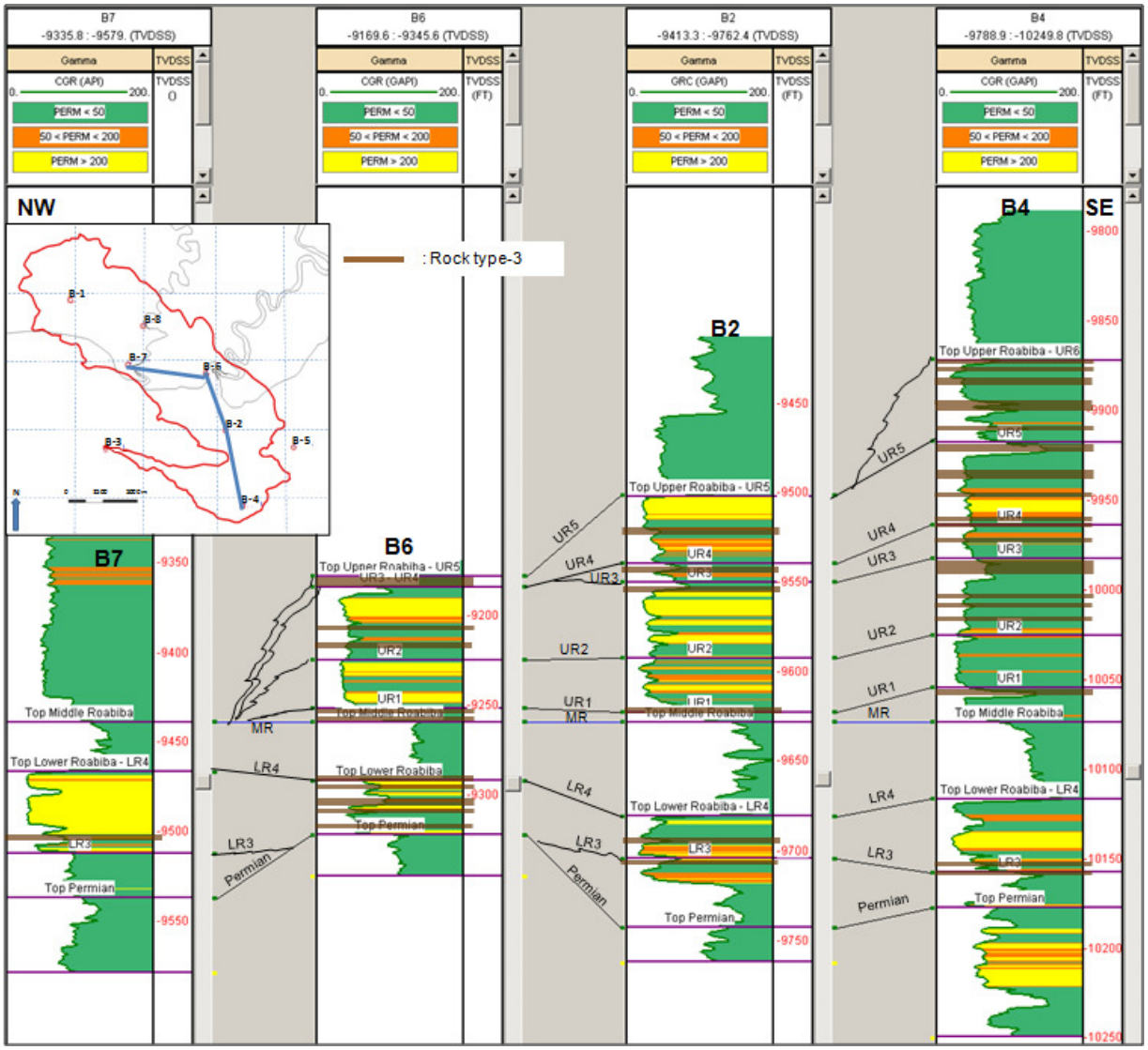

Cross-section in NW-SE direction showing distribution of rock type-3

VITA

Name	Riene Vera
Education	Texas A&M University College Station, Texas, USA M.S., Geology, 2009
	Trisakti University Jakarta, Indonesia B.S., Geology, 1998
Address	Raffles Hills Block O1/22, Cibubur, Depok, West Java, Indonesia, 16454
E-mail	riene_vera@yahoo.com